U.S. Department
of Transportation
Federal Railroad
Administration

Office of Research,
Development and Technology
Washington, DC 20590

Torsional Strength and Stiffness of a Passenger Car Coupling System

DOT/FRA/ORD-23/24

Final Report | September 2023

REPORT DOCUMENTATION PAGE

Form Approved
OMB No. 0704-0188

1. REPORT DATE *(DD-MM-YYYY)*	**2. REPORT TYPE**	**3. DATES COVERED** *(From - To)*
29-06-2022	Technical Report	9/30/2019 – 6/30/22

4. TITLE AND SUBTITLE
Torsional Strength and Stiffness of a Passenger Car Coupling System

5a. CONTRACT NUMBER
693JJ618D000006 / 693JJ619F000113

5b. GRANT NUMBER

5c. PROGRAM ELEMENT NUMBER

6. AUTHOR(S)
Robert Trent (0000-0001-8506-1408)
Bora Jang (0000-0002-5685-2726)
Matt Radovich (0000-0001-5719-0640)
Anuradha Guntaka (0000-0003-1253-1127)
Anand Prabhakaran (0000-0002-4940-9988)

5d. PROJECT NUMBER

5e. TASK NUMBER

5f. WORK UNIT NUMBER

7. PERFORMING ORGANIZATION NAME(S) AND ADDRESS(ES)
Sharma & Associates, Inc.
5810 S Grant Street
Hinsdale, IL 60521

8. PERFORMING ORGANIZATION REPORT NUMBER

9. SPONSORING/MONITORING AGENCY NAME(S) AND ADDRESS(ES)
U.S. Department of Transportation
Federal Railroad Administration
Office of Railroad Policy and Development
Office of Research, Development, and Technology
Washington, DC 20590

10. SPONSOR/MONITOR'S ACRONYM(S)

11. SPONSOR/MONITOR'S REPORT NUMBER(S)
DOT/FRA/ORD-23/24

12. DISTRIBUTION/AVAILABILITY STATEMENT
This document is available to the public through the FRA website.

13. SUPPLEMENTARY NOTES
COR: Jeffrey Gordon

14. ABSTRACT
Between September 2019 and June 2022, the Federal Railroad Administration (FRA) sponsored a research team from Sharma & Associates to model and test the torsional strength of a passenger car coupling system to understand the performance of coupling systems in train accidents and to enhance current specifications. The team designed a test fixture to apply a controlled torque to a complete coupling system comprising a coupler, yoke, draft gear, and draft sill, and developed a Finite Element (FE) model of the test fixture to assess its structural integrity and to predict the applied torque necessary for failure. The team identified two modes of failure, draft sill failure and coupler shank failure. The mode of failure was found to depend on the degree of constraint provided by the draft sill. Researchers found the results of full-scale testing agreed reasonably well with those measured in the FE model tests. Classical overturning calculations indicated that an applied torsional moment of 297 kip-ft, the lowest measured torsional capacity of the tested coupling system, would likely rollover a single rail car. Such an applied torsional moment will likely be near or beyond the yield capacity of modern car structures and would need to be evaluated on a case-by-case basis in possible future work.

15. SUBJECT TERMS
Full Scale Testing, H couplers, Coupler Torsion, Torsional Transmission

16. SECURITY CLASSIFICATION OF:			**17. LIMITATION OF ABSTRACT**	**18. NUMBER OF PAGES**	**19a. NAME OF RESPONSIBLE PERSON**
a. REPORT	**b. ABSTRACT**	**c. THIS PAGE**		79	**19b. TELEPHONE NUMBER** *(Include area code)*

Standard Form 298 (Rev. 8/98)
Prescribed by ANSI Std. Z39.18

METRIC/ENGLISH CONVERSION FACTORS

ENGLISH TO METRIC	METRIC TO ENGLISH
LENGTH (APPROXIMATE)	**LENGTH (APPROXIMATE)**
1 inch (in) = 2.5 centimeters (cm)	1 millimeter (mm) = 0.04 inch (in)
1 foot (ft) = 30 centimeters (cm)	1 centimeter (cm) = 0.4 inch (in)
1 yard (yd) = 0.9 meter (m)	1 meter (m) = 3.3 feet (ft)
1 mile (mi) = 1.6 kilometers (km)	1 meter (m) = 1.1 yards (yd)
	1 kilometer (km) = 0.6 mile (mi)
AREA (APPROXIMATE)	**AREA (APPROXIMATE)**
1 square inch (sq in, in^2) = 6.5 square centimeters (cm^2)	1 square centimeter (cm^2) = 0.16 square inch (sq in, in^2)
1 square foot (sq ft, ft^2) = 0.09 square meter (m^2)	1 square meter (m^2) = 1.2 square yards (sq yd, yd^2)
1 square yard (sq yd, yd^2) = 0.8 square meter (m^2)	1 square kilometer (km^2) = 0.4 square mile (sq mi, mi^2)
1 square mile (sq mi, mi^2) = 2.6 square kilometers (km^2)	10,000 square meters (m^2) = 1 hectare (ha) = 2.5 acres
1 acre = 0.4 hectare (he) = 4,000 square meters (m^2)	
MASS - WEIGHT (APPROXIMATE)	**MASS - WEIGHT (APPROXIMATE)**
1 ounce (oz) = 28 grams (gm)	1 gram (gm) = 0.036 ounce (oz)
1 pound (lb) = 0.45 kilogram (kg)	1 kilogram (kg) = 2.2 pounds (lb)
1 short ton = 2,000 pounds (lb) = 0.9 tonne (t)	1 tonne (t) = 1,000 kilograms (kg)
	= 1.1 short tons
VOLUME (APPROXIMATE)	**VOLUME (APPROXIMATE)**
1 teaspoon (tsp) = 5 milliliters (ml)	1 milliliter (ml) = 0.03 fluid ounce (fl oz)
1 tablespoon (tbsp) = 15 milliliters (ml)	1 liter (l) = 2.1 pints (pt)
1 fluid ounce (fl oz) = 30 milliliters (ml)	1 liter (l) = 1.06 quarts (qt)
1 cup (c) = 0.24 liter (l)	1 liter (l) = 0.26 gallon (gal)
1 pint (pt) = 0.47 liter (l)	
1 quart (qt) = 0.96 liter (l)	
1 gallon (gal) = 3.8 liters (l)	
1 cubic foot (cu ft, ft^3) = 0.03 cubic meter (m^3)	1 cubic meter (m^3) = 36 cubic feet (cu ft, ft^3)
1 cubic yard (cu yd, yd^3) = 0.76 cubic meter (m^3)	1 cubic meter (m^3) = 1.3 cubic yards (cu yd, yd^3)
TEMPERATURE (EXACT)	**TEMPERATURE (EXACT)**
[(x-32)(5/9)] °F = y °C	[(9/5) y + 32] °C = x °F

QUICK INCH - CENTIMETER LENGTH CONVERSION

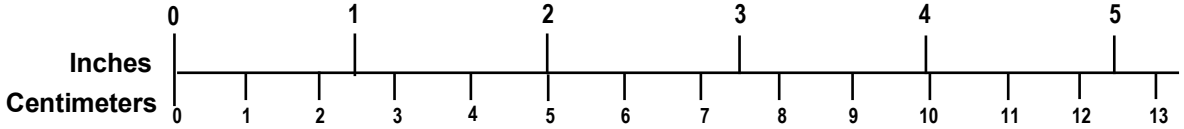

QUICK FAHRENHEIT - CELSIUS TEMPERATURE CONVERSIO

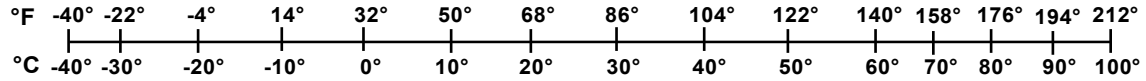

For more exact and or other conversion factors, see NIST Miscellaneous Publication 286, Units of Weights and Measures. Price $2.50 SD Catalog No. C13 10286

Updated 6/17/98

Contents

Illustrations

Tables

Executive Summary

Between September 2019 and June 2022, the Federal Railroad Administration (FRA) sponsored a research team from Sharma & Associates to model and test the torsional strength of a passenger car coupling system. The results can be used to understand the performance of coupling systems in train accidents and to enhance the current specifications, which only include requirements for the strength of couplers in the vertical and axial directions.

The team designed a test fixture to apply a controlled torque to a complete coupling system comprising a coupler, yoke, draft gear, and draft sill. Researchers developed a Finite Element (FE) model of the test fixture to assess its structural integrity and to predict the applied torque necessary for failure. The team identified two modes of failure, draft sill failure and coupler shank failure. The mode of failure was found to depend on the degree of constraint provided by the draft sill.

The research team found that draft sill failure occurred when the coupler, yoke, and draft gear were nominally constrained in the draft sill (as is the case in normal operating conditions) and coupler shank failure occurred when the draft sill provided full restraint. The latter situation might arise following structural deformation caused by an accident or with particularly stiff draft sill designs.

Researchers tested long shank, H-type Tightlock couplers. The first test resulted in failure of the draft sill at an applied torque of 297 kip-ft, with a coupler rotation angle of 25.8 degrees recorded at failure. The team then modified the test fixture so that a second test resulted in the failure of the coupler shank, which occurred at an applied torque of 390 kip-ft and a coupler rotation angle of 16.9 degrees. The third and final test used the modified test fixture from the second test with the coupler from the first test, and resulted in coupler shank failure at an applied torque of 351 kip-ft and a coupler rotation angle of 24.4 degrees.

The research team created FE models to simulate both failure modes that produced results which agreed reasonably well with those measured in the tests. The validated FE models also can be used to research the torsional performance of other coupling systems.

Classical overturning calculations indicated that an applied torsional moment of 297 kip-ft, the lowest measured torsional capacity of the tested coupling system, would likely rollover a single rail car. Such an applied torsional moment will likely be near or beyond the yield capacity of modern car structures and would need to be evaluated on a case-by-case basis in possible future work.

One potential next step in this research could be the evaluation of more modern draft sill designs and couplers with pushback elements. In addition, the team recommends derailment modeling of a string of cars using the evaluated torsional characteristics to identify conditions under which adjacent cars may be stabilized or experience rollover.

1. Introduction

This report describes modeling and testing to quantify the torsional strength of a passenger car coupling system. The Federal Railroad Administration (FRA) sponsored a research team from Sharma & Associates to conduct the research between September 2019 and June 2022.

1.1 Background

In addition to their obvious role of connecting cars to makeup a train, couplers play a vital role in keeping trains together and aligned under derailment conditions. Crashworthiness paradigms, whether traditional (relying on strong, unyielding car bodies), or more modern Crash Energy Management (CEM) systems (relying on structural collision energy dissipation), depend at least to some degree on couplers providing climb resistance, jack-knifing resistance, and rollover resistance for crash protection. Keeping cars aligned is particularly critical to ensure CEM benefits are realized in a crash event.

Climb resistance requirements for passenger equipment, including the climb resistance offered by H-type and F-type couplers, are addressed by federal regulations 49 CFR 238.205 and 238.207. American Public Transportation Association (APTA) and Association of American Railroads (AAR) standards and recommended practices address the strength requirements of couplers. In general, however, these strength requirements are only defined in the vertical[1] and axial (i.e., buff and draft) conditions. In addition, APTA S-034-99 (section 5.5.2.2 Bypass resistance) implies that the lateral strength of coupler connections needs to be at least the same as the climb resistance. However, coupler torsional strength requirements remain undefined.[2] While the coupler torsional strength of H-type and F-type couplers is considered 'adequate' to provide the needed resistance in a derailment or collision event, its magnitude has not been quantified in publicly available research.

Couplers play a key role in determining the inter-car rollover behavior in derailments. The torsional stiffness of coupler connections, particularly couplers with top and bottom shelves (i.e., E-type couplers) have caused strings of tank cars to derail under strong lateral load (e.g., high wind) and empty car conditions. Figure 1 shows an example where a train collision in the Missoula rail yard (Montana Rail Link) on February 7, 2017, resulted in the derailment of 30 tank cars. However, it also is likely that torsionally stiff coupler connections can prevent cars from derailing by helping to keep cars upright. Previous FRA research, through both analytical and test efforts [1], has studied the torsional stiffness of E-type couplers with and without top and bottom shelves and quantified the torsional stiffness (i.e., kip-ft of torsional resistance per degree of rotation) of these connections under elastic conditions. However, the connections were not tested to failure to estimate the ultimate torsional strength. Further, the study did not draw a conclusion regarding the potential of a stiff coupler connection to induce a chain derailment,

[1] Generally defined as the capacity of the coupler and its carrier to resist an anti-climbing vertical upward or downward load of 100,000 lbf without permanent deformation.

[2] One exception is the APTA pushback coupler recommended practice PR-CS-RP-019-11, which recommends that couplers provide torsional resistance of ±150 kip-ft (203 kNm) before pushback function. The document also notes that such a level of resistance is only expected to keep cars upright under minor derailment conditions, and not under serious derailments.

noting, “It is possible that for every ‘domino’ effect multicar rollover, there are also some potential rollovers that are eliminated because of the shelf-type coupler.”

Figure 1. Domino Derailment of Tank Cars

The concern for passenger cars is that if the torsional resistance of the coupler (and its structural attachments) is overwhelmed, resistance to carbody roll will be compromised, which could lead to significantly unsafe conditions. The intent of this research was to quantify the torsional resistance of H-type coupler connections through analytical and test means so that the risks of such an event can be evaluated and, if necessary, mitigated.

While freight and passenger car coupler systems are relatively strong, they are generally designed to be the weakest link in the train as they are most readily accessible for inspection, maintenance, and replacement in case of failure. As an example, H-type coupler shanks with Grade C steel are expected to be fully elastic up to an axial load of 300 kips, and they can take on a permanent set in as little as 450 kips and have a minimum ultimate strength of 725 kips. In contrast, the minimum elastic capacity of the passenger cars the coupler connects is at least 800 kips, with the ultimate capacity being two to three times that value.

The prior FRA study on coupler torsional stiffness focused on E-type couplers, as these are currently the most used on freight vehicles [1]. E-type couplers have a few key differences when compared to F-type and H-type couplers. E-type couplers allow relative vertical movement at the knuckle interface, their shanks rest on solid (i.e., non-sprung) carriers, and they further connect to the yoke through a horizontal key. In the derailments that drove the initial research, the ultimate strength of the couplers was not a concern as the coupler systems survived the derailment. Rather, the focus of that research was on the torsional stiffness of the couplers.

In contrast, F-type and H-type coupler knuckles and heads are designed to interface in a way that allows a limited amount of rotation but no relative vertical displacement at the knuckle interface (see Figure 2). Rotation in the coupling system[3] is therefore accommodated using a sprung coupler carrier that allows relative vertical movement at the carrier. Further, the coupler shank connects to the yoke through a vertical coupler pin that allows free rotation about the vertical

[3] This report uses the term ‘coupling system’ to mean the coupler, draft sill, yoke, draft gear, and related small components.

axis. The key difference between H-type and F-type couplers is that H-type knuckles and coupler heads are machined (i.e., post-casting) to tighter tolerances, and therefore result in less slack and slop at the interface (i.e., a Tightlock connection). This research focused on the ultimate strength of the coupling system, not just its stiffness.

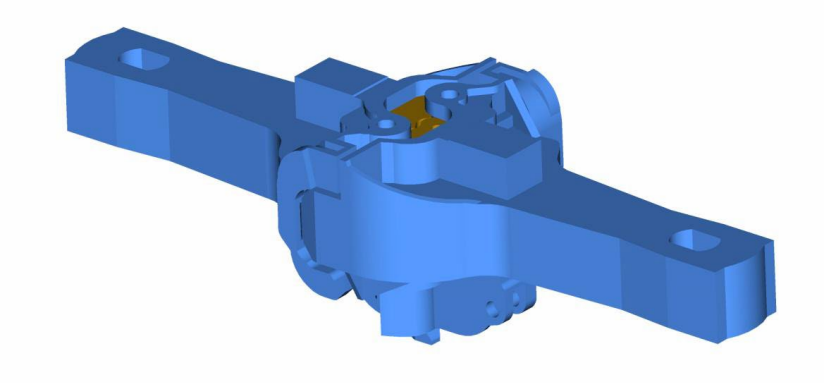

Figure 2. H-type Couplers – Coupled

1.2 Objectives

The objectives of the research were to determine the torsional strength of both a coupling system and a coupler alone, using a H-type coupler in its draft sill and recording the resulting failure modes through FE modeling and full-scale testing, and validate the FE modeling by comparing the results with those from full-scale testing. The goal was to demonstrate a repeatable method in which coupling systems can be tested for torsional strength in their draft sills and obtain data to be used in future car-to-car FE models, for the purpose of quantifying torsional transmission between the cars.

1.3 Overall Approach

The team first reviewed available accident reports and data to determine if any useful information could be obtained and used in this study. Researchers created a Computer Aided Design (CAD) model of an H-type Tightlock coupler and used it to generate an FE model. The team designed and built a test fixture to apply sufficient torque to fail the test specimens. Full scale tests were completed on three test specimens under two different constraint conditions. The team then compared the results of the FE modeling with those of the full-scale tests.

1.4 Scope

The scope of this research was to model and test a H-type Tightlock coupler system. However, the analytical approach and test fixture design are adaptable for use on other types of couplers, including those used in freight equipment.

1.5 Organization of the Report

The report is organized as follows:

- Section 2 discusses the accident data that was available and indicates whether this information was useful in setting up the modeling and testing.
- Section 3 describes the test articles and test fixture.

- Section 4 describes the coupler CAD model.
- Section 5 discusses the FE modeling and results.
- Section 6 describes the full-scale tests, providing details of the test apparatus, testing procedure, and test results.
- Section 7 compares the results from the full-scale testing to those from the FE modeling.
- Section 8 provides conclusions including a summary of the torsional strengths and stiffnesses from the full-scale testing.
- Appendices A and B provide additional images and results from the full-scale testing.
- Appendix C provides classical calculations to determine whether the carbody will roll over based on torque applied to the coupler shank.

2. Accident Survey

The research team gathered and reviewed publicly available information on rail accidents, including FRA data, National Transportation Safety Board (NTSB) reports, trade journals and newspaper reports, with the goal of obtaining insight into coupler torsional performance from accident statistics and details.

2.1 RAIRS Data

Data was gathered on coupler related accidents by reviewing FRA's Railroad Accident and Incident Reporting System (RAIRS). This system records the accident cause code and consequences for most derailments and incidents in the United States.

Cause codes in the series E3xx identify incidents that were initiated by coupler or draft system failure. Figure 3 shows the trend in these accidents from 2004 through 2018. On average, approximately 30 incidents each year were caused by coupler or draft system failures in this timeframe.

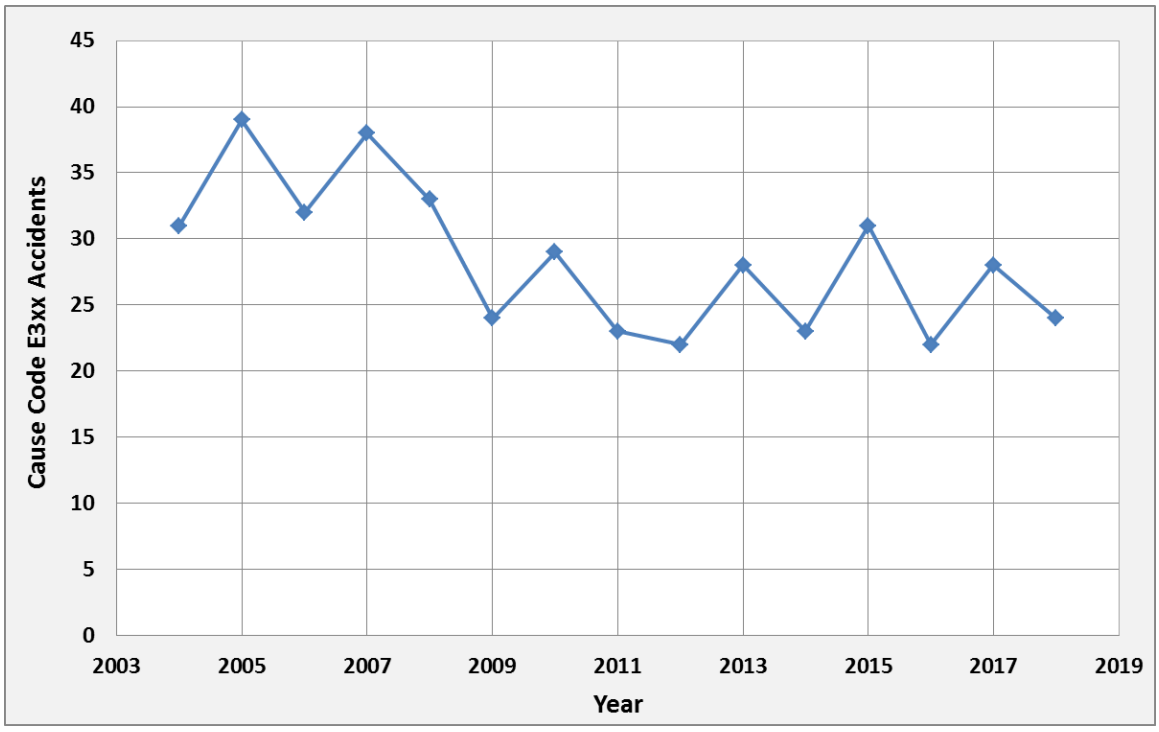

Figure 3. Annual Trend in E3xx Caused Accidents

Table 1 lists the cause codes in the E3xx series. It shows the total number of accidents from 2004 to 2018 inclusive, where each code was identified as the primary or secondary cause.

Table 1. E3xx Cause Code Definitions and Accidents – 2004 to 2018

Cause Code	Number of Accidents (Primary Cause)	Number of Accidents (Secondary Cause)	Description
E30C	55	8	Knuckle broken or defective
E30L	2	0	Knuckle broken or defective (LOCOMOTIVE)
E31C	18	0	Coupler mismatch, high/low
E31L	1	0	Coupler mismatch, high/low (LOCOMOTIVE)
E32C	27	1	Coupler drawhead broken or defective
E32L	2	0	Coupler drawhead broken or defective (LOCOMOTIVE)
E33C	106	0	Coupler retainer pin/cross key missing
E33L	1	0	Coupler retainer pin/cross key missing (LOCOMOTIVE)
E34C	63	2	Draft gear/mechanism broken or defective (including yoke)
E34L	1	0	Draft gear/mechanism broken or defective (including yoke) (LOCOMOTIVE)
E35C	31	0	Coupler carrier broken or defective
E35L	0	0	Coupler carrier broken or defective (LOCOMOTIVE)
E36C	9	0	Coupler shank broken or defective (includes defective alignment control)
E36L	1	0	Coupler shank broken or defective (includes defective alignment control) (LOCOMOTIVE)
E37C	6	0	Failure of articulated connectors
E37L	0	0	Failure of articulated connectors (LOCOMOTIVE)
E39C	87	4	Other coupler and draft system defects, (CAR) (Provide detailed description in narrative)
E39L	2	0	Other coupler and draft system defects, (LOCOMOTIVE) (Provide detailed description in narrative)

Table 2 breaks down the data in Table 1 by the type of train consist. These accidents all involved freight trains. There were 14 reported injuries in the timeframe and no fatalities.

Table 2. Cause Code Breakdown

Consist Type	Accidents Caused by E3
Freight Train	225
Work Train	2
Single Car	3
Cut of Cars	21
Yard/ Switching	169
Light Loco(s)	4
Unknown	3
	427

Unfortunately, the E3xx records from RAIRS did not include details about coupler performance in the accidents. Likewise, RAIRS records for accidents from other causes (e.g., track failure, collision) do not provide details about how well the couplers performed.

2.2 NS Steam Excursion Accident 1986

NTSB published a rail accident report on a derailment that occurred in 1986 where the type of coupler played a significant role [2]. The accident was referenced in a Trains Magazine article on May 1, 2006, "Couplers The Durable Link," by Kevin P. Keefe. The following excerpt highlights the anticipated benefits of H-type Tightlock couplers:

> *Evidence of the value of Type H couplers was provided in the May 18, 1986, derailment of a Norfolk Southern steam excursion train in the Great Dismal Swamp near Suffolk, VA. The train had 23 cars, all equipped with tight-locks except for the three older ex-Southern heavyweight cars, two of which jackknifed. Most of the 18 people who were seriously injured were riding in those two cars.*

The accident sent a shock wave throughout the recreational railroad industry and led passenger excursion operators to adopt the Type H coupler as standard. All cars on Amtrak's roster are now equipped with tight-lock couplers, and the company requires them on all privately owned passenger cars the company hauls. This requirement has led most active owners of older, non-streamlined cars to install Type H couplers, while others have removed their cars from mainline activity.

2.3 Philadelphia Derailment 2015

Some useful information on coupler performance was found in NTSB's report on the December 8, 2015, Amtrak derailment near Philadelphia, PA [3]. In this accident, a passenger train entered a 50 mph speed-restricted curve at 103 mph and subsequently derailed. Figure 4 shows an aerial view of the derailment. The red circle indicates the connection between the fourth car, which rolled onto its side, and the fifth car, which remained more upright.

Figure 4. Aerial View of Philadelphia Accident [3]

Figure 5 shows the end of the fourth car in the train that was coupled to the fifth car. The coupler shank casting failed across its transverse section. The draft sill remained intact without any extreme deformation.

Figure 5. Fourth Car Coupler Shank Failure

2.4 Chatsworth Accident 2008

On September 12, 2008, a passenger train collided with a freight train at a combined speed of over 80 mph in Chatsworth, CA. The following information was obtained from FRA's report on the accident [4].

The passenger train was seen to have experienced inter-car forces sufficient to exceed the strength of multiple couplers. Figure 6 shows how the coupler on the lead freight locomotive failed and draft gear on the lead freight and passenger locomotives was damaged. Figure 7 shows that the couplers on the trailing end of the first passenger car and the leading end of the second passenger car were severely damaged. Table 3 summarizes key information about the performance of the couplers and draft gear in the accident.

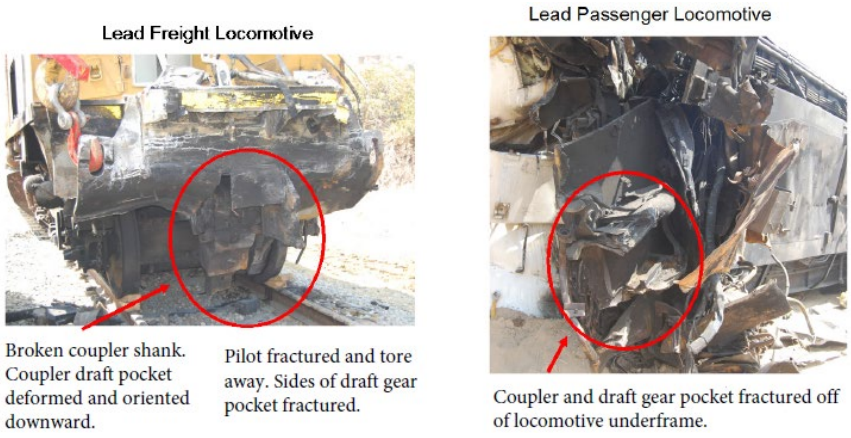

Figure 6. Coupler and Draft Gear Damage, Lead Freight and Passenger Locomotives [4]

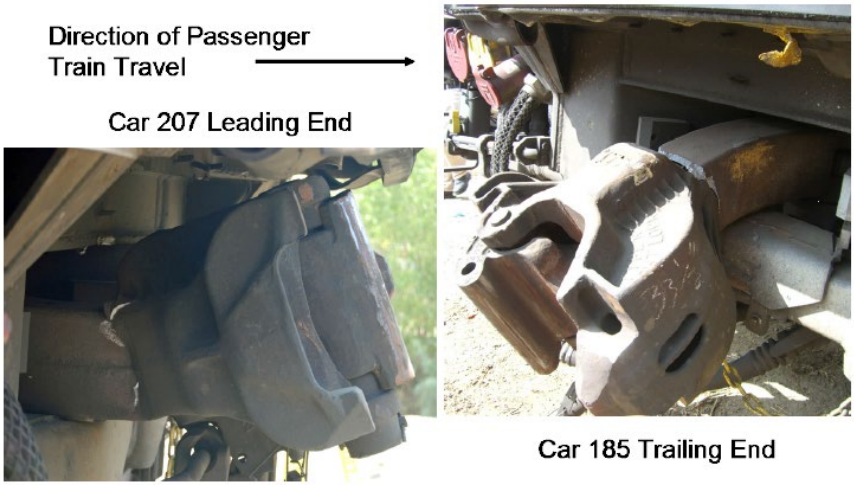

Figure 7. Coupler Damage to Trailing End of First Passenger Car and Leading End of Second Passenger Car [4]

Table 3. Chatsworth Crash Data (from [4])

Front end Lead Freight Loco	Front end Pass Loco	Rear end Pass Loco	Front end 1st pass car (185)	Rear end 1st pass car (185)	Front end 2nd Pass Car (207)	Rear end 2nd Pass Car (207)	Front end 3rd Pass Car (617)
Coupler shank fractures through	Coupler shank fractures	No info	No info	Coupler bent downward and cracked at head/shank int. (angle of bend not mentioned)	Coupler bent upward ~30 deg and cracked at head/shank int.	No info	No info
Draft gear pocket deforms downward	Draft gear pocket fractures off of loco frame	No info	No info	No info	No info	No info	No info

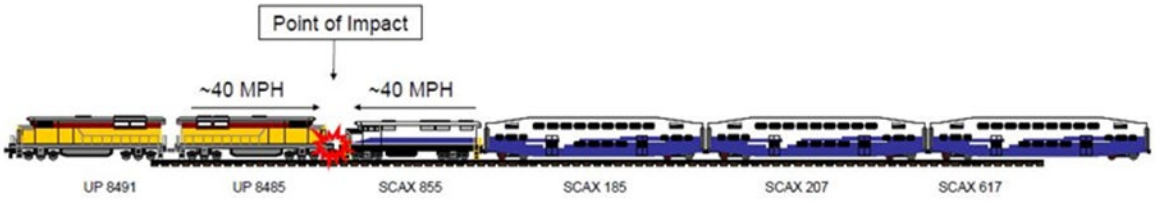

Note: Pass Loco and 1st pass car appear to roll over after the lead couplers of locos fracture through (on UP), unkown for Pass loco

3. Test Articles and Test Fixture

Researchers conducted full-scale testing to obtain the relationship between applied torque and coupler rotation and to characterize the failure modes of the coupling system. The test results were also used to validate the FE modeling and analysis.

Two types of tests were performed:

- Coupler/Draft Sill System Test
- Coupler Failure Test

3.1 Coupler/Draft Sill System Test Articles

The team selected the CH81E H-type Tightlock coupler with a radial connector and a WM-5-6 yoke with twin cushion draft gear for the test. This arrangement is common on many passenger cars.; This coupler setup is available with multiple coupler shank lengths. Although longer shank couplers are less common among current passenger car designs, one was chosen for this test effort as it is the most torsionally flexible and thus a conservative option. The longer coupler shank length also allows for the torque to be applied through a specially designed clamp-on torque arm assembly.

Figure 8 shows a drawing of the CH81E with the yoke and draft gear. Figure 9 shows details of the yoke, radial connector, and associated pins and bushings.

The coupler body was a grade E steel casting in accordance with AAR M-201 standards with a published tensile yield strength of 100 ksi and ultimate tensile strength of 120 ksi.

The yoke and radial connector were also AAR M-201 grade E steel castings.

Table 4 lists the quantities of the individual test pieces procured for the testing.

Table 4. Test Piece Quantities

Component	Qty.
Tightlock coupler with knuckle	6
Yoke and radial connector assembly	4
Y44A follower block	2
WM-5-6 draft gear	2

One of the coupler bodies and knuckles was used for scanning and characterizing both the exterior and interior geometry. Since both components were cut into several sections to accomplish this, they were not available for use in the testing. One coupler with knuckle was used as the actuating coupler and placed in the test fixture. The remaining four couplers with knuckles were available for testing with the four yoke and radial connectors. Other components were reused in the test as needed.

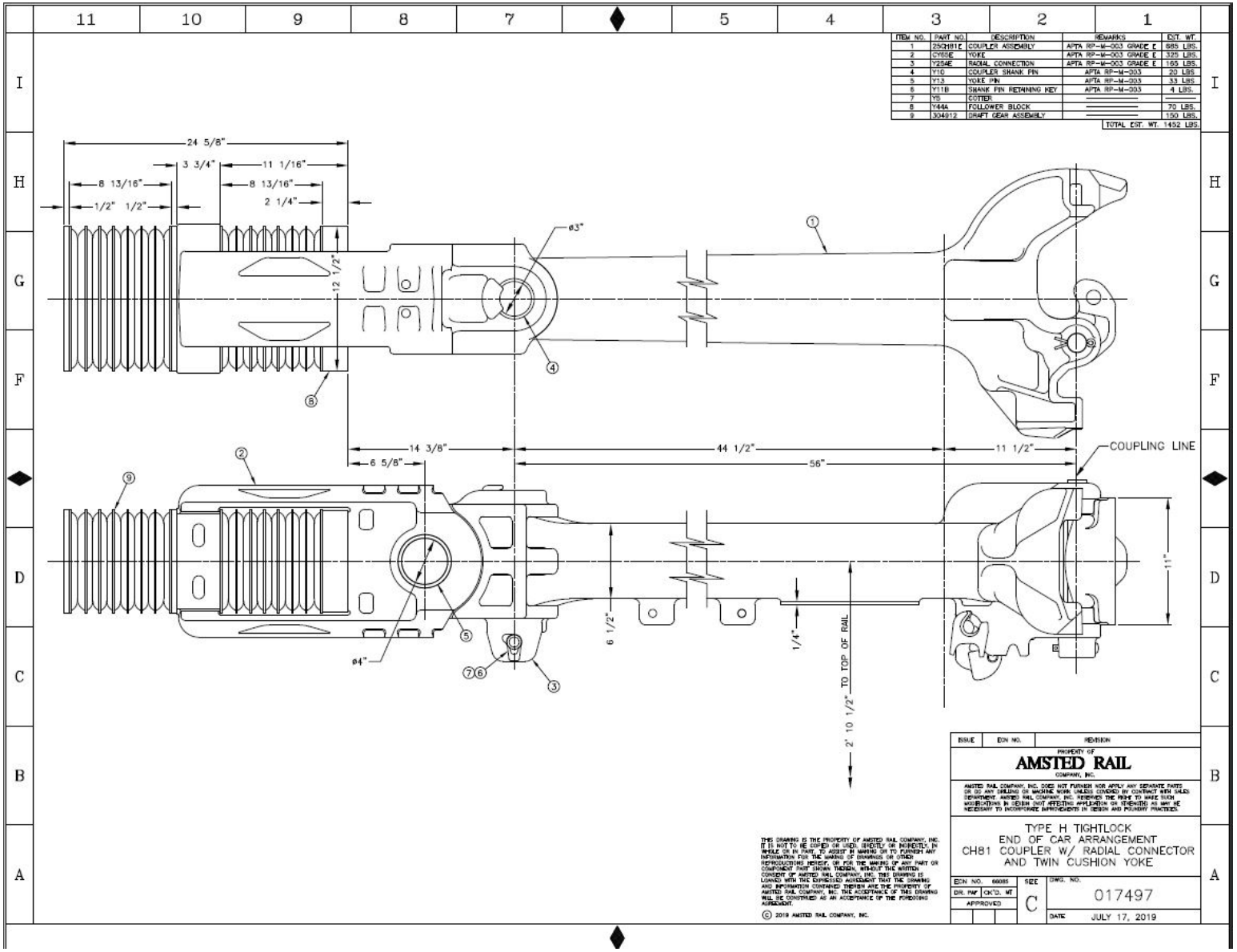

Figure 8. H-type Tightlock Coupler, Yoke, and Draft Gear

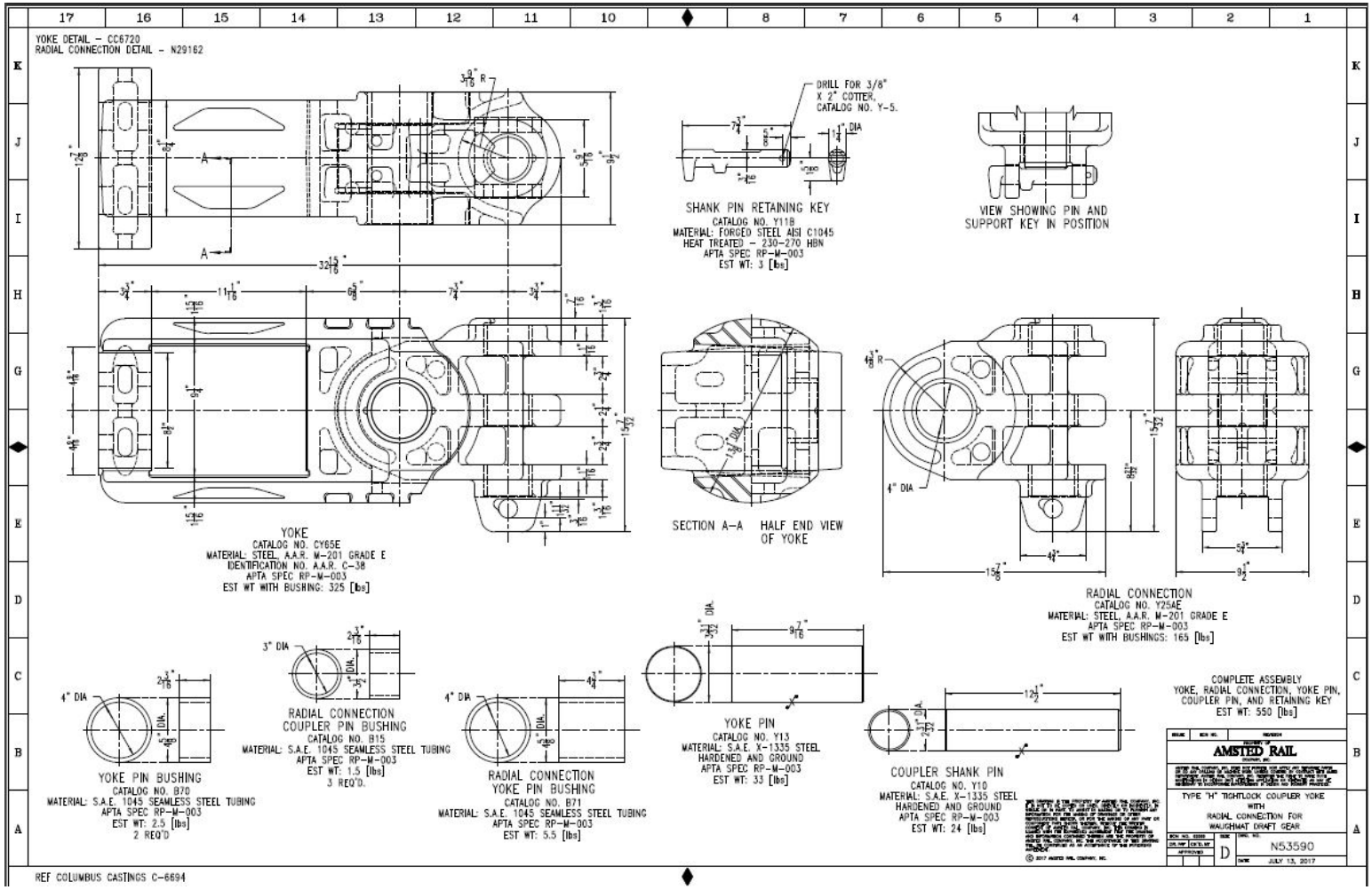

Figure 9. Radial Connector and Yoke Details

Measurements on an Illinois Central (IC) Grill-Coach #3345 (former Missouri Pacific 568) built by American Car and Foundry (lot # 2905) were used to design the draft sill for the full-scale tests. This car had an H-type coupler arrangement like that of the CH81E. Some original manufacturer's drawings of this car were also obtained to aid in the design. Figure 10 shows the end of the coach and Figure 11 is an example of the original drawings.

Figure 10. Illinois Central Grill-Coach #3345

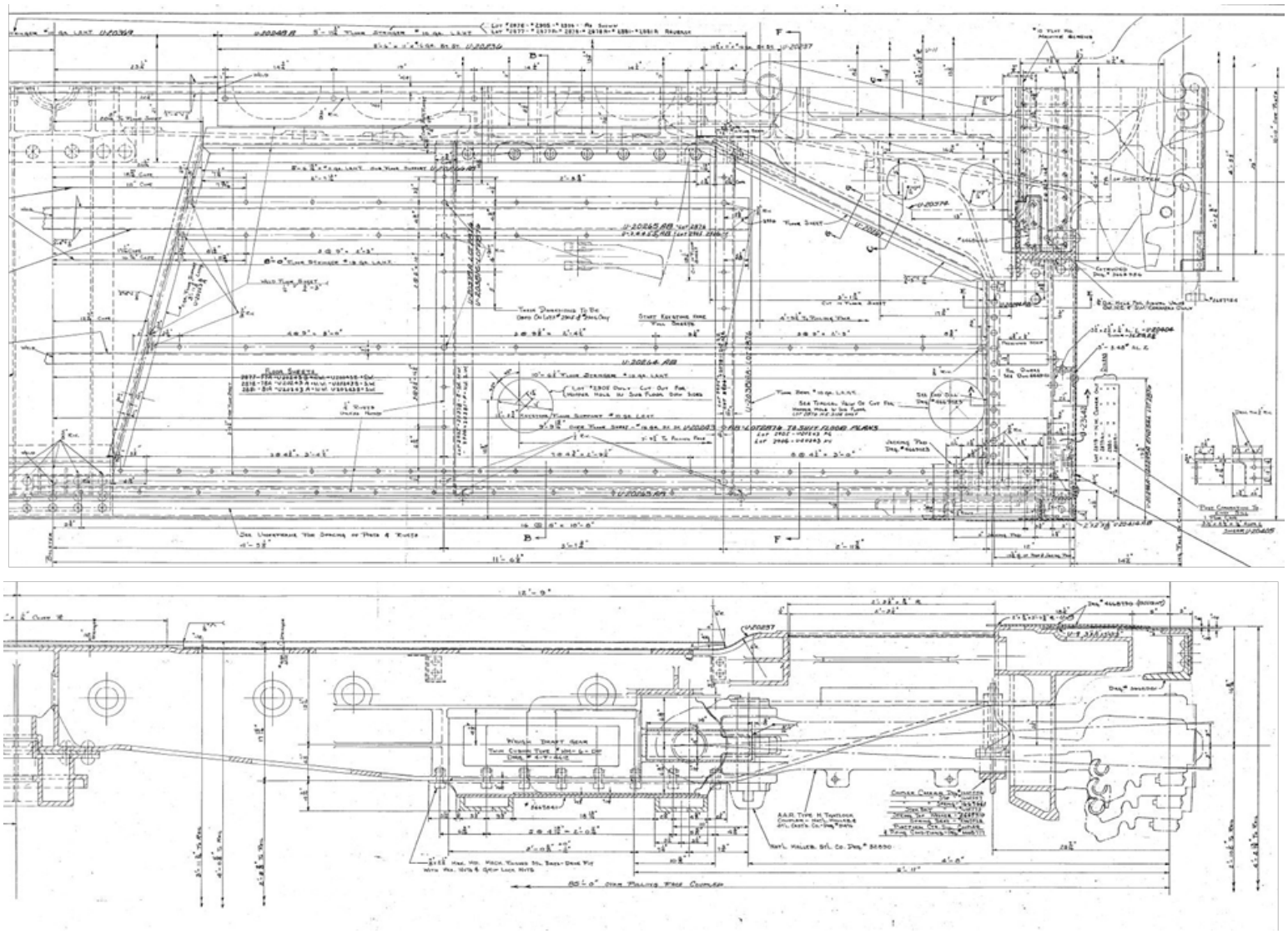

Figure 11. Example Draft Sill Arrangement Drawing

The draft sill was fabricated from ASTM A588 (Corten) steel with a yield strength of 50 ksi. It was fabricated from steel plate rather than being cast like that on an actual car. It included all the interior features such as draft lugs and stiffeners to accept the draft gear, yoke, and coupler. A sprung carrier accommodated vertical movement of the coupler, and a retaining plate assembly supported all the installed components, just as in an actual car. Material and thicknesses used for the test article were like that of the measured car. Some simplifications of the complex casting geometry were made to make the fabrication practical. Figure 12 shows the draft sill model created for the coupler/draft sill system test with the coupler and yoke installed.

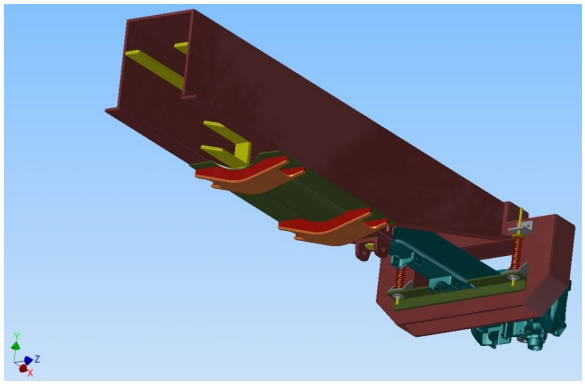

Figure 12. CAD Model of Draft Sill with Sprung Carrier and Carrier Plate Assembly

3.2 Coupler/Draft Sill System Test Fixture

The test fixture consisted of a large test frame comprised of several bolted structural steel I-beams forming a structure that houses and reacts two smaller test fixtures: an actuation fixture designed to accept the actuating coupler, and a reaction fixture designed to accept the Coupler/Draft Sill test specimen and react the torsional load in conjunction with the larger frame. The load was applied by a hydraulic actuator to a lever arm connected to the shaft of the actuating coupler. Figure 13 shows a general arrangement of the test fixture, hydraulic actuator, and test coupling system.

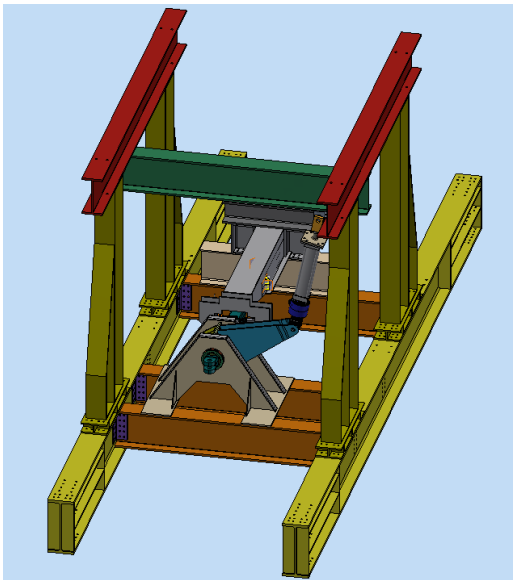

Figure 13. Test Fixture – CAD 3D View (diagonal beams not shown for clarity)

Figure 14 shows the end of the finished test fixture with the hydraulic actuator. The diagonal beams were included to increase the torsional stiffness of the test fixture.

Figure 14. Test Fixture – End View

Figure 15 shows the actuating fixture used to convert force in the hydraulic actuator to torque on the test coupling system. Two main 'A' shaped upright web assemblies accommodated the coupler shank adapter and a Nylatron® GSM plain bearing. This arrangement allowed the actuating coupler to rotate as the torque was applied. The shank adapters had a rectangular bore to fit the varying section of the coupler shank.

A lever arm comprised of two welded sub-assemblies was used to clamp over the coupler shank adaptors. It was connected to the clevis on the hydraulic actuator. Shims were used to create a tight fit between the coupler shank and the arm.

Figure 15. Actuating Fixture and Lever Arm

3.3 Coupler Failure Test Articles and Test Fixture

A modified draft sill was used for the coupler failure test; Figure 16 shows the modifications made to the draft sill. In this case, the draft sill was used only as a support and to react the loads; the yoke and twin cushion draft gear were absent. Two steel blocks were machined and welded into the draft sill to replace the lugs of the yoke where the radial connector interfaced with the yoke to strengthen and stiffen the fixture. Additional plates were welded on the blocks connecting them at their lower surface. A bottom close-off plate along with several internal plates spanning cross-wise inside the sill were also welded in to prevent widening of the draft sill. The radial connector was used to connect the coupler to the fixture.

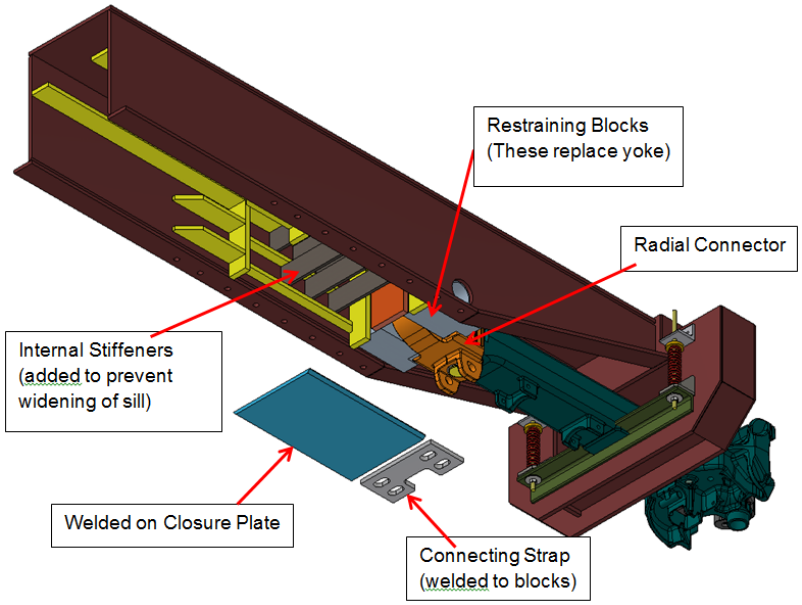

Figure 16. Modifications to Draft Sill

The modified draft sill was mounted to the test fixture closer to the coupler to better support and restrain the fixture and prevent widening of the sill during testing; this was the only modification to the test fixture. Figure 17 shows the modified mounting position. This modification stiffened the fixture in torsion and made coupler failure more likely.

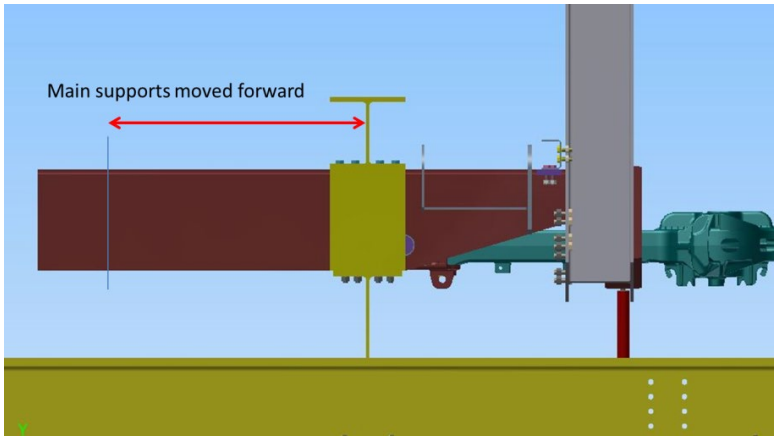

Figure 17. Modified Draft Sill Mounting Position

4. Coupler CAD Model

A 3-D coupler CAD model was created by scanning the exterior and interior surfaces of the H-type Tightlock coupler components including the coupler shank, coupler knuckle, lift lock, thrower, yoke, and radial connector. Some parts were sacrificed and cut into sections to obtain the interior surface configuration. Then, the 3D CAD files were adjusted to remove artifacts and non-critical features such as raised lettering, machine lines, and other small irregularities.

Figure 18 shows example results of the 3D scans. Local variations in wall thicknesses may not be consistent across couplers and may not correspond to the design intent; wall thicknesses varied from coupler to coupler, even within the small batch of couplers that SA received. The CAD model was prepared from the 3D scan, removing the local thickness variations to represent the design intent. In Figure 18, the areas colored red indicate material that was removed and the areas in blue indicate material that was added to prepare a consistent CAD model.

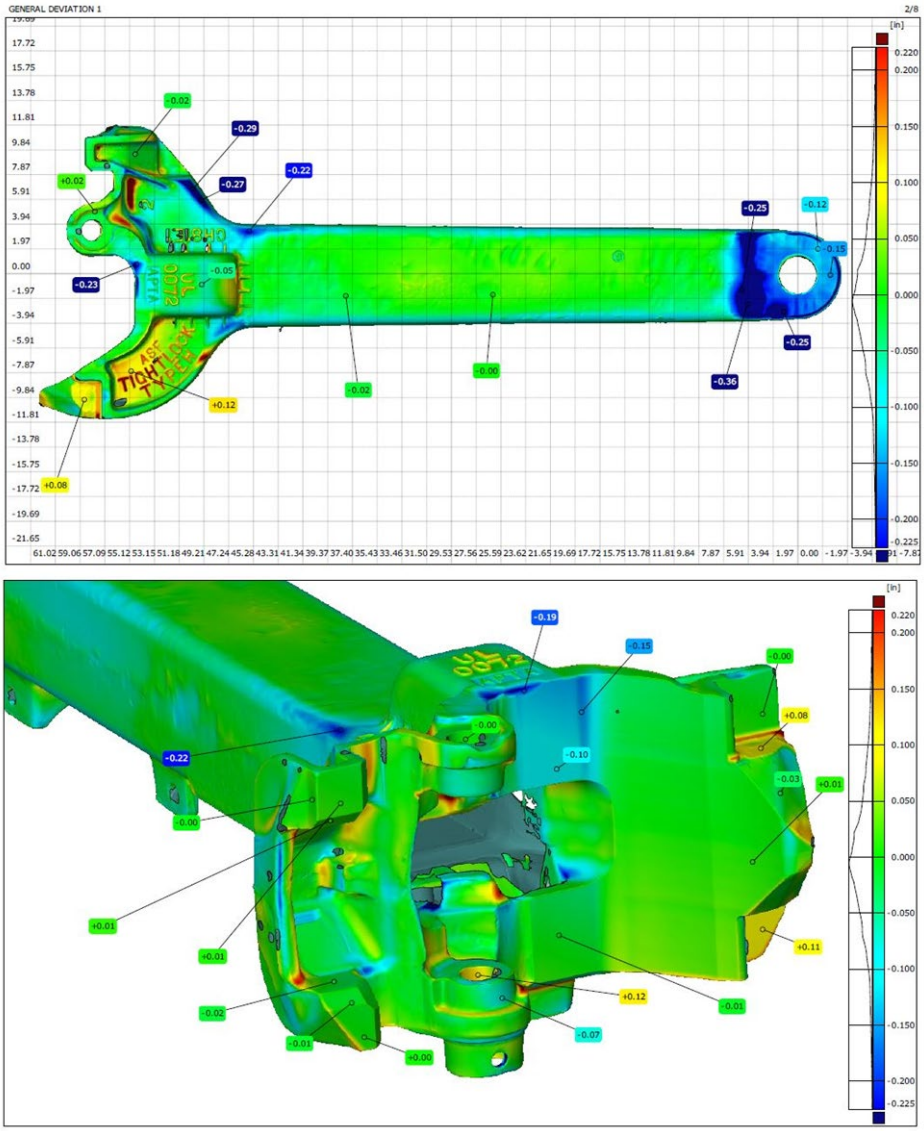

Figure 18. Examples of 3D Coupler Scans

The CAD model shown in Figure 18 was used for the FE modeling of both coupler-draft sill system and coupler failure. Post-test sectioning and inspection of the coupler shank (after the coupler failure test) revealed smaller thicknesses in the top wall and greater thicknesses in the bottom wall of the shank near the failure area. Revisions were made to the Coupler Failure FE Model to account for differences between the original CAD model and the geometry measured in the coupler used for the first coupler failure test. A post-test FE Analysis (FEA) was performed for the Coupler Failure model. Figure 19 shows the differences. There were also differences in the geometry around the lugs near the failure that were corrected (Figure 20). No other changes were made to the FE Model.

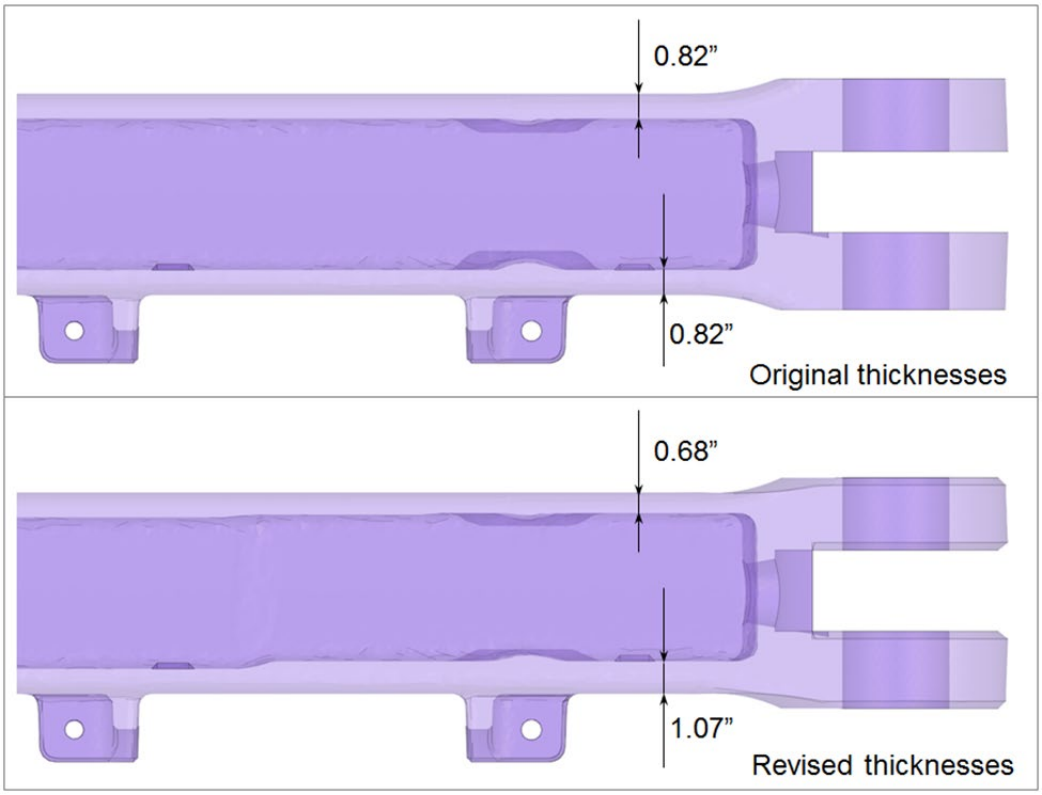

Figure 19. Coupler FE Model Thickness Revisions

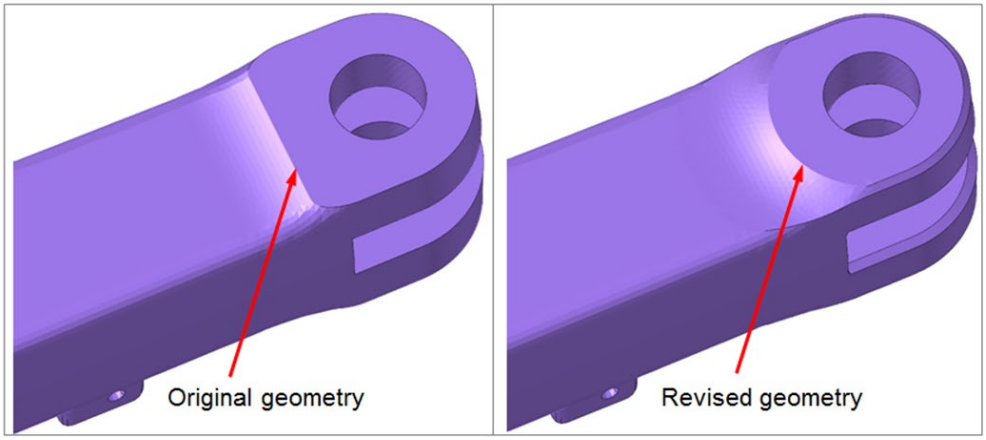

Figure 20. Coupler FE Model Geometry Correction

5. Finite Element Modeling and Analysis

The FE models of the test fixture and the test articles were developed from 3D CAD models. These FE Models were used to verify the structural integrity of the test fixture and to predict the relationship between torque and angular deflection of the coupling system under test conditions.

Two FE models were developed and used to simulate the tests:

- Coupler/Draft Sill System Model
- Coupler Failure Model

Both models include the complete test fixture.

The coupler/draft sill system model was simulated with the coupler, yoke, and draft gear nominally constrained in the draft sill, as is the case in normal operating conditions.

The coupler failure model was simulated with full restraint of the coupler shank in the draft sill. This situation might arise following structural deformation resulting from an accident or with particularly stiff draft sill designs. Researchers also obtained the torsional strength and deflection of the coupler alone from the coupler failure model.

Subsection 5.1 provides details of the FE models. Subsections 5.2 and 5.3 describe the results from the analyses.

5.1 FE Model Details

The FE mesh was generated in Altair HyperMesh and the FEA was performed using LS-DYNA, an explicit solver.

5.1.1 Meshing

The FE mesh was constructed in Altair HyperMesh software using solid and shell elements with all possible contacting surfaces between the components (i.e., automatic single surface contact type). The draft gear was represented by elastomeric elements in the FE model.

A second order tetrahedral solid mesh with 0.5 inch elements was used for the coupler, its bushings and pins, and the draft gear. The draft sill and test fixture components (e.g., large frame, coupler torsion reaction fixture, actuating fixture, etc.) used a linear quad shell mesh with element size ranging from 0.5 to 1.0 inch. The resulting FE model had 1,920,901 elements and 740,564 nodes with 87 components.

Figure 21 shows the FE model of the test fixture, couplers, draft gear, and draft sill.

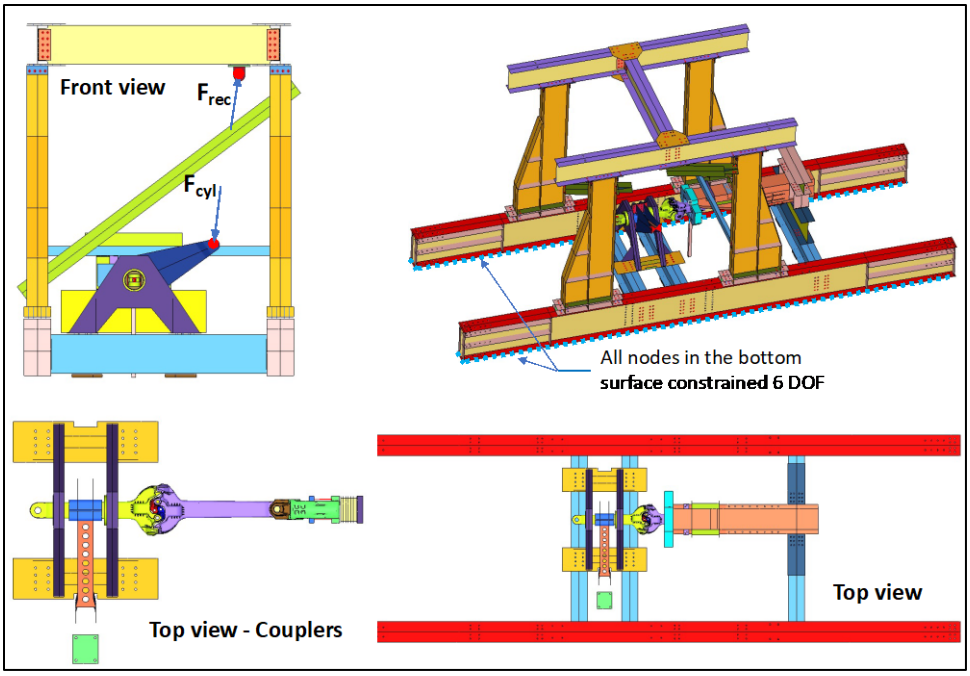

Figure 21. FE Model of Test Fixture with the Test Article

5.1.2 Materials

The materials used for different components in this study are shown in Table 5.

Table 5. Materials used for the components in FE Model

Material	Component
M201 Steel Casting Grade E – Coupler from Lab Coupon Test	Couplers
M201 Steel Casting Grade E – Yoke from Lab Coupon Test	Yoke
M201 Steel Casting Grade E	Radial connector, knuckles, throwers, lift locks
ASTM A992 Steel	I-Beams
ASTM A572 Grade 50	All other components
ASTM A36 Steel	Shims (for Coupler shank and Shank adapter)
ASTM A519 Grade 1026	Bearing housing
SAE X-1335 Steel	Coupler pin, Yoke pin, Knuckle pins
SAE 1018, Cold Drawn Steel	Shank adapter
SAE 1045, Seamless Steel Tubing	Bushings (for Coupler, Radial connector, Yoke)

Tensile tests were conducted on three 0.5 inch round coupon samples from each coupler and yoke in accordance with ASTM A370-2020 [5] and ASTM E8/E8M-2016a [6]. The material properties obtained from these tests are shown in Table 6, along with the material properties for other components used in the FE model. All materials were modeled with a Poisson ratio of 0.3.

Table 6. Material Properties used in FE Model

Material	Elastic Modulus (ksi)	Yield Strength (ksi)	Tangent Modulus (ksi)	Ultimate Strength (ksi)
M201 Steel Casting Grade E – Coupler from Lab Coupon Tests	29,896	117.5	202.8	131.9
M201 Steel Casting Grade E – Yoke from Lab Coupon Tests	30,647	118.4	152.5	136.9
M201 Steel Casting Grade E	29,000	100.0	144.9	119.8
ASTM A992 Steel	29,000	50.0	72.1	65.0
ASTM A572 Grade 50	29,000	50.0	72.1	65.0
ASTM A36 Steel	29,000	36.0	96.2	58.0
ASTM A519 Grade 1026	29,000	47.0	82.6	70.0
SAE X-1335 Steel	29,000	44.0	153.5	79.1
SAE 1018, Cold Drawn Steel	29,000	54.0	67.5	64.0
SAE 1045, Seamless Steel Tubing	29,000	45.0	233.5	82.0

5.1.3 Loading

The magnitudes of the applied load were based on levels that could cause rollover (or near-rollover) of a loaded car and levels that can cause failure of the coupler system.

Considering the coupler as a thin-walled, closed section, an estimated torque of 380 kip-ft would result in torsional failure (i.e., yield) at the smallest cross section along the coupler. The coupler would reach its yield strength at this load due to the twist produced by the torque. The hydraulic actuator force corresponding to this torque was estimated to be 85 kips.

Figure 22 shows the bi-linear loading history used in the simulation. The initial high loading rate was used to take up slack in the system and to reduce the amount of time to complete the simulation. It was followed by a lower rate to capture the details of component failures.

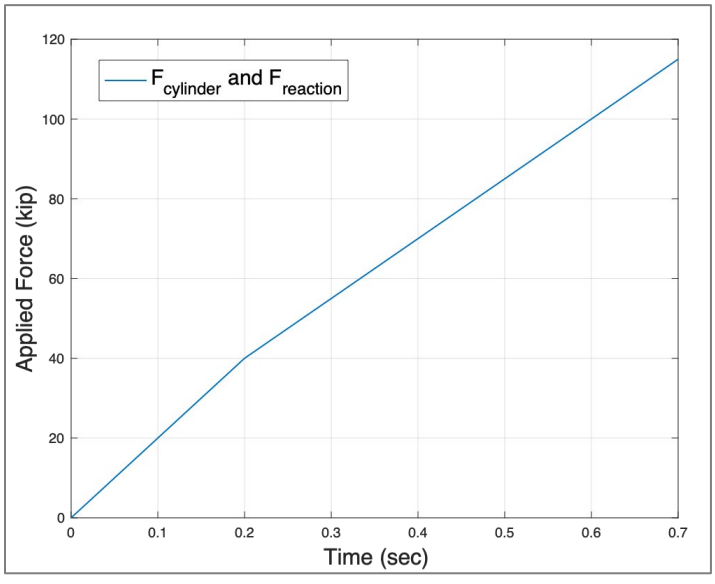

Figure 22. Bi-linear Loading History

5.2 Coupler/Draft Sill System Simulation Results

Investigating the time of first element failure (i.e., material ultimate strength, based on the material failure strain) of critical components of the coupling system shows the contact between components and stress concentration areas.

In Figure 23, the von-Mises stress contour images from the Coupler/Draft Sill System simulation are superimposed onto the loading history.

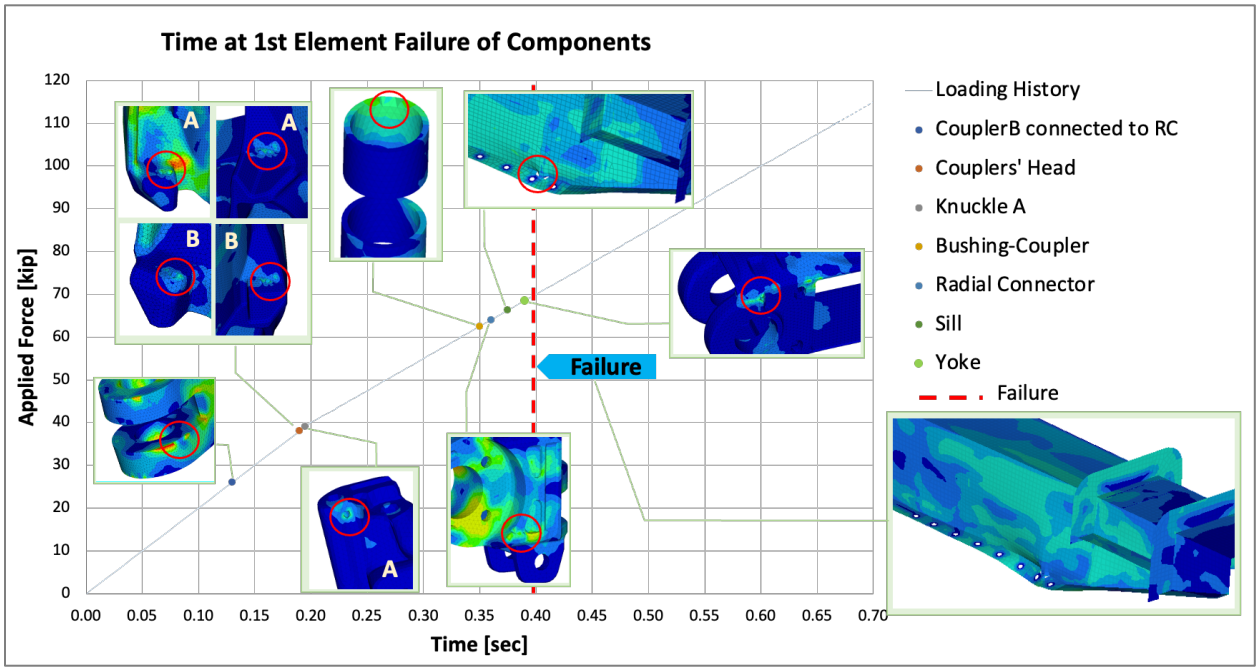

Figure 23. First Element Failures – Coupler/Draft Sill System Model

The elements in the lugs of the test coupler, where it is connected to the radial connector, were the first to fail at 25 kips. Around 40 kips, the elements of both knuckles joining the two couplers started to fail. As the force increased, the radial connector, sill, and yoke reached the failure point one after the other. At 70 kips, the draft sill failed due to widening near the radial connector and yoke.

Figure 24 shows the relationship between the applied torque and the rotation of the lever arm.[4] The trend of this curve represents the overall slipping, yielding and torsional deflection of the system. The curve shows a relatively linear relationship until the inflection point at around 28 degrees, where yielding of the system and widening of the sill became dominant. System failure occurs around 65 degrees of lever arm rotation.

[4] The waviness in this plot and further plots is due to the dynamic effect of the explicit solver that was used for the simulation. The initially higher loading rate (the first part of the bi-linear loading curve) also contributes to this waviness by causing instability/oscillations, which propagates further as the simulation progresses. Another critical factor which influences this waviness is components losing elements beyond their failure strain in the FE simulations, resulting in sudden changes in the angle of rotation.

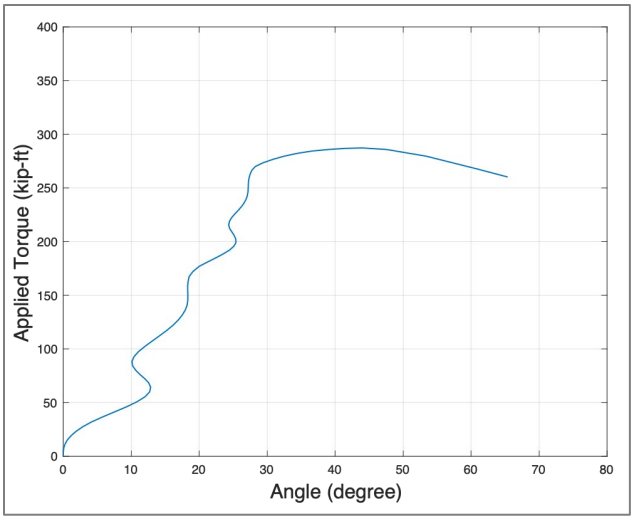

Figure 24. Applied Torque vs. Lever Arm Rotation

Figure 25 and Figure 26 show the relationship between the applied torque and the rotation of the yoke and draft sill, respectively. Figure 26 shows the two reference lines used to measure the rotation of the draft sill.

Figure 27 shows the von-Mises stress contours for the test coupler and draft sill. As seen in this image, when the test coupler reached the maximum stress (at point II in the loading history), the stresses were concentrated on the side of the coupler shank near the connection to the radial connector and distributed on the top and bottom of the coupler at the middle of its shank. The draft sill stress contours show that the coupling system failed due to the increase in width of the draft sill's side plates (at point III in the loading history).

The widening of the sill and the failed bolted connection shown in the results of the coupler/draft sill system simulation indicate that the draft sill itself is the weakest link in the system. As a result, the draft sill widening/failure occurred before significant deformation/failure of the other components.

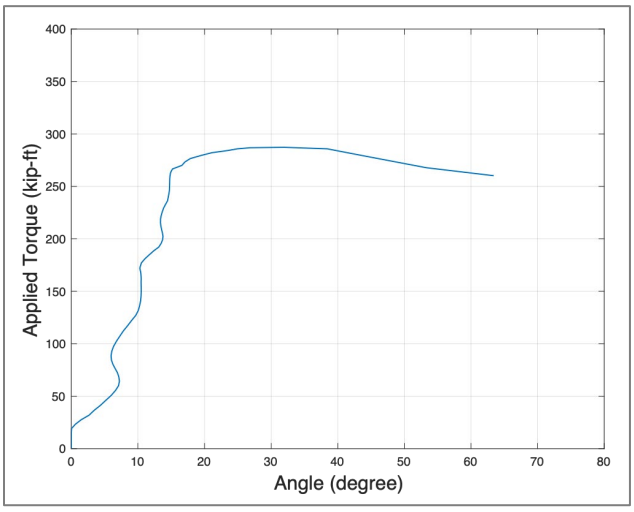

Figure 25. Applied Torque vs. Yoke Rotation

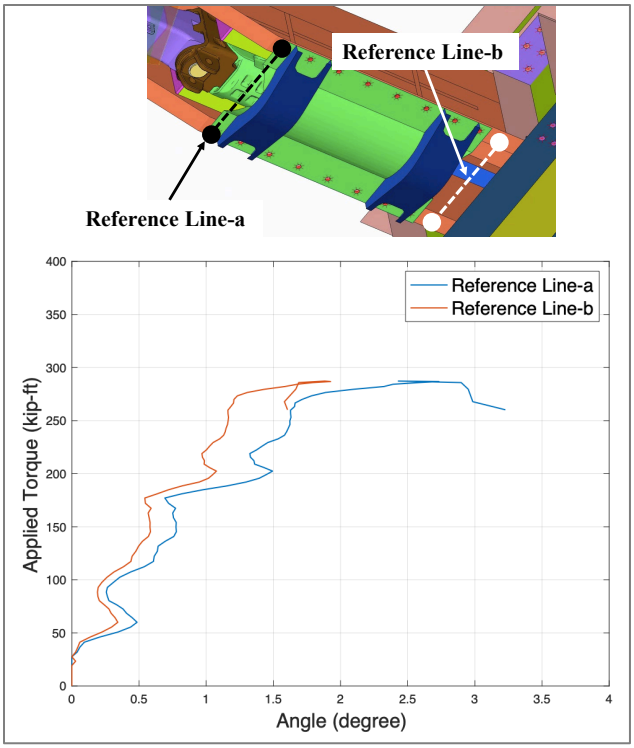

Figure 26. Applied Torque vs. Draft Sill Rotation

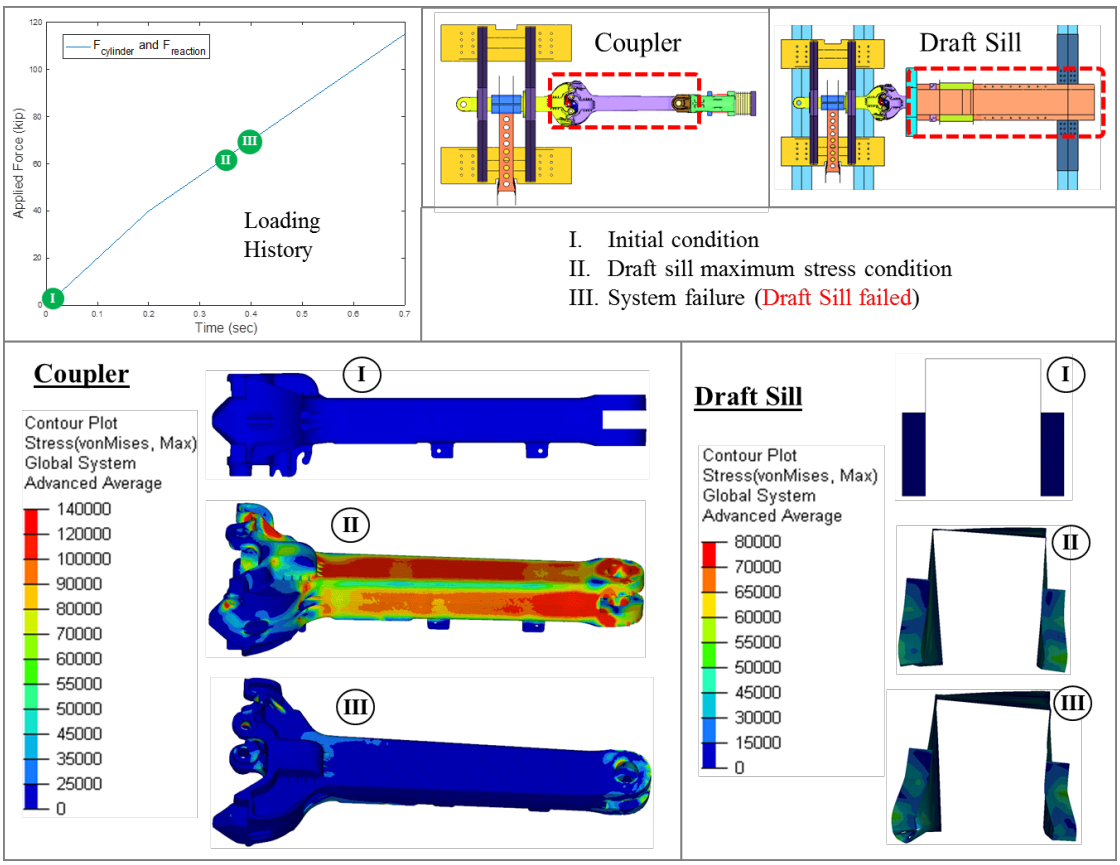

Figure 27. von-Mises Stress Contours - Coupler/Draft Sill System FE Model

5.3 Coupler Failure Simulation Results

Investigating the time of the first element failure (i.e., material ultimate strength, based on the material failure strain) of the critical components of the coupling system shows the contact between components and stress concentration areas. In Figure 28. images from the FE analysis are superimposed onto the loading history.

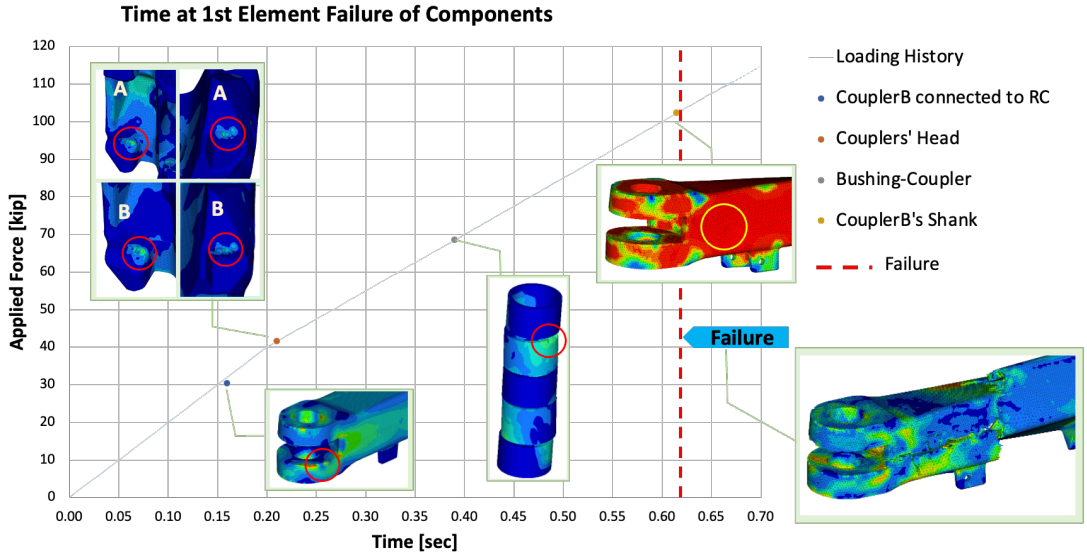

Figure 28. First Element Failure – Coupler Failure Simulation

The elements in the lugs of the test coupler where it is connected to the radial connector were the first to fail at 30 kips. Around 42 kips, the elements of both knuckles joining the two couplers started to fail. Next, the coupler bushing and radial connector reached the failure point, and at 102 kips the coupler shank experienced ultimate failure in torsion.

Figure 29 shows the relationship between the applied torque and the rotation of the lever arm. The curve shows a relatively linear relationship until the point where the coupler starts to yield. The coupler failure occurred around 48.5 degrees of lever arm rotation.

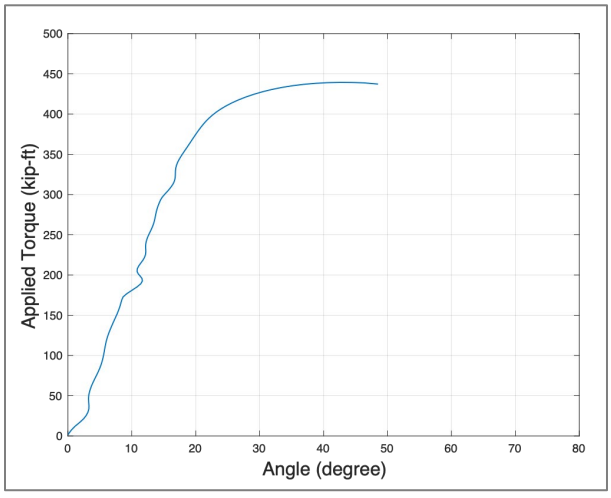

Figure 29. Applied Torque vs. Lever Arm Rotation

Figure 30 shows the von-Mises stress contours for the test coupler at progressive levels of twist. The maximum coupler stress can be observed at point III, directly before the failure. The coupler shank fracture can be seen in the last image (at point IV in the loading history) where the fracture is shown from two side views.

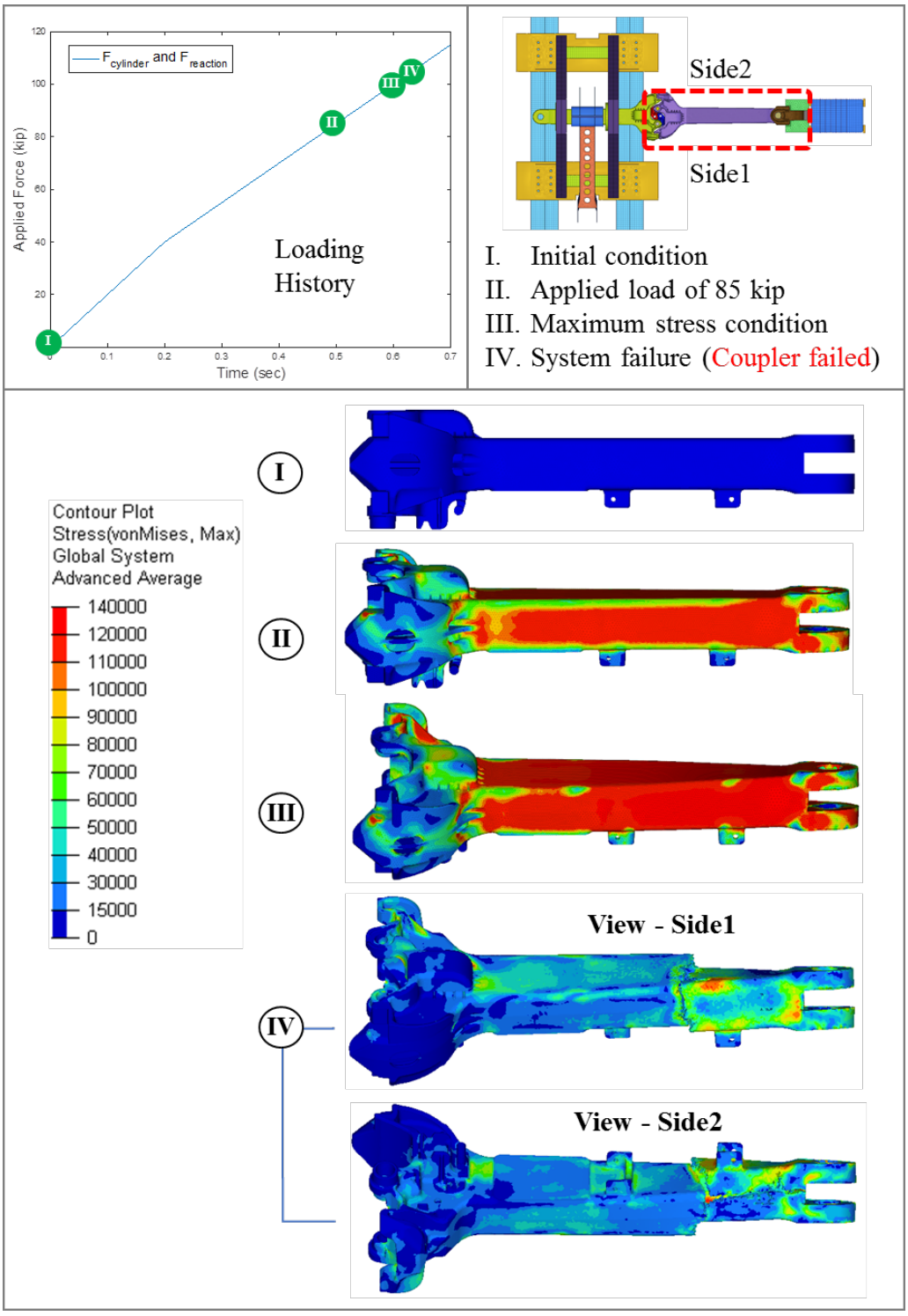

Figure 30. von-Mises Stress Contours - Coupler Failure Model

6. Full-scale Testing

Researchers conducted full-scale testing to study the relationship between applied torque and coupler rotation and to characterize the failure modes of the coupling system. The test results were also used to validate the FE modeling and analysis.

Two types of tests were performed:

- Coupler/Draft Sill System Test
- Coupler Failure Test

6.1 Test Apparatus

The test apparatus consisted of:

- Test fixture and test articles (discussed in Section 3 of this report)
- Hydraulic system
- Instrumentation

6.1.1 Hydraulic System

The hydraulic system consisted of the following components:

- Electric induction pump
- Hydraulic fluid reservoir
- 150-kip double-acting hydraulic actuator with 55 in stroke
- Hydraulic control system
- Flow control valve
- High pressure piping including valves, hoses, couplers, etc.

6.1.2 Video

Four video cameras and two teleconferencing video cameras were used to capture the testing operation from different viewpoints.

6.1.3 Instrumentation

Instrumentation was used to capture and record relevant forces, rotations, deflections, and strains, as described below:

- An Interface, standard, 100-kip capacity load cell (1232-AF-100K) was connected on the extension end of the hydraulic actuator piston to record the force applied to the lever arm.
- Extension of the Parker 2H series hydraulic actuator was recorded using a WaveScale linear displacement transducer integral with the actuator.
- Inclinometers were applied to the actuating coupler and to the coupling end of the draft sill to measure rotation angles.

- Strain gauges were applied to the test coupler and the draft sill to measure strains and for comparison with the FE simulation results. The stress contours from the FE model were used to select appropriate locations for the strain gages. The team selected locations close to areas of interest but far enough away from steep strain gradients.

Figure 31 shows the Somat e-DAQ lite data acquisition system used in the testing. The sample rate was 100 samples/second with a 33 Hz filter on the strain and displacement channels and a 15 Hz filter on the force and tilt channels.

Figure 31. Data Acquisition System

6.1.3.1 Instrumentation for the Coupler/Draft Sill System Test

Eight displacement sensors (i.e., string potentiometers) were attached along the draft sill lower flange to measure draft sill deflection. Two were also applied horizontally on the draft sill web at a location expected to have the most deflection. Figure 32 shows the deflection measurement locations for the Coupler/Draft Sill System Test.

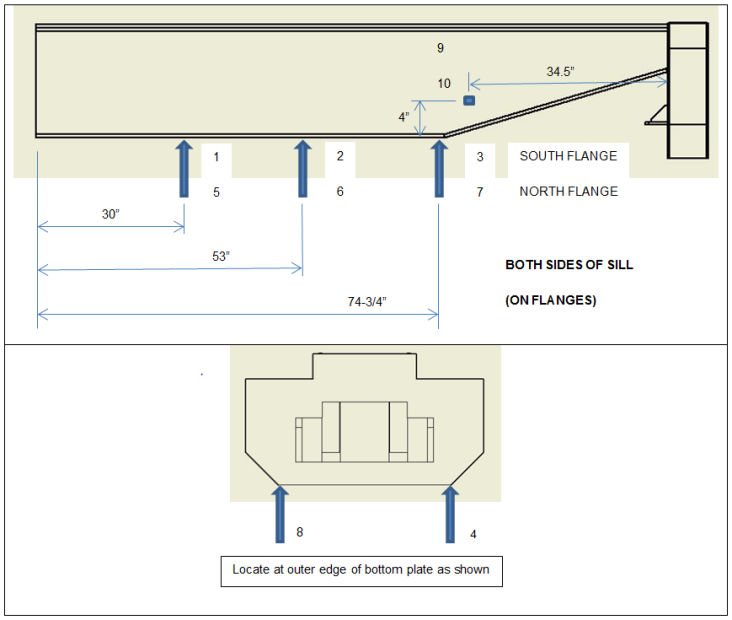

Figure 32. Displacement Sensors on Draft Sill – Coupler/Draft Sill System Test

Figure 33 shows the locations of the strain gauges on the coupler. The same locations and orientations were used in both the Coupler/Draft Sill System Test and the Coupler Failure Tests.

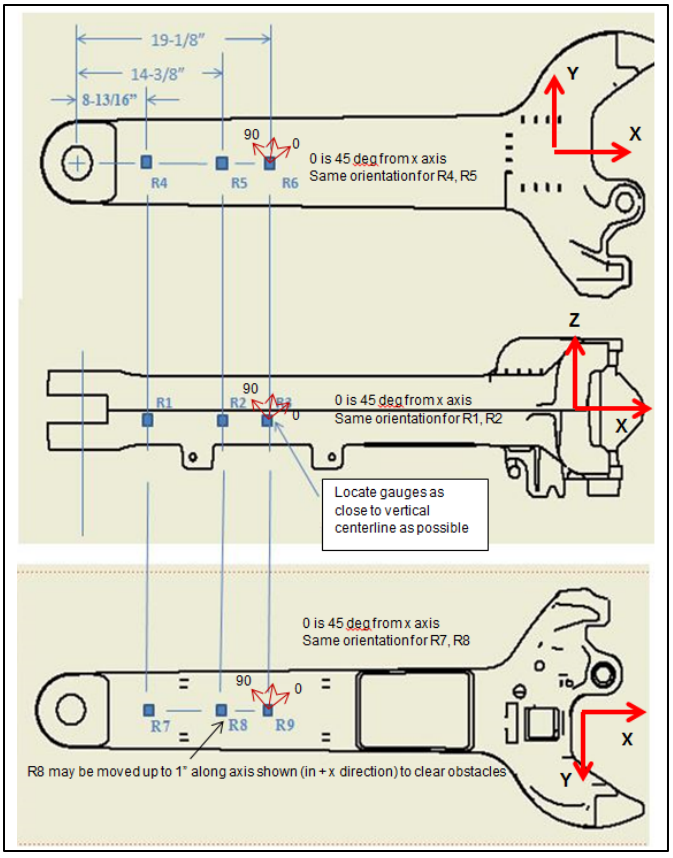

Figure 33. Locations of Strain Gages on Coupler

Figure 34 shows the locations of the strain gauges on the draft sill for the Coupler/Draft Sill System Test.

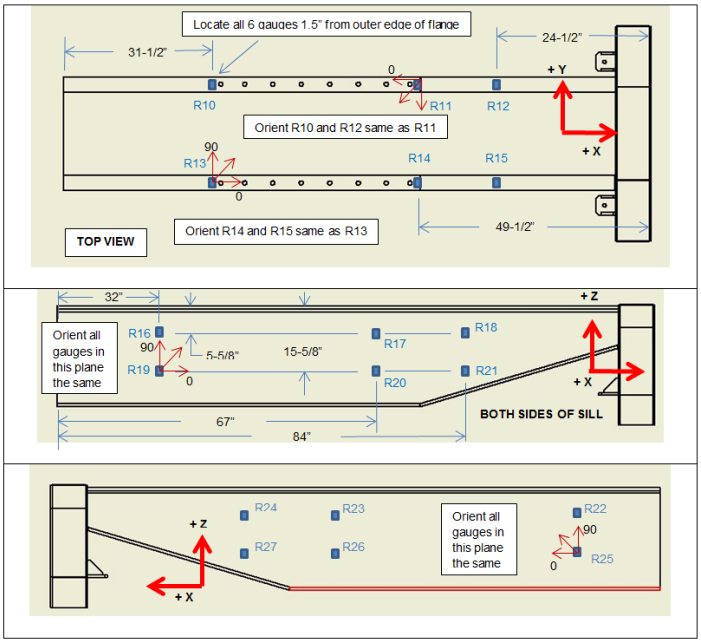

Figure 34. Strain Gage locations on Draft Sill

6.1.3.2 Instrumentation for the Coupler Failure Test

Figure 35 shows a simpler arrangement of displacement transducers used for the Coupler Failure Test.

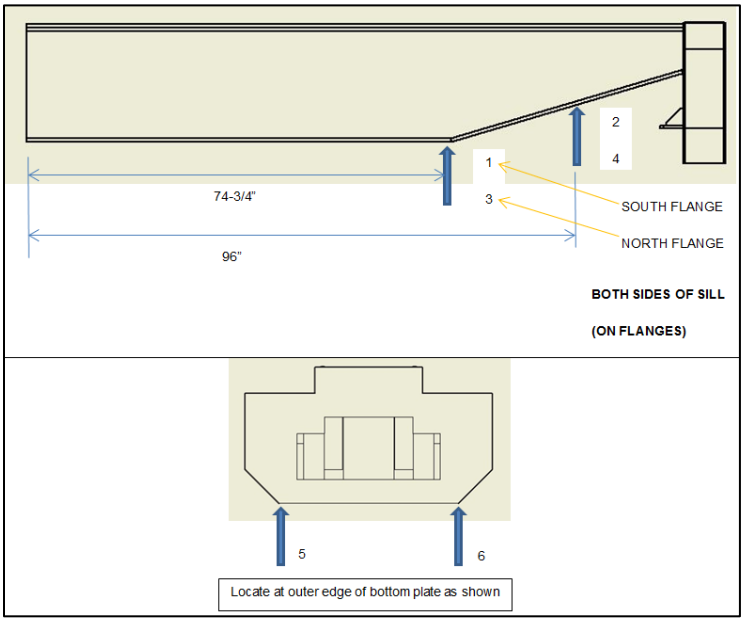

Figure 35. Displacement Transducer Locations – Coupler Failure Test

Figure 36 shows the location of tilt sensors installed on the coupler for the Coupler Failure Test. These allowed the twist in the coupler shank to be measured.

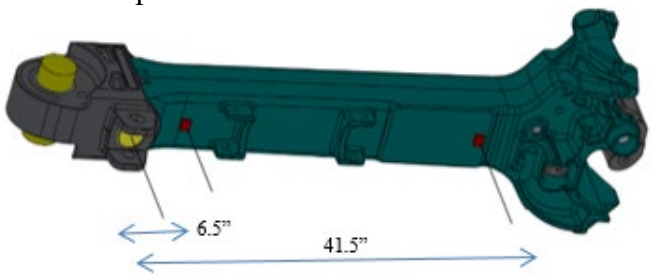

Figure 36. Tilt Sensor Locations – Coupler Failure Test

Four additional displacement transducers were positioned on the coupler for the coupler failure test as a backup to obtain deflections in case the tilt sensors failed. Figure 37 shows the locations of these additional transducers.

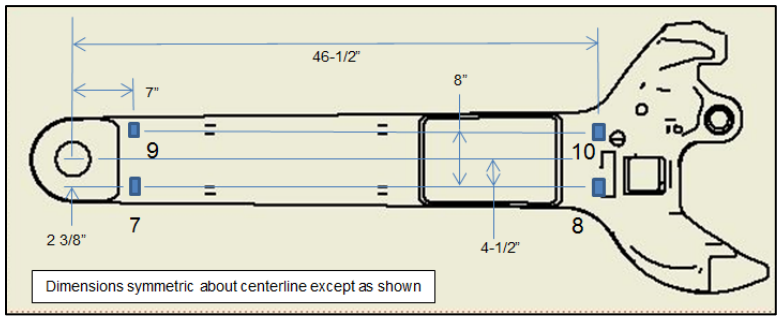

Figure 37. Additional Displacement Transducers – Coupler Failure Test

Figure 38 shows the locations of the strain gauges on the coupler. These are the same locations and orientations used in both the Coupler/Draft Sill System and the Coupler Failure Tests.

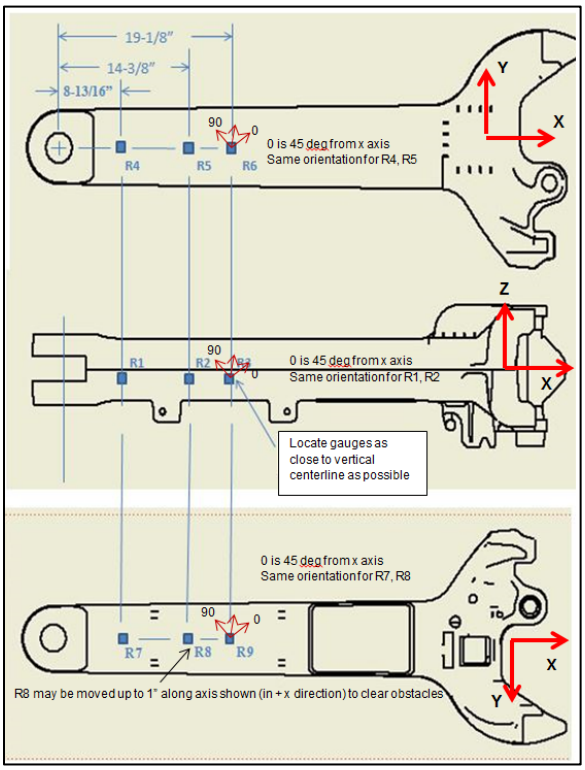

Figure 38. Locations of Strain Gages on Coupler

Strain gages on the sill were reduced to 6 rosettes for the Coupler Failure Test. Figure 39 shows their locations. These gauges were used only to monitor the sill's integrity during the test.

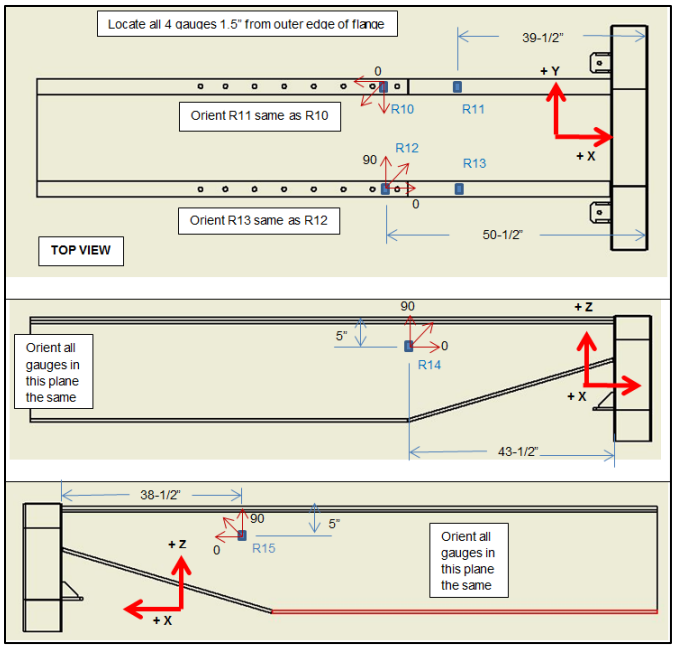

Figure 39. Draft Sill Rosette Gauge Locations – Coupler Failure Test

6.2 Coupler/Draft Sill System Testing

The MTS hydraulic control system was used to gradually increase actuator force. Initially, 2-kip increments were used (up to 30 kips), then 1-kip increments were used to capture events as failure was approached. Load cell actuator force data was fed into the MTS to control the actuator extension and the system recorded actuator force and extension.

Researchers measured the cylinder force data and lever arm angle at each load step. Figure 40 shows the relationship between applied cylinder force and actuating coupler rotation in the Coupler/Draft Sill System Test. The resulting torque values were calculated and plotted against the angle of rotation, as shown in Figure 41.

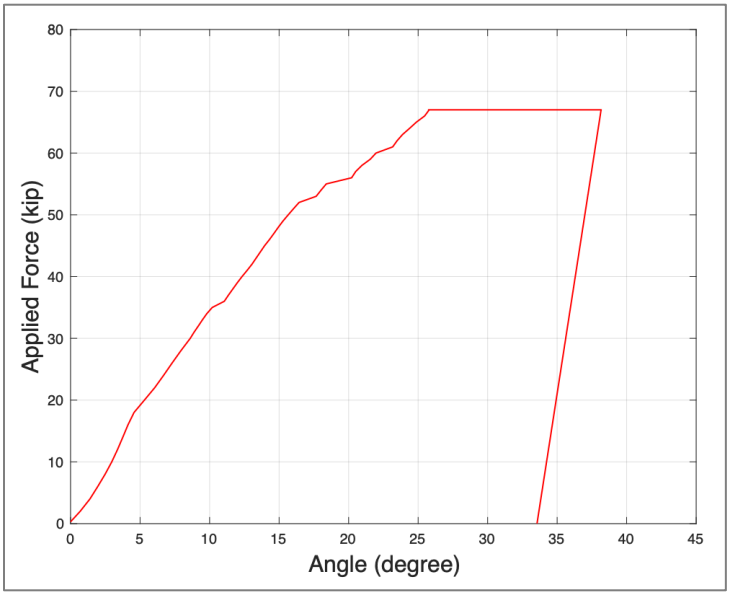

Figure 40. Applied Force vs. Actuating Coupler Rotation - Coupler/Draft Sill System Test

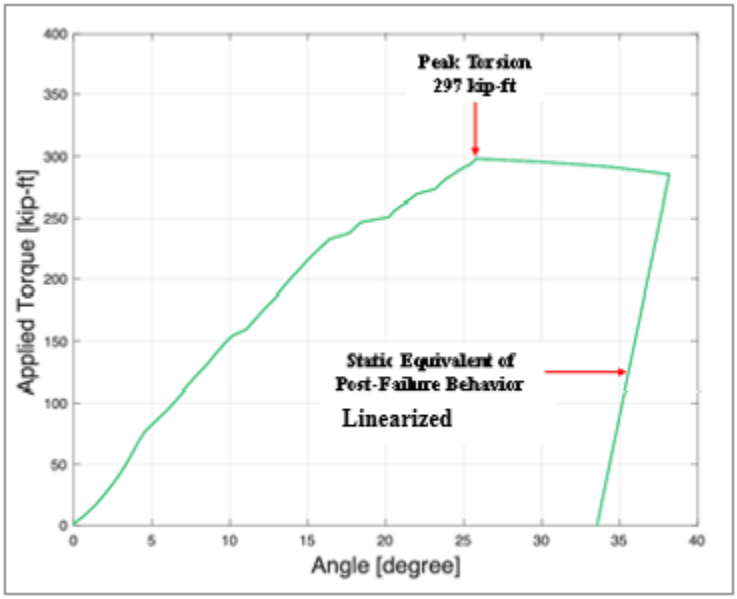

Figure 41. Applied Torque vs. Actuating Coupler Rotation – Coupler/Draft Sill System Test

As the load on the lever arm increased, researchers observed changes in strain and deflection of all measured components. Figure 40 shows the actuating coupler rotation continued to increase almost linearly until a force of 67 kips was reached at a rotation of 25.5 degrees. This was the point when the draft sill assembly failed. After this point, the angle increased to approximately 38 degrees with no corresponding increase in force. This maximum force equates to a torque of 297 kip-ft and represents the draft sill system capacity, as shown in Figure 41.

Inspection of the test coupling system after failure showed that widening of the draft sill forced a shearing and separating action on the connection of the draft sill to the carrier assembly. The draft sill assembly failed by the shearing of four bolts along one of its flanges and plastic deformation of the sill's webs, flanges, and other interior reinforcement structures. The bolts that failed were among the 16 fasteners used to connect the draft gear retaining plate to the draft sill. Figure 42 through Figure 44 show photos of the failures.

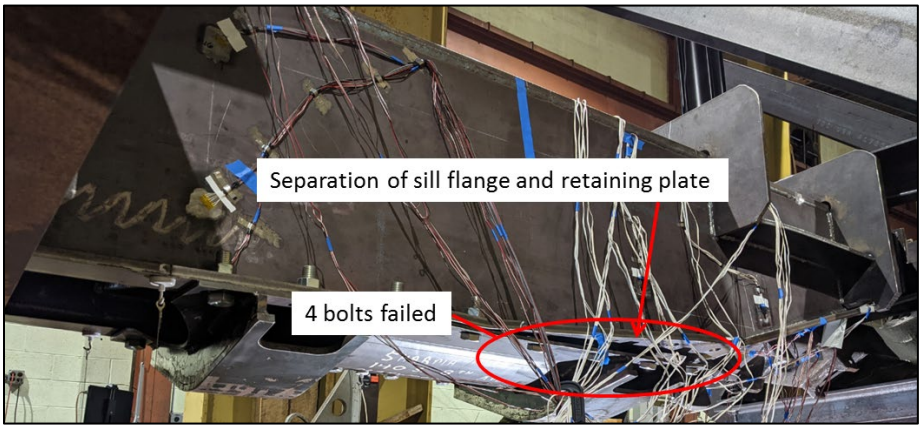

Figure 42. Draft Sill and Bolt Failure – View 1

Figure 43. Draft Sill and Bolt Failure – View 2

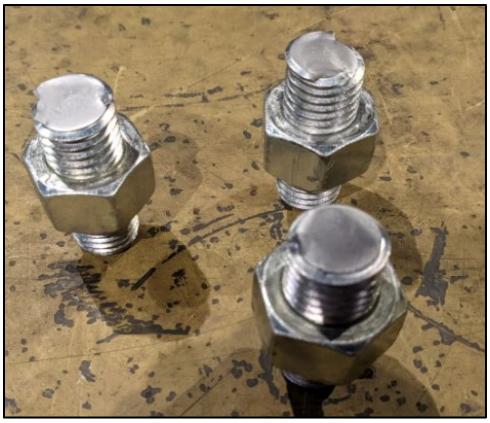

Figure 44. Shear Failure of Bolts

Figure 45 shows that all the holes used to connect the retaining plate to the draft sill flange experienced various amounts of elongation.

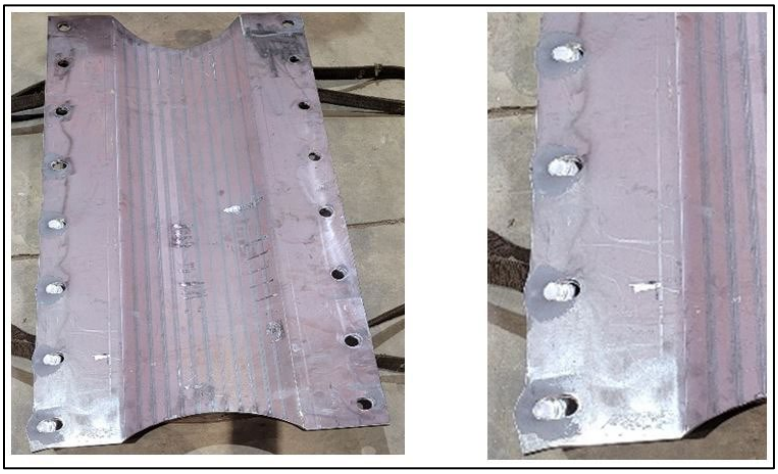

Figure 45. Hole Elongation on Retainer Plate

Figure 46 and Figure 47 show the contacts made between the draft gear, radial connector, and follower block and the draft sill after failure. The yoke had grabbed on to one of the draft sill's longitudinal stiffeners and deformed it. The radial connector had also dug into the draft stops of the draft sill.

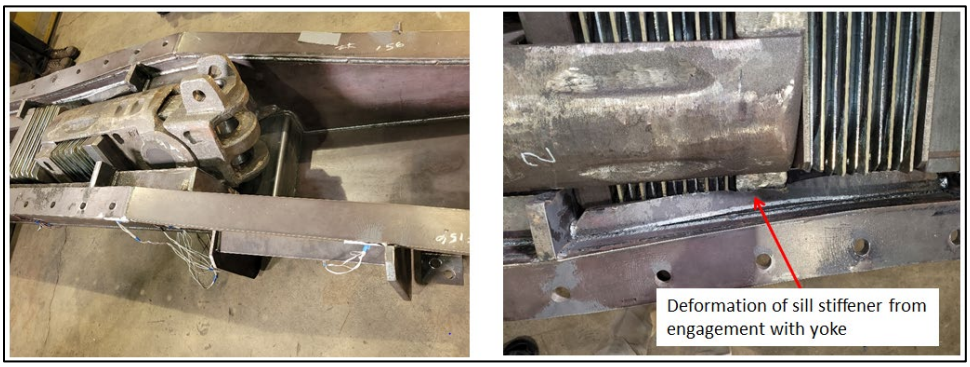

Figure 46. Post Test After Disassembly – View 1

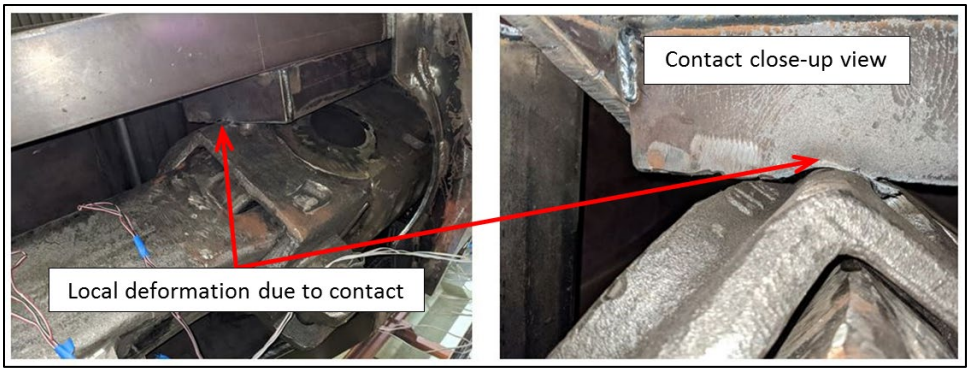

Figure 47. Post Test After Disassembly – View 2

Figure 48 is a post-test view of the test coupler engagement and rotation. A 1-degree permanent twist of the test coupler was measured after removal from the test fixture.

Figure 48. Rotation of Couplers – Post Test

Figure 49 shows the underside of the coupler after the test. The strains from the gauges on the coupler indicated stresses would be at or (in some small local areas) beyond yield. No measurable deformation occurred to the radial connector or yoke.

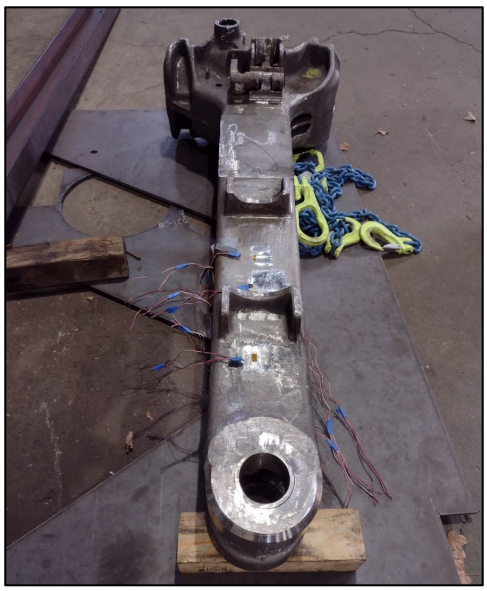

Figure 49. Test Coupler Underside - Post Test

From these results, the team estimated that the stress state at peak load on the test coupler was independent of the coupler/draft sill system failure mode. In other words, based on the load path, the stresses on the coupler would have been similar even if the system had taken the coupler failure path.

The permanent structural twist and permanent widening of the draft sill was observed from hand measurements, displacement transducers, and strain gauges. Sizeable areas on the draft sill experienced deformation well into the plastic range. Appendix A provides additional details of the manual measurements made of the draft sill width at several locations of interest.

No measurable permanent deformation of the actuating coupler assembly occurred. The test fixture also survived with no noticeable permanent deformations, except for local permanent deformation of the channel supporting the coupler head end of the draft sill (this channel was used to roughly simulate the draft sill connection to a car floor structure).

The draft sill failure (as opposed to coupler failure) is most likely due to the AAR grade E cast components comprising the items inside the draft sill, which have a much higher strength and hardness than the A572 grade 50 steel used in the fabrication of the draft sill. This difference and the higher material thicknesses of the draft components inside the sill forced its deformation and failure.

6.3 Coupler Failure Testing

Draft sill widening and sheared bolts were the mode of failure in the Coupler/Draft Sill System Test described in Section 6.2, which was intended to result in failure of the coupler. Two coupler specimens were tested: a stepped ramped loading of the applied torque was used for the first specimen and a continuous ramped loading was applied for the second specimen.

For the first test specimen, the actuator force was gradually increased in 5-kip increments to 65 kips. It was then increased in 2-kip increments to 84 kips. Finally, 1-kip increments were added until failure occurred. The final, smaller 1-kip load increments allowed the events to be captured accurately as failure was approaching.

A continuous ramped loading was used for the second test specimen. This specimen was previously used in the Coupler/Draft Sill System Test and remained undamaged from that test except for a 1-degree permanent twist. This coupler specimen was used to evaluate a scenario where the coupling system would experience torsional loading in a derailment causing a draft sill failure and subsequent loading and failure of the coupler.

The two couplers were tested sequentially. In both tests, as the cylinder force was gradually applied, the strains and the angle of coupler rotation increased. The twist of the test coupler shank increased with the applied torque as shown by the difference in the front and rear tilt sensors.

Figure 50 shows photos of the first coupler after it failed. Three visible cracks formed during the failure. The first crack appeared at approximately 84 kips of actuator force (375 kip-ft. of torque on the test coupler), corresponding to an actuating coupler rotation of approximately 15 degrees and a test coupler twist of 5 degrees. The crack was seen from video taken of the test and occurred on the right side of the shank near the rear lugs. The largest crack extended across the top of the test coupler at about a 45-degree angle and down both sides of the shank near the rear lugs. Cracks also formed laterally along the lug radii.

The cracks propagated until the applied force automatically shut off at an actuator force of 87 kips (391 kip-ft of torque) corresponding to an actuating coupler angle of 17 degrees. The automatic shut off was accomplished by a trip switch based on absolute error between the measured and applied load.

Figure 51 shows photos of the cracks in the second coupler. Cracks started at the sides of the coupler shank at an applied force of approximately 79 kips (351 kip-ft. of torque), progressed across the top of the coupler shank, and then joined. A branch crack then propagated longitudinally along the shank toward the coupler head.

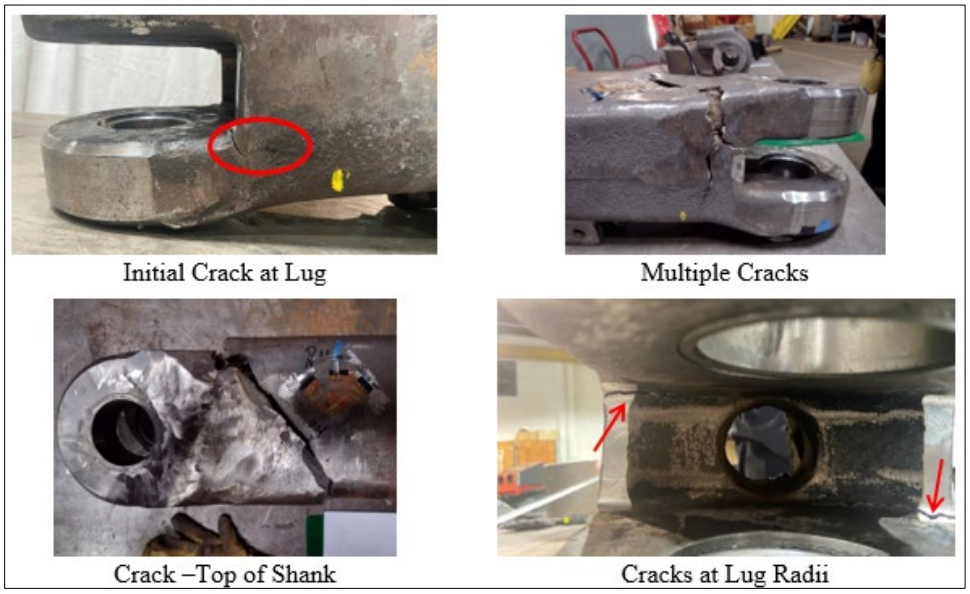

Figure 50. Crack Locations – Coupler Failure Test Specimen 1

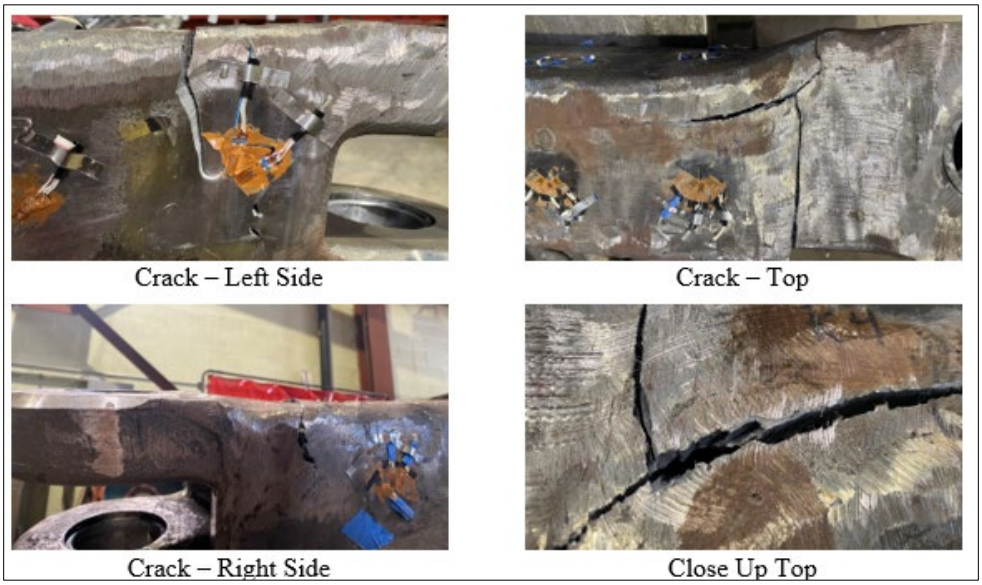

Figure 51. Crack Locations – Coupler Failure Test Specimen 2

Appendix B provides details of the strain gauge data recorded in the Coupler Failure Tests. The strain results agree well with the nature of the crack propagation. Gauges near the crack initiation

site started showing higher strains first and reached higher levels than the gauges away from the failure. Overlays of the von-Mises stresses obtained from the gauges on the FE modeling results also showed very good correlation.

Figure 52 shows the relationship between applied torque and rotation for the Coupler/Draft Sill System Test and the two Coupler Failure Tests. Angular deflection in the Coupler/Draft Sill System Test reached approximately 38 degrees compared to a maximum of approximately 24 degrees in the Coupler Failure Tests. Angular deflection curves are steeper (i.e., more rigid in torsion) in the Coupler Failure Tests than in the Coupler/Draft Sill System Test. This was expected since the test fixture was stiffened to encourage the coupler shanks to fail. In addition, the support location of the draft sill was moved forward closer to the coupler. The coupler is inherently stiffer in torsion than the overall draft sill system.

The second coupler specimen failed at a lower moment (351 kip-ft.) than the first coupler specimen (390 kip-ft.). This was due to the thinner wall of the second coupler (0.40 in) specimen compared to that of the first specimen (0.68 in).

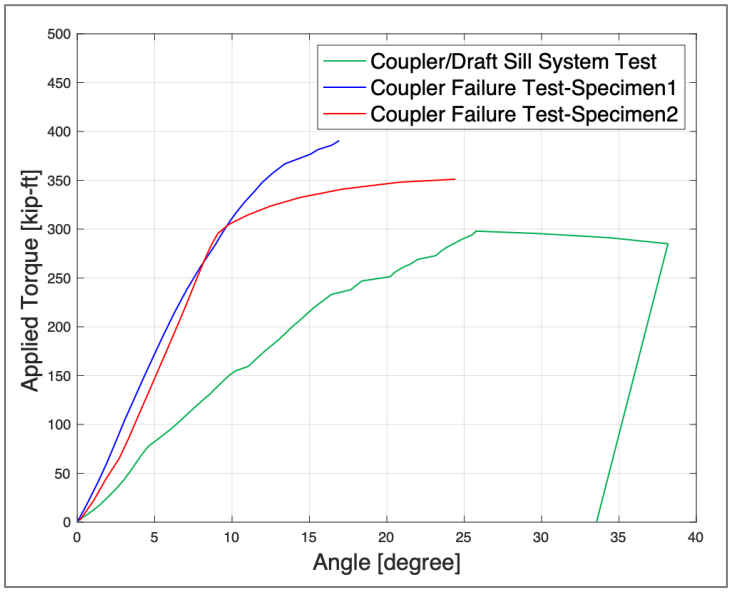

Figure 52. Torque vs. Rotation for all Tests Results

6.4 Test Summary

The test effort described in this chapter characterized two modes of failure for the system, a draft sill failure mode and a coupler failure mode. These two modes reasonably bookend the torsional performance of the coupler system, with draft sill failure occurring at about 297 kip-ft of torsional moment, and coupler failure occurring at about 390 kip-ft of torsional moment.

Classical rollover calculations (see Appendix C) suggest that even the lower of the two capacities measured (297 ft-kips) would rollover an individual passenger car. The effects of such a loading on a string of cars would require additional modeling that is outside the scope of this work, and the team recommends that this work be conducted as part of future research.

7. Comparison Between Test and FEA Results

7.1 Coupler/Draft Sill System: Test vs. FEA

Overall, the FE simulation results and the test results showed reasonable correlation. The red line in Figure 53 shows the applied torque-rotation relationship measured in the Coupler/Draft Sill System Test overlaid with the results from the FE modeling (blue line). The relationship was approximately linear until the draft sill failed.

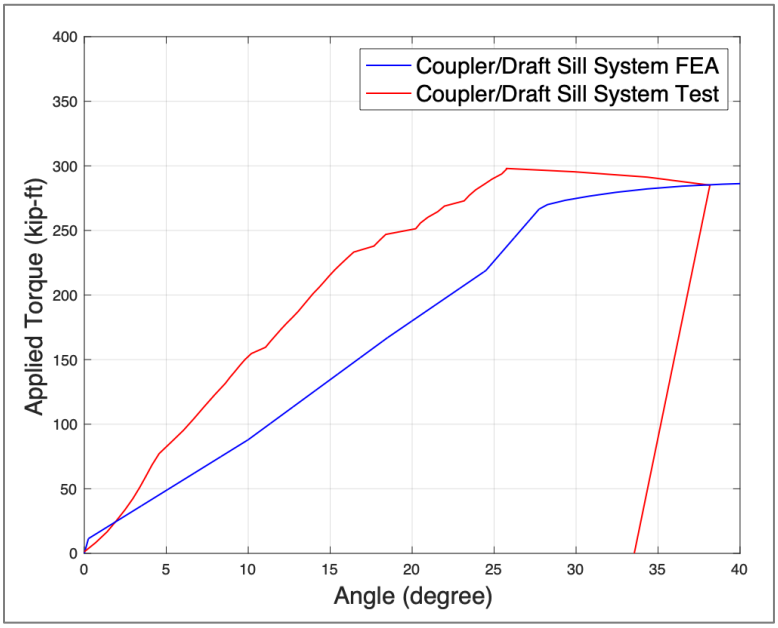

Figure 53. Coupler Rotation vs. Applied Torque Comparison

Figure 54 shows the front part of the draft sill in the area where the failure occurred. The FE image is a contour plot of von-Mises stress showing stresses around the yield point. The amount of coupler rotation is similar, as seen in both images.

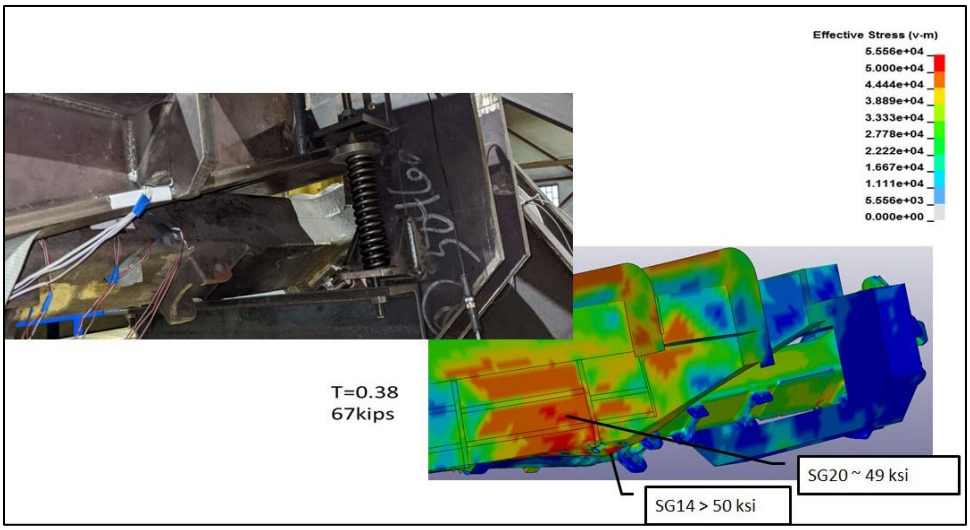

Figure 54. Comparison – Draft Sill and Coupler Rotation

Figure 55 shows the contact between the radial connector and the draft stops after failure, when the corner of the radial connector dug into the draft stop. The same condition can be observed in the FE model.

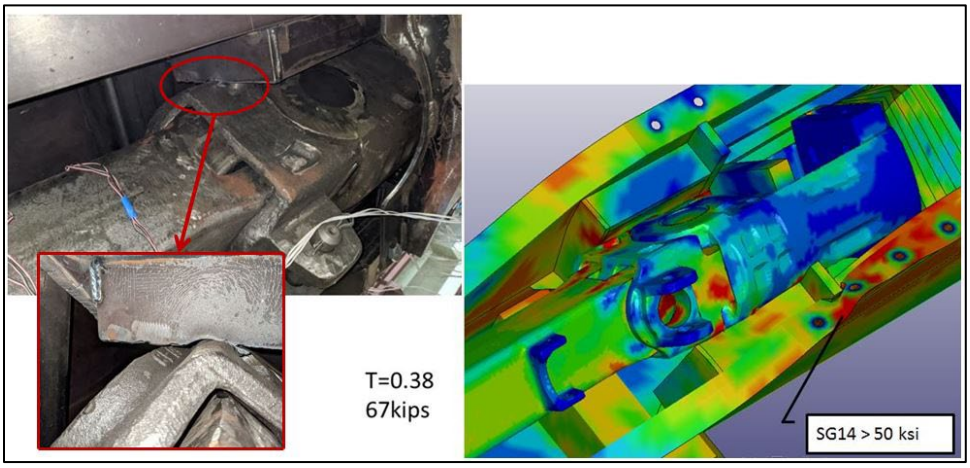

Figure 55. Radial Connector and Yoke Inside Draft Sill Contact Comparison

Figure 56 shows a comparison of the interaction of the yoke with the longitudinal stiffener inside the draft sill in the test and in the FE Model. In the Coupler/Draft Sill System Test, the end of the yoke contacted the stiffener and deformed it upward. The FE Model did not predict this as there was adequate nominal clearance. Part and assembly manufacturing tolerances and deformations from the forces applied during rotation could be responsible for the differences between test and modeling.

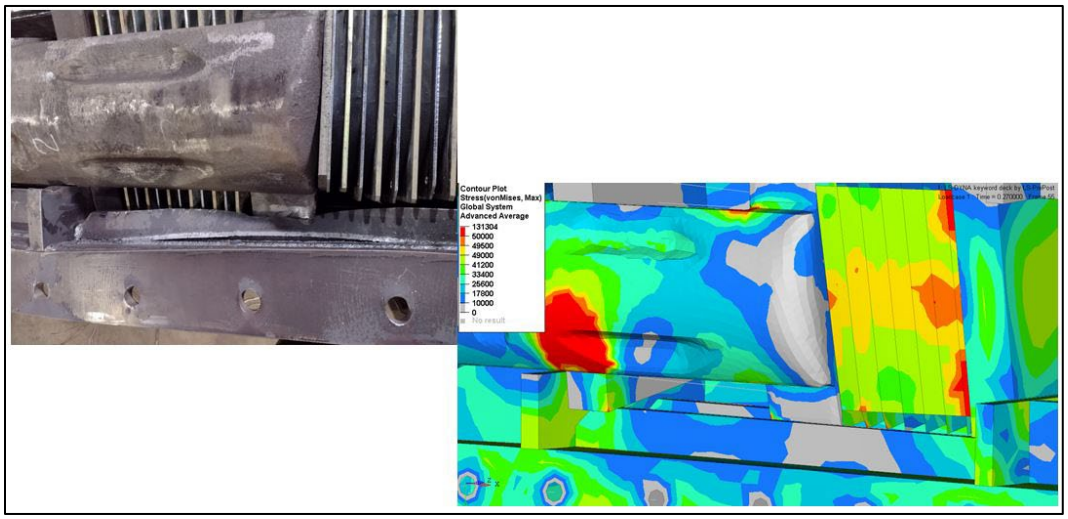

Figure 56. Yoke and Draft Gear Inside Sill Contact Comparison

Figure 57 compares the deformation where the bolt failed (as seen after the test) with that from the FE Model. Deformation of the sill flange is shown to be similar between the test and the FE modeling. Failure of the fasteners was not explicitly captured by the FE Model since the bolts were modeled as beam elements.

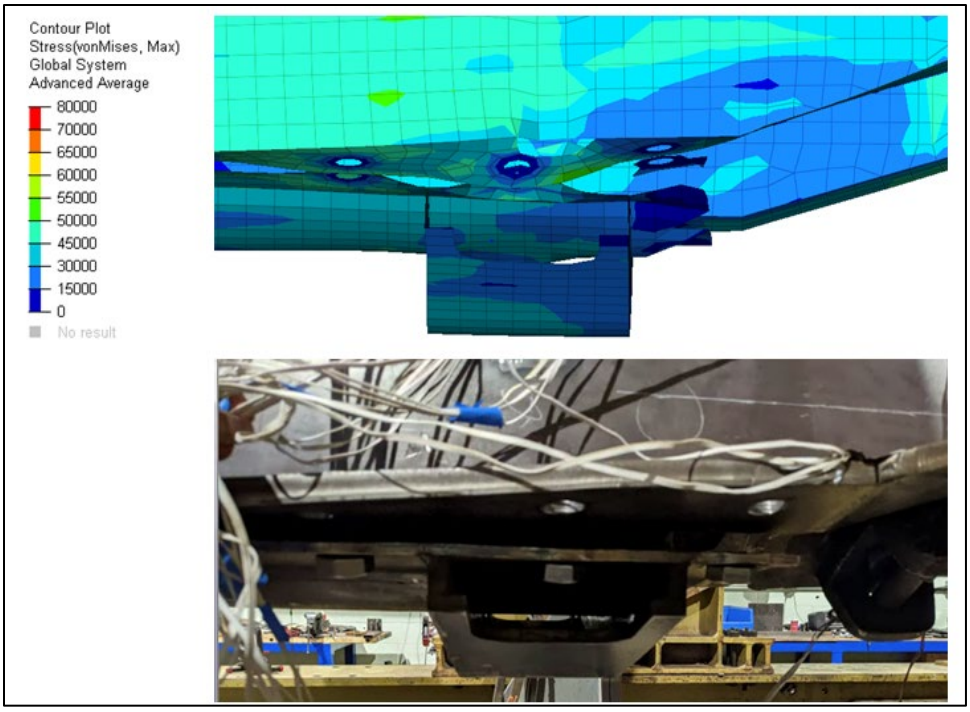

Figure 57. Area of Bolt Failure Deformation Comparison

Figure 58 shows three points of progressive failure on the curve of yoke rotation vs. applied torque. The photo on the top shows the area of interest from the full-scale test; the images from the FE simulation on the bottom (identified as 1, 2, and 3) show the corresponding conditions of the draft sill and retainer plate at the same moments.

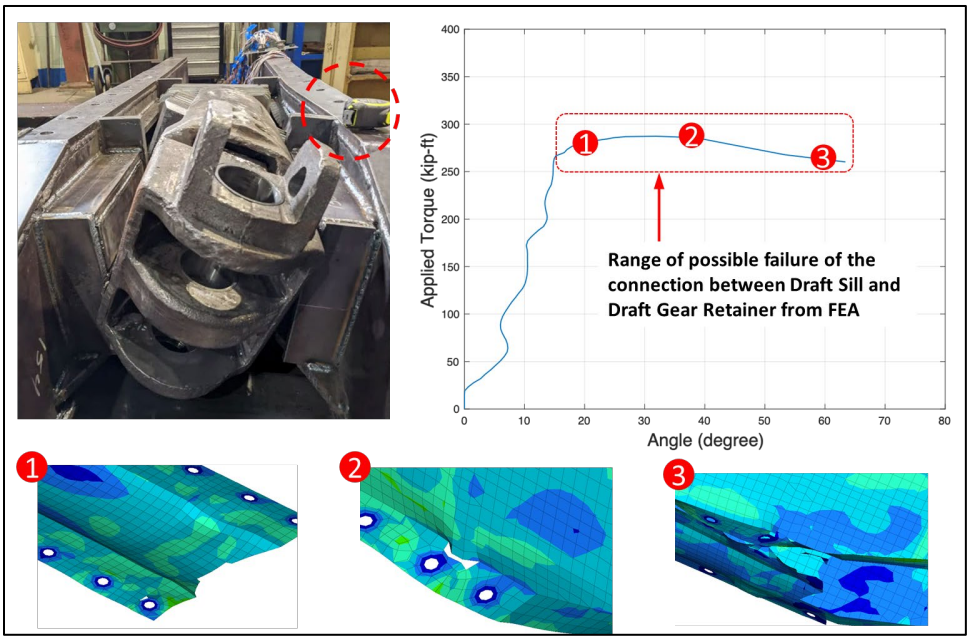

Figure 58. Progressive Failure of Draft Sill Comparison

Figure 59 shows a comparison of the draft sill displacements measured in the Coupler/Draft Sill System Test with those from the FE Model. As expected, displacement transducer 8 (DT8) had

the highest positive displacement in the FE modeling due to the direction of rotation imposed on the sill and it being the transducer farthest from the sill center support. DT4 correspondingly shows the greatest negative value. The displacements were similar in the physical test.

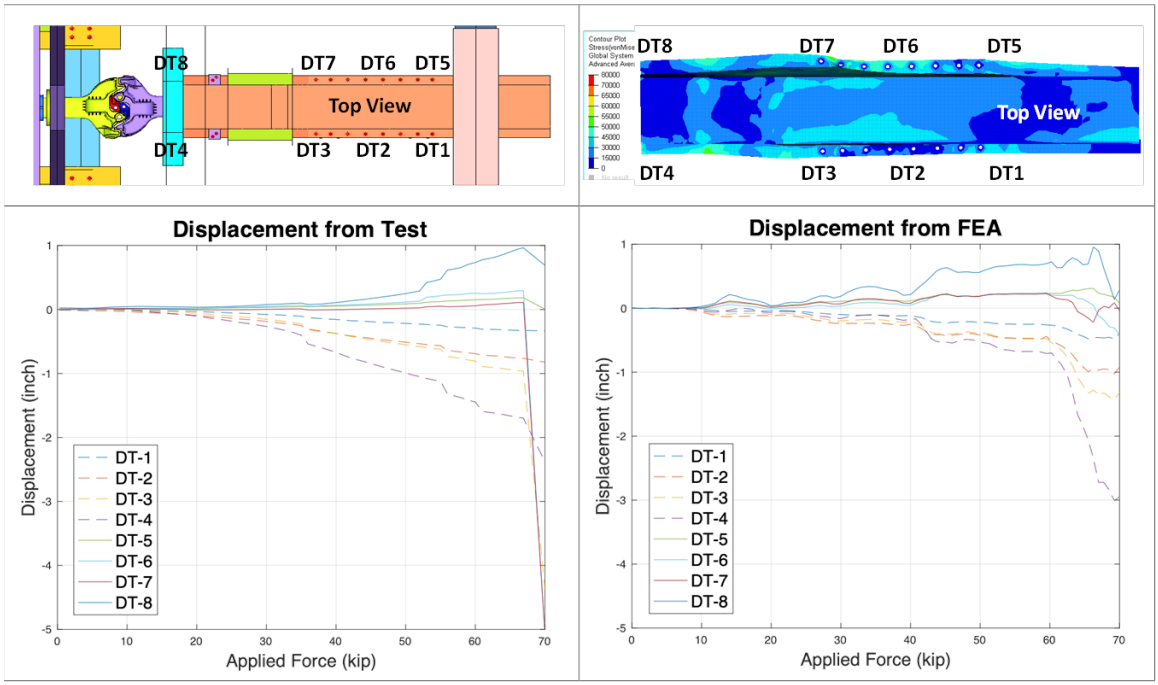

Figure 59. Draft Sill Displacement Comparison

Figure 60 shows a comparison of measurements made on the draft sill weldment after the test to those from the FE Model. The measured widening of the sill at its maximum point along its length is slightly higher than that predicted by the FE model.

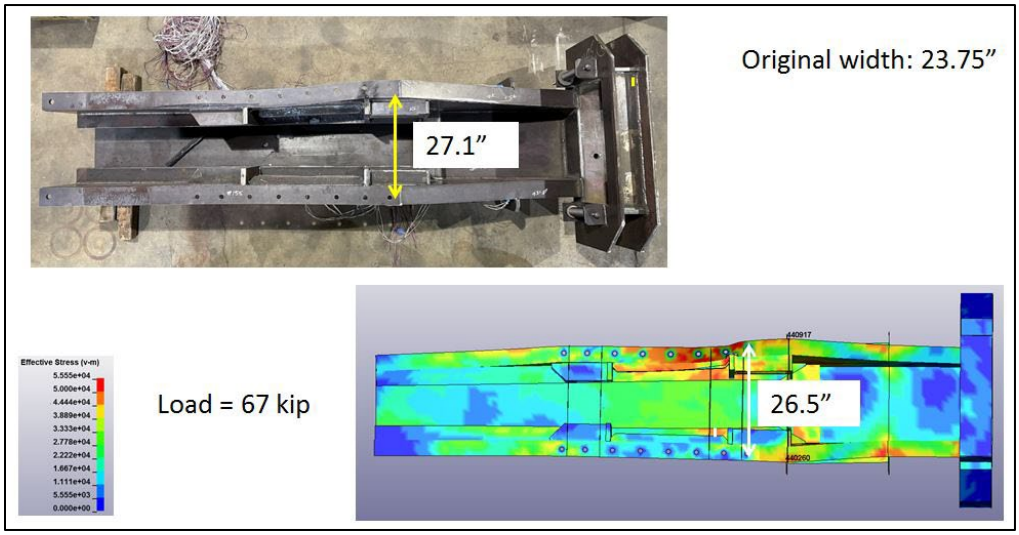

Figure 60. Draft Sill Deformed Width Comparison

Figure 61 shows a comparison of the cross-channel connection deformation to the sill seen in the Coupler/Draft Sill System Tests with that from the FE model. As seen in the figure, the results are very similar between the FE modeling and the test.

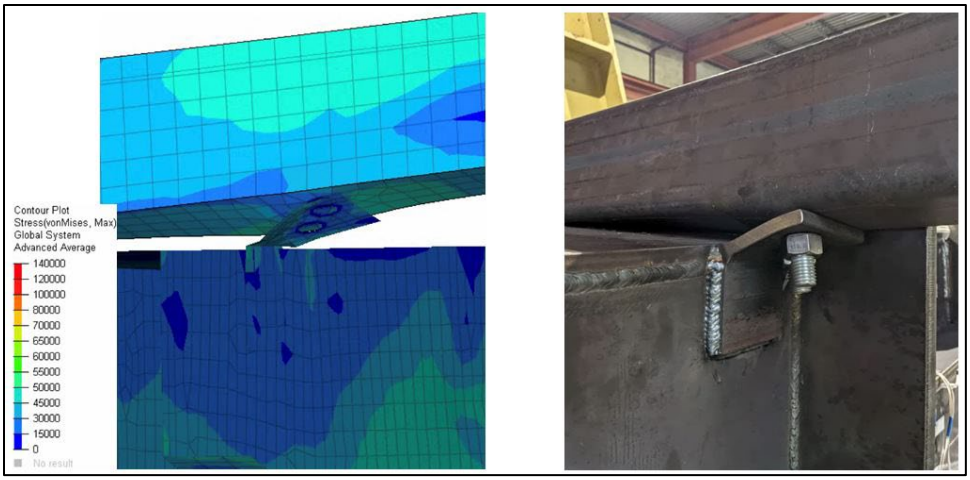

Figure 61. Cross-Channel Connection Deformation Comparison

7.2 Coupler Failure Test/FEA

Figure 62 depicts a comparison of the torsional deflection results from the two Coupler Failure Tests to those from the FE model in its original form ($FEA_{pre\text{-}test}$) and as modified post-test ($FEA_{post\text{-}test}$). The modified FE model geometry was based on the first specimen of the Coupler Failure Test. There is reasonable agreement in the shapes of the curves. However, the FE models show rotation of more than 30 degrees at failure compared to the test specimens that failed at 17 and 25 degrees. The test results show slightly higher torsional stiffness in the linear portions than the FE model predictions. This difference is most likely a result of differences in gap locations and sizes between the FE model and the test assembly, local element failure in areas away from the fracture location, and differences in the actual material properties from those in the FE model. In the coupling system, the torsional stiffness is affected by not only the coupler itself, but also the component connections.

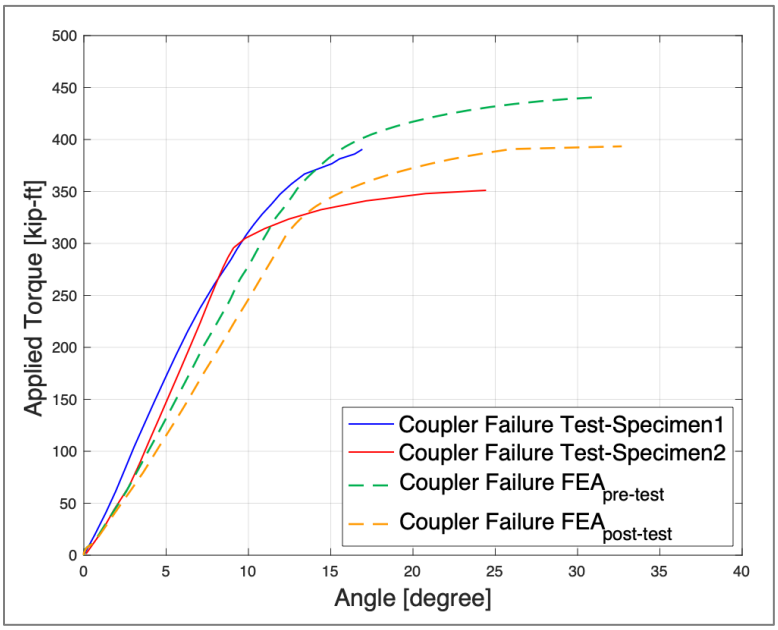

Figure 62. Coupler Failure Torsional Deflection Comparison

Figure 63 shows a comparison of the twist in the coupler shank measured in the two Coupler Failure Tests to those from the FE model in its original form and as modified post-test. The second specimen exhibited greater twist than the first since it had thinner coupler shank walls in some areas.

For both test specimens, the torsional stiffness of the test coupler shank was the same as that from the FE models in the linear portion but was slightly lower in the non-linear portion of the curve. The predicted twist from $FEA_{post\text{-}test}$ model falls between the results of the two Coupler Failure Test specimens.

Table 7 provides a summary of the torque and deflection results from the coupler failure tests. Table 8 shows a summary of the basic system capacity data obtained from all the tests.

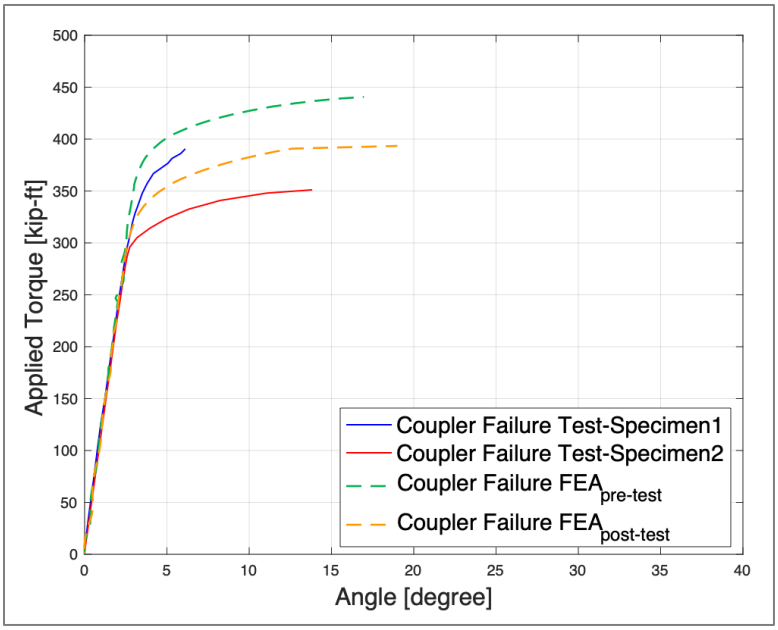

Figure 63. Coupler Shank Twist Comparison

Table 7. Torque-Deflection Summary – Coupler Failure Test

Specimen	Torque (kip-ft)	Coupler Shank Twist Angle (deg.)	Actuation Coupler Angle (deg.)
1	390	6.1	16.9
2	351	13.8	24.4
Average	371	10.0	20.7

Table 8. Coupling System Capacity Summary

Test	Initial Failure Torque (kip-ft)	Initial Failure Actuating Coupler Angle (deg.)	Ultimate Failure Torque (kip-ft)	Ultimate Failure Actuating Coupler Angle (deg.)
Coupler/draft sill system	160 [5]	11.1 [5]	297	25.8
Coupler Failure Specimen-1	375 [6]	15.0 [6]	390	16.9
Coupler Failure Specimen-2	310 [6]	10.5 [6]	351	24.4

[5] Measured at the time of draft sill flange yield

[6] Measured at the time of coupler crack initiation

8. Conclusions

A research team performed analyses and testing of H-type coupling systems to determine the relationship between the applied coupler torque and resulting rotation of the systems; the torsional system capacity at failure was also obtained. The team found that for this draft sill system design, draft sill widening and bolt failure at the draft gear retaining plate resulted in failure with a system capacity of approximately 297 kip-ft.

The coupler itself was loaded beyond its yield strength in the Coupler/Draft Sill System Test but showed only a 1 degree permanent twist and likely had 25-33 percent more capacity to failure. Sizeable areas on the draft sill experienced plastic deformation. The test compared favorably with the FE simulation and showed similar results, with stress levels and deformations consistent with predictions for the coupler and draft sill. Based on classical rollover calculations, it is likely that an applied torsion of 297 kip-ft would rollover an uncoupled single level passenger rail car.

To obtain performance data on the coupler itself, the team performed additional testing of two coupler specimens in a manner that forced the coupler to fail. These tests showed a coupler torque capacity of 371 kip-ft. and a coupler shank twist angle to failure of 10 degrees. This corresponded to an actuating coupler angle of 20.7 degrees. These values were an average of both specimens.

Potential next steps in this research could be evaluation of more modern sill designs and couplers with pushback elements. The team also recommends simplified modeling of a string of cars using the evaluated torsional characteristics to identify conditions where adjacent cars may be stabilized or may rollover.

9. References

1. Trent, R., Prabhakaran, A., & Sharma, V. (2010). Torsional Stiffness of Railroad Coupler Connections (Report No. DOT/FRA/ORD–07/16). Federal Railroad Administration.
2. National Transportation Safety Board (1987). Derailment of Steam Excursion Train Norfolk and Western Railway Company Train Extra 611 (Report No. NTSB/RAR-87/05).
3. National Transportation Safety Board (2016). Derailment of Amtrak Passenger Train 188, Philadelphia, PA, May 12, 2015 (Report No. NTSB/RAR/16/02).
4. Tyrell, D., Severson, K., Jacobsen, K., Carolan, M., Lapre, P., Whelan, C., Schuster, J., Sandler, M., & Marceau, P. (2017). Passenger/Freight Train Collision September 12, 2008, Chatsworth, CA: Main Report (Report No. DOT/FRA/ORD-17/20). Federal Railroad Administration.
5. ASTM International (2021). Standard ASTM A370-20.
6. ASTM International (2020). Standard ASTM E8/E8M-16a.

Appendix A.
Additional Images and Data - Coupler/Draft Sill System Test

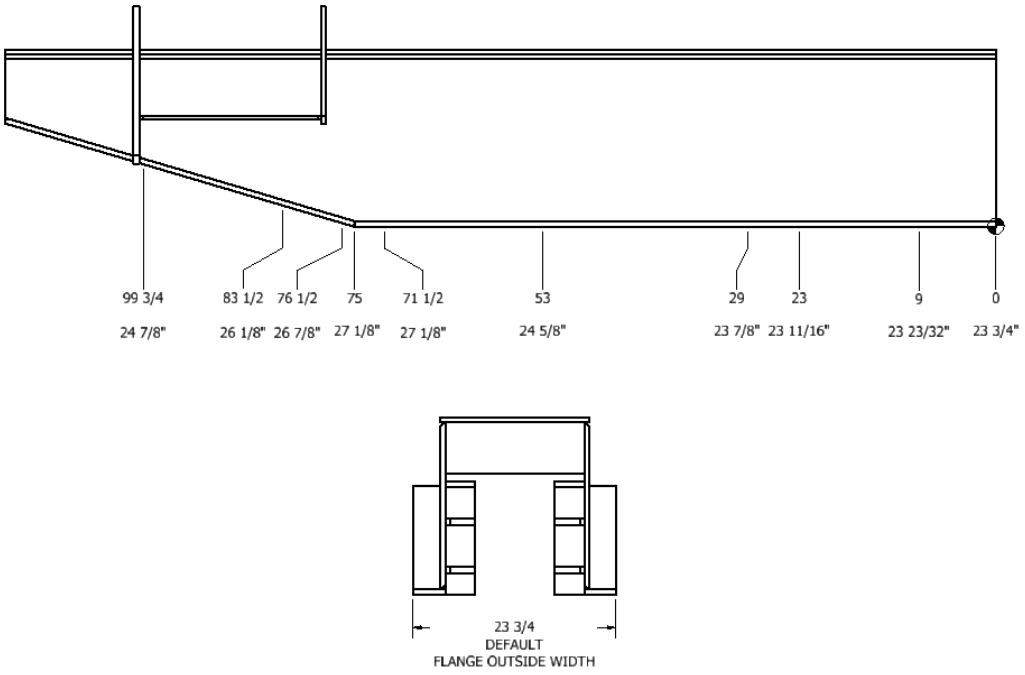

Figure A 1. Post Test width measurements of Draft Sill (Outer Flange)

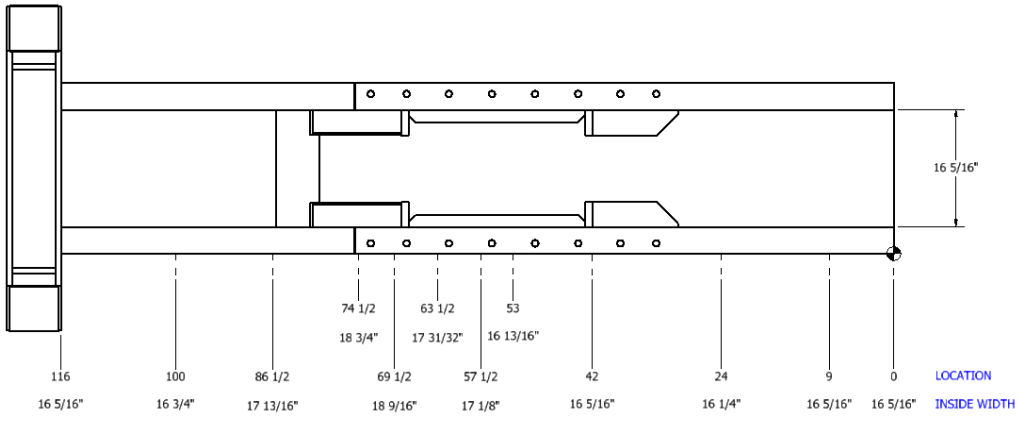

Figure A 2. Post Test width measurements of Draft Sill (Inside)

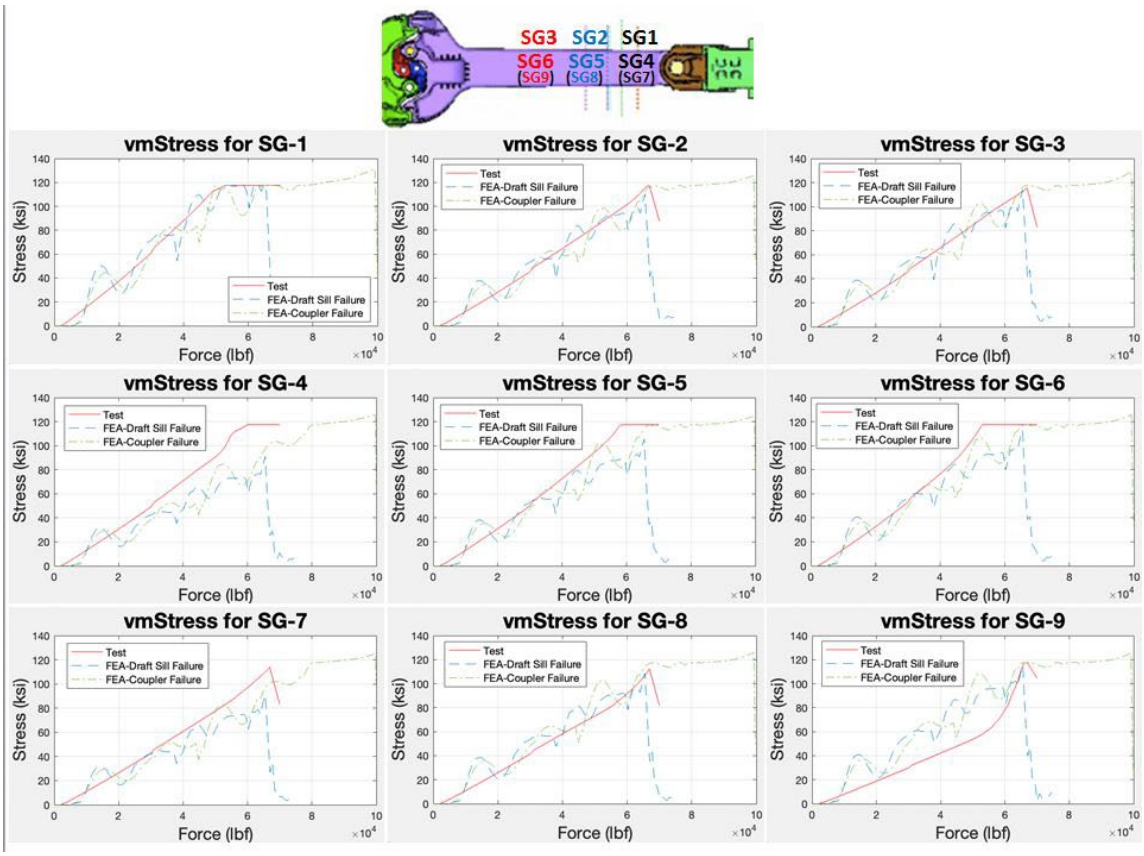

Figure A 3. Coupler Strain Gage comparison, Test to FEA

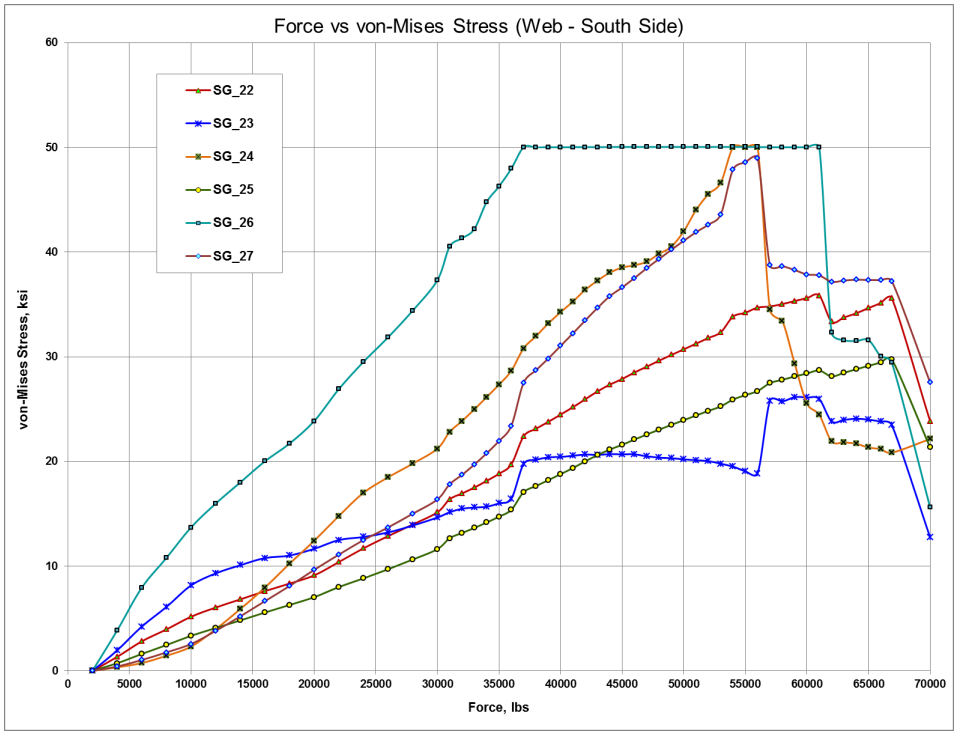

Figure A 4. Stresses on Draft Sill (South Web)

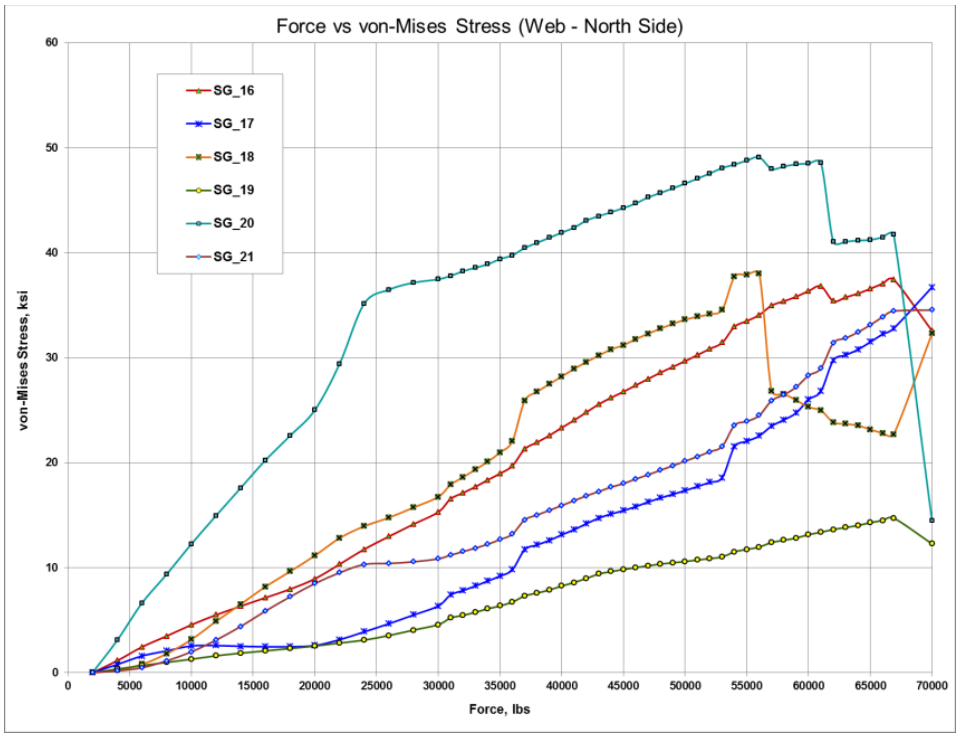

Figure A 5. Stresses on Draft Sill (North Web)

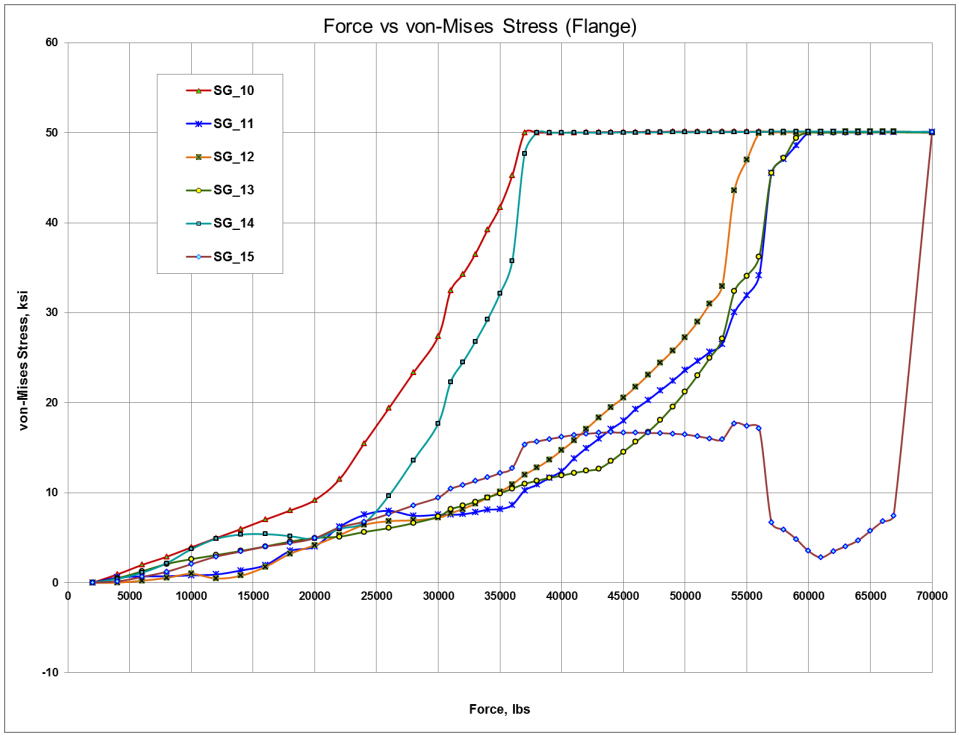

Figure A 6. Stresses on Draft Sill (Flange)

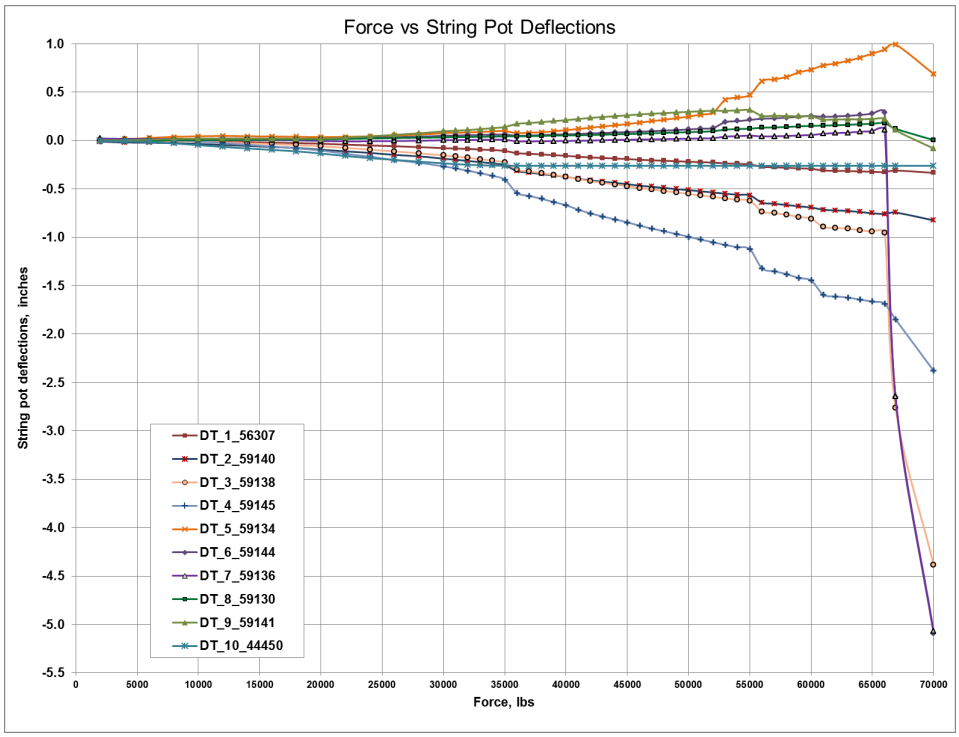

Figure A 7. Deflection Data – Draft Sill

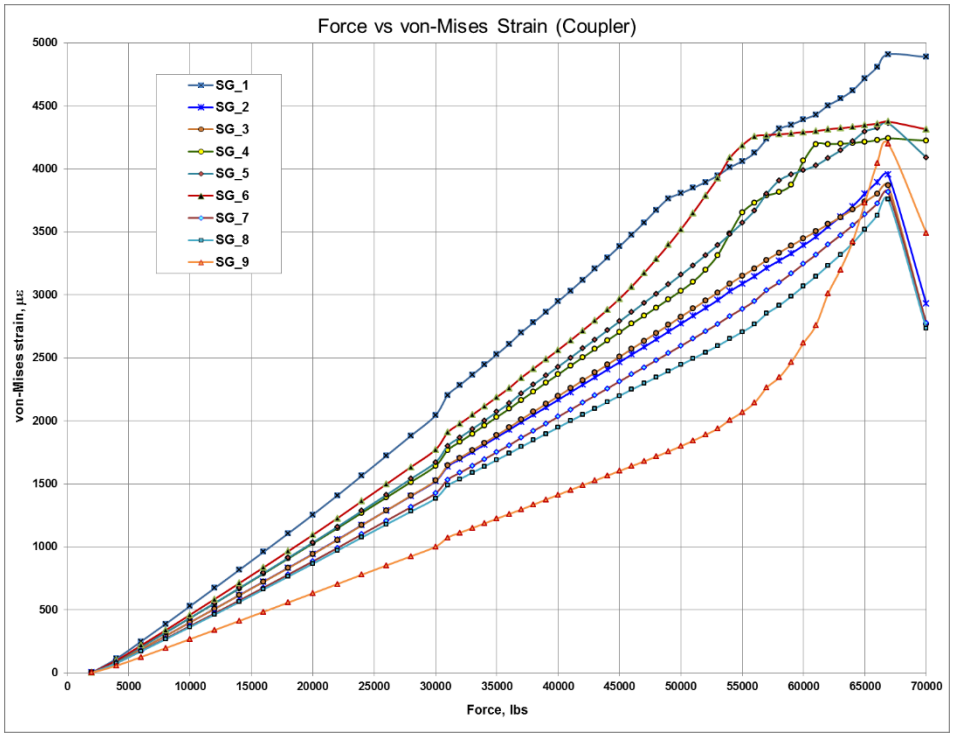

Figure A 8. Strain Data - Coupler

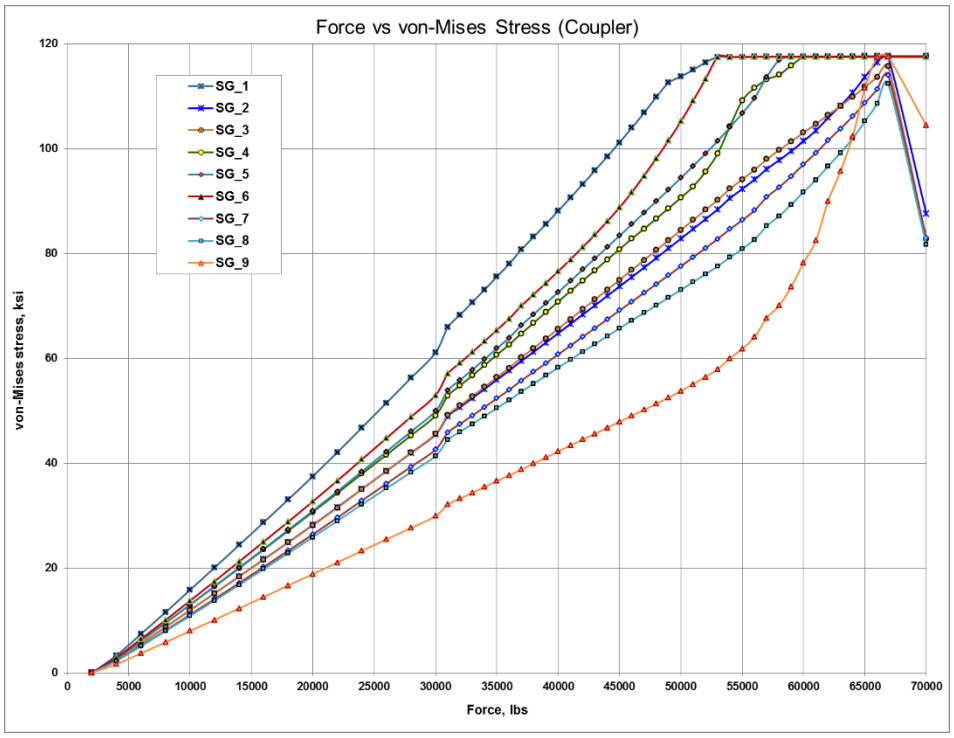

Figure A 9. Stress Plots – Coupler

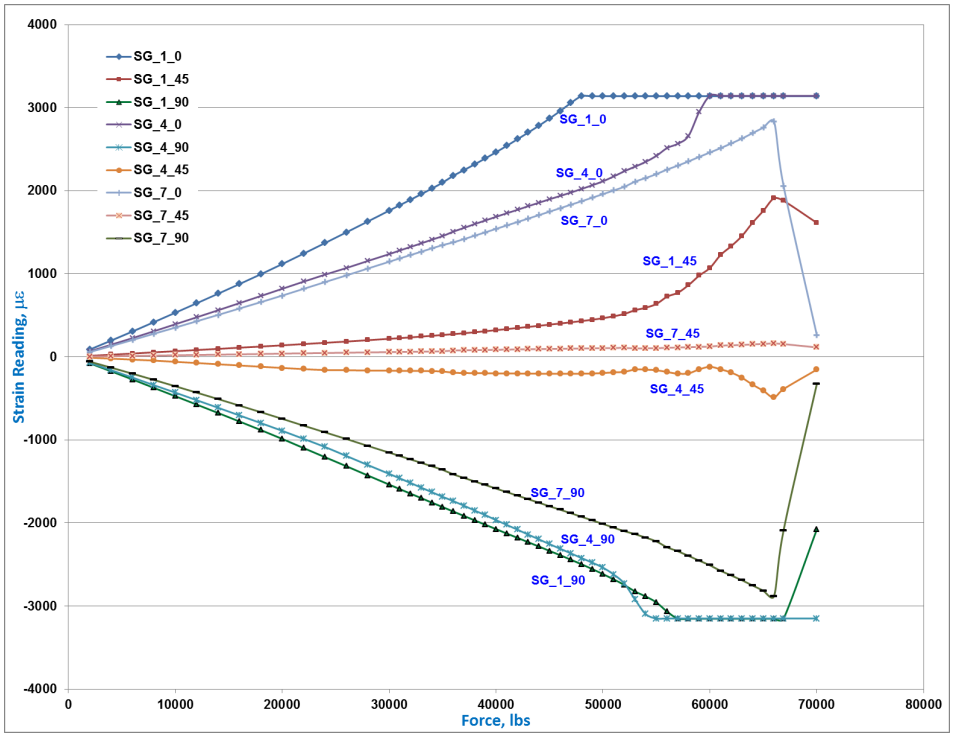

Figure A 10. Strain Gage Data #'s (1,4,7) – Coupler

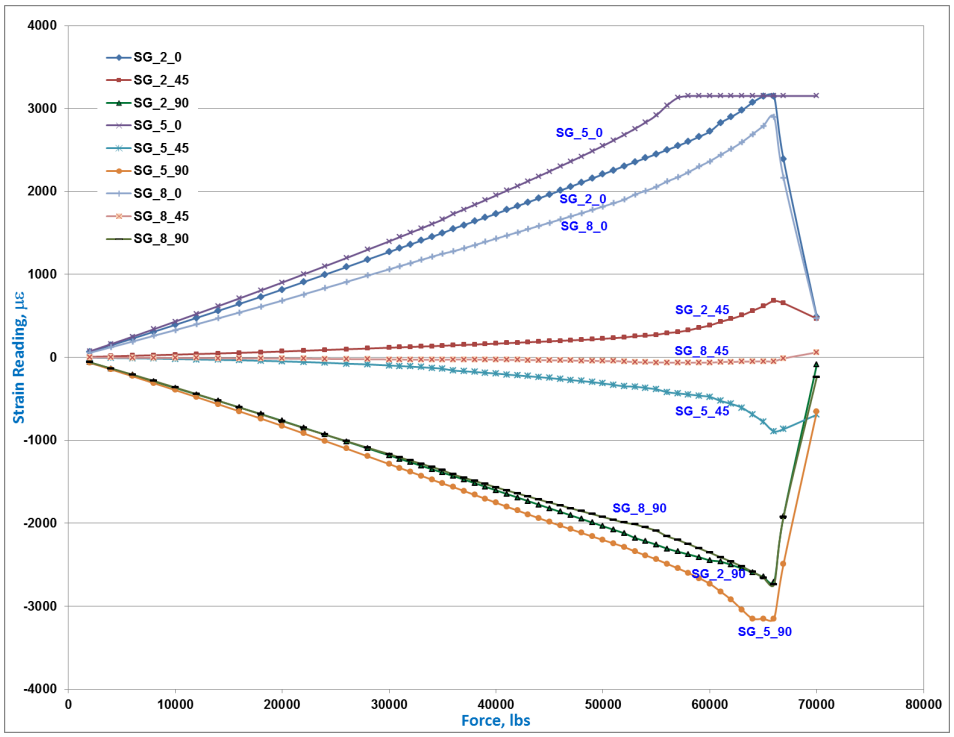

Figure A 11. Strain Gage Data #'s (2,5,8) - Coupler

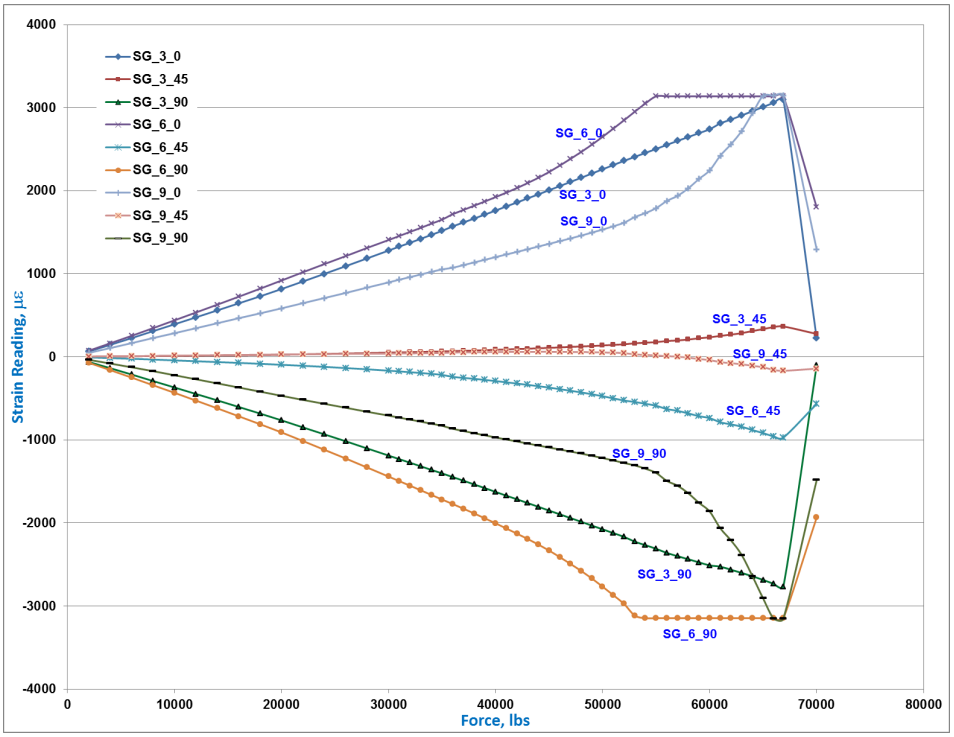

Figure A 12. Strain Gage Data #'s (3,6,9) – Coupler

Appendix B.
Additional Images and Data - Coupler Failure Test

Figure B 1. Example Strain Gauge Application

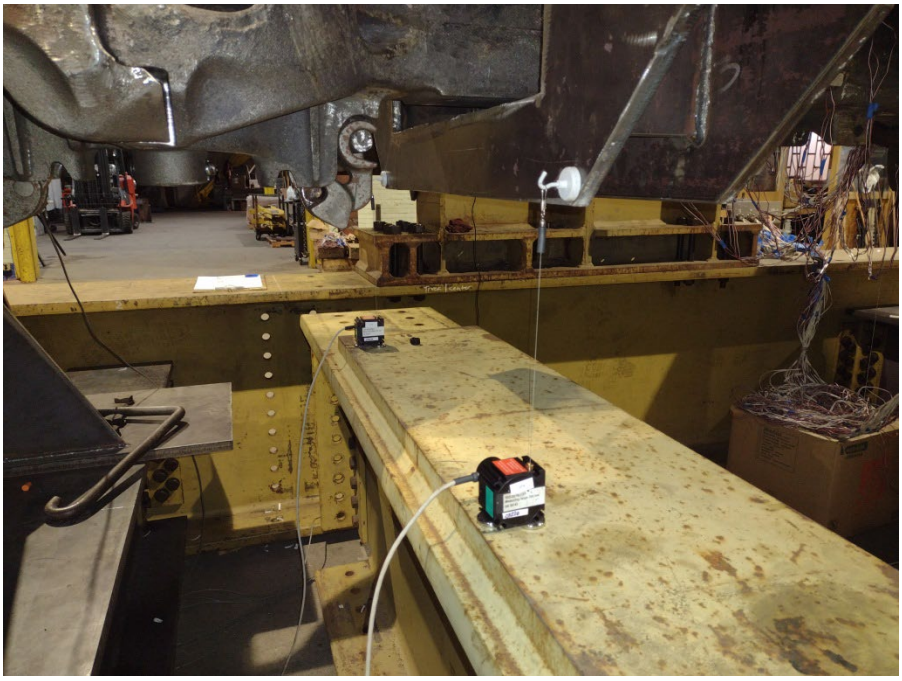

Figure B 2. Example Displacement Transducer Application

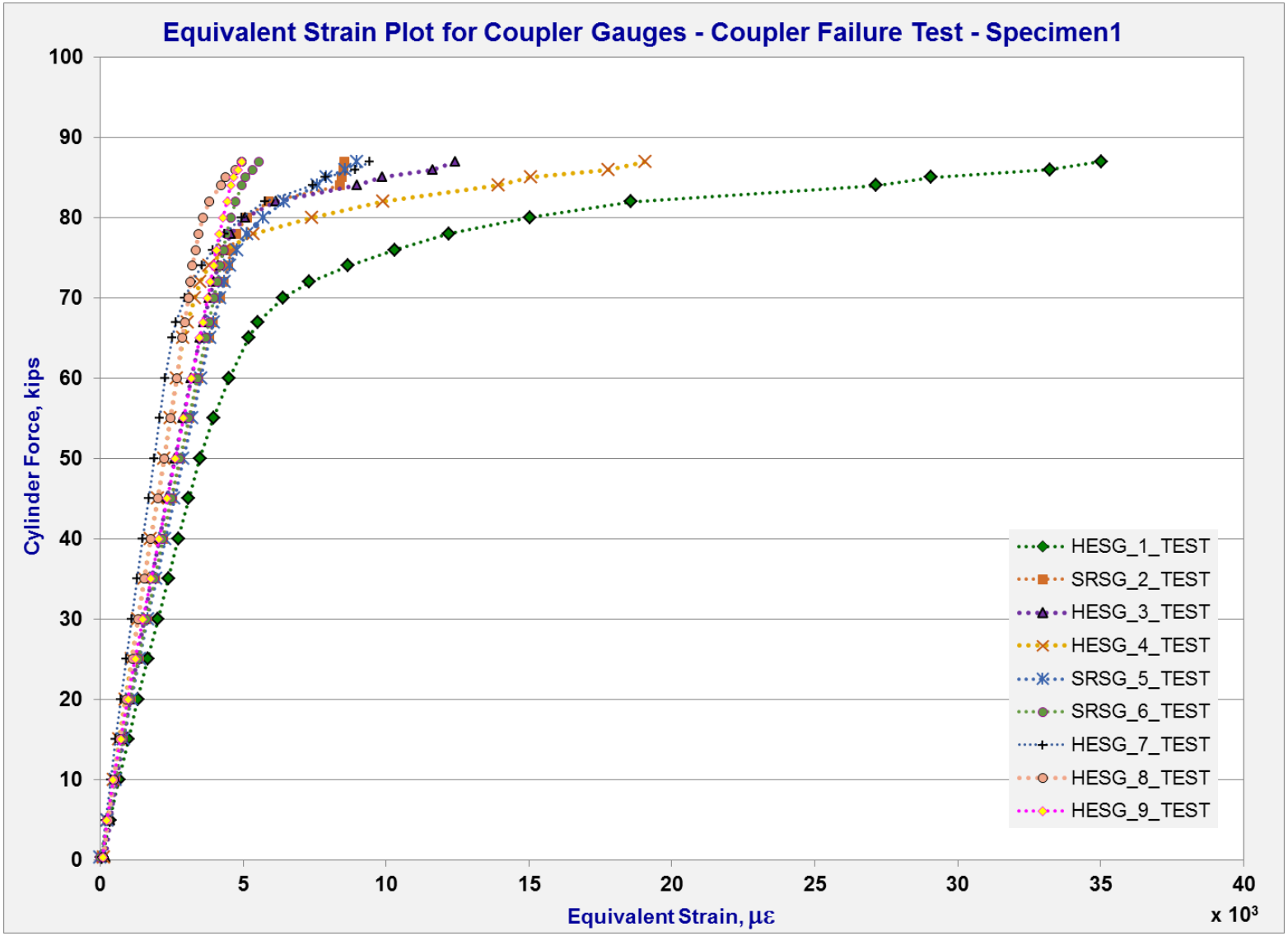

Figure B 3. Equivalent Strain Plot for the Coupler Gauges – Coupler Failure Test – Specimen 1

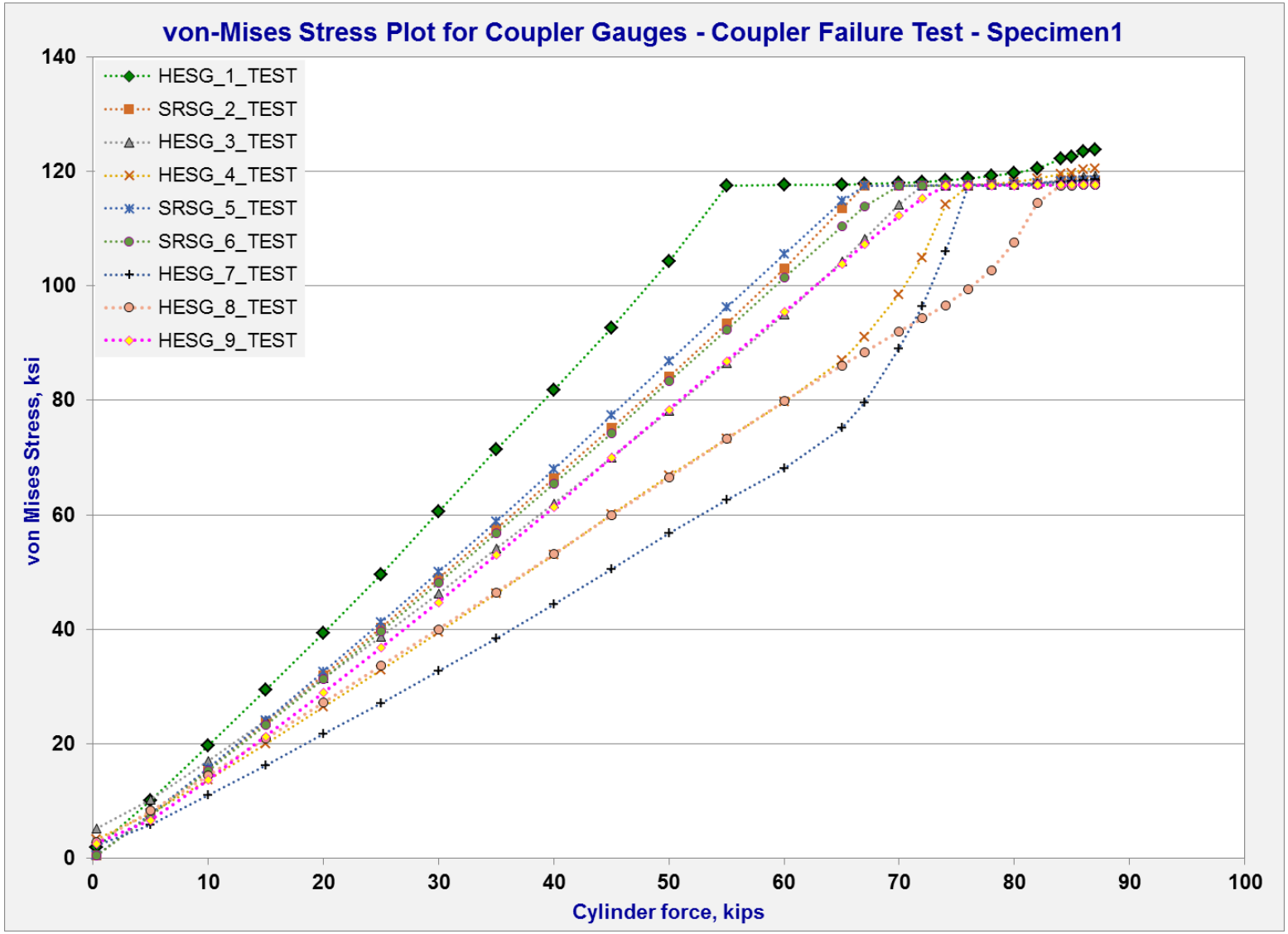

Figure B 4. Equivalent Stress Plot for the Coupler Gauges – Coupler Failure Test – Specimen 1

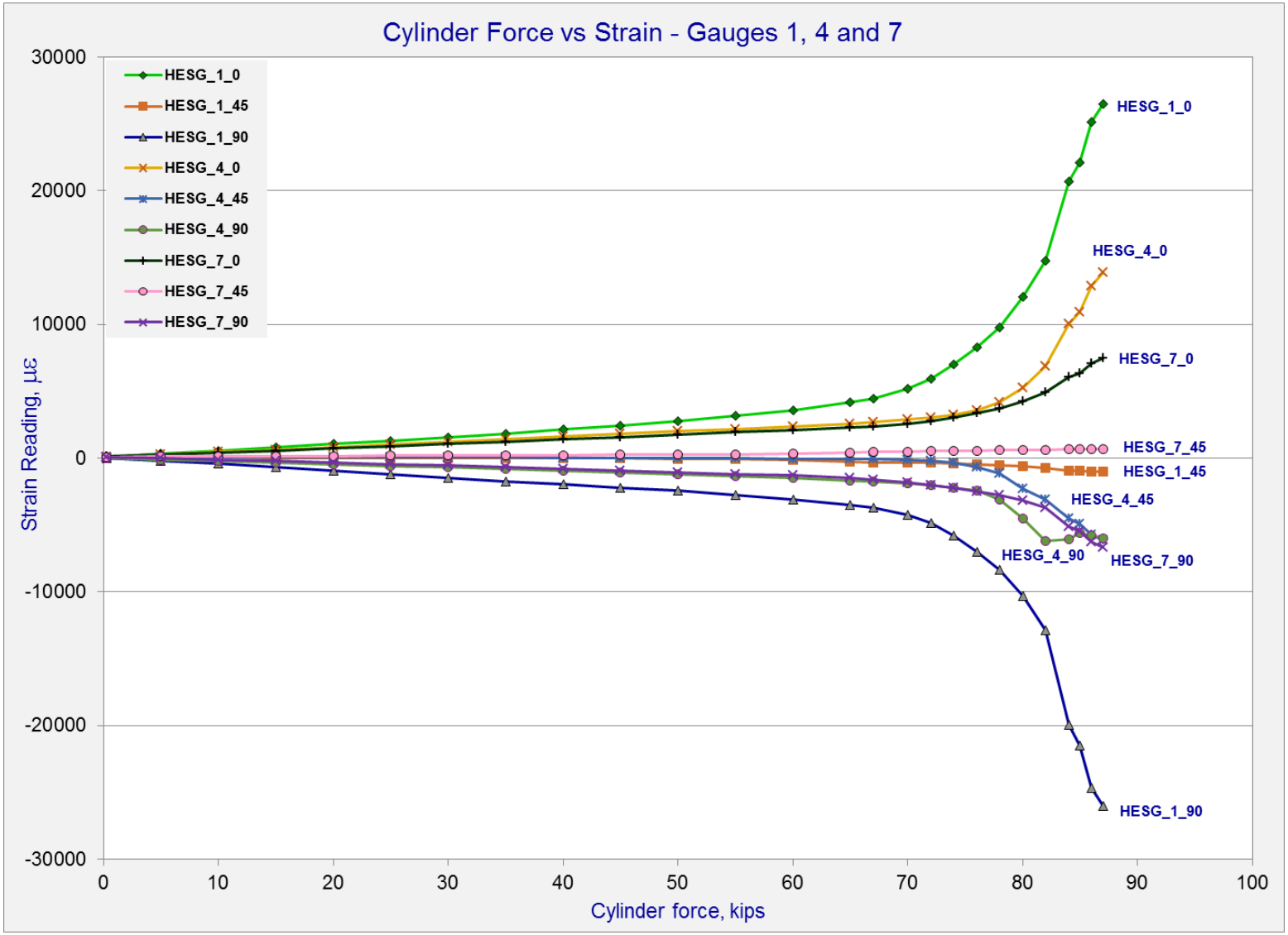

Figure B 5. Test Strains Plot for the Coupler Gauges 1, 4 and 7 – Coupler Failure Test – Specimen 1

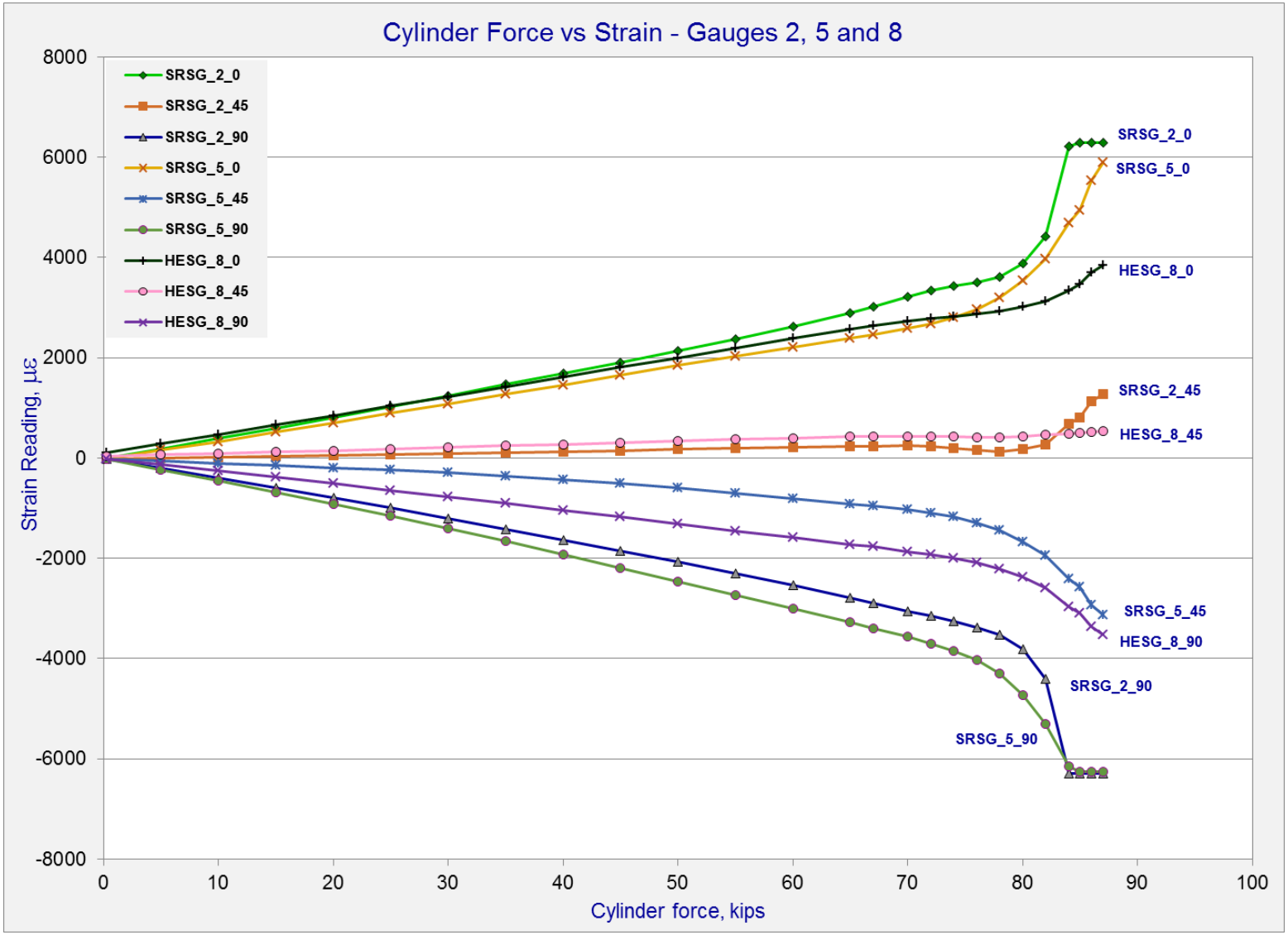

Figure B 6. Test Strains Plot for the Coupler Gauges 2, 5 and 8 – Coupler Failure Test – Specimen 1

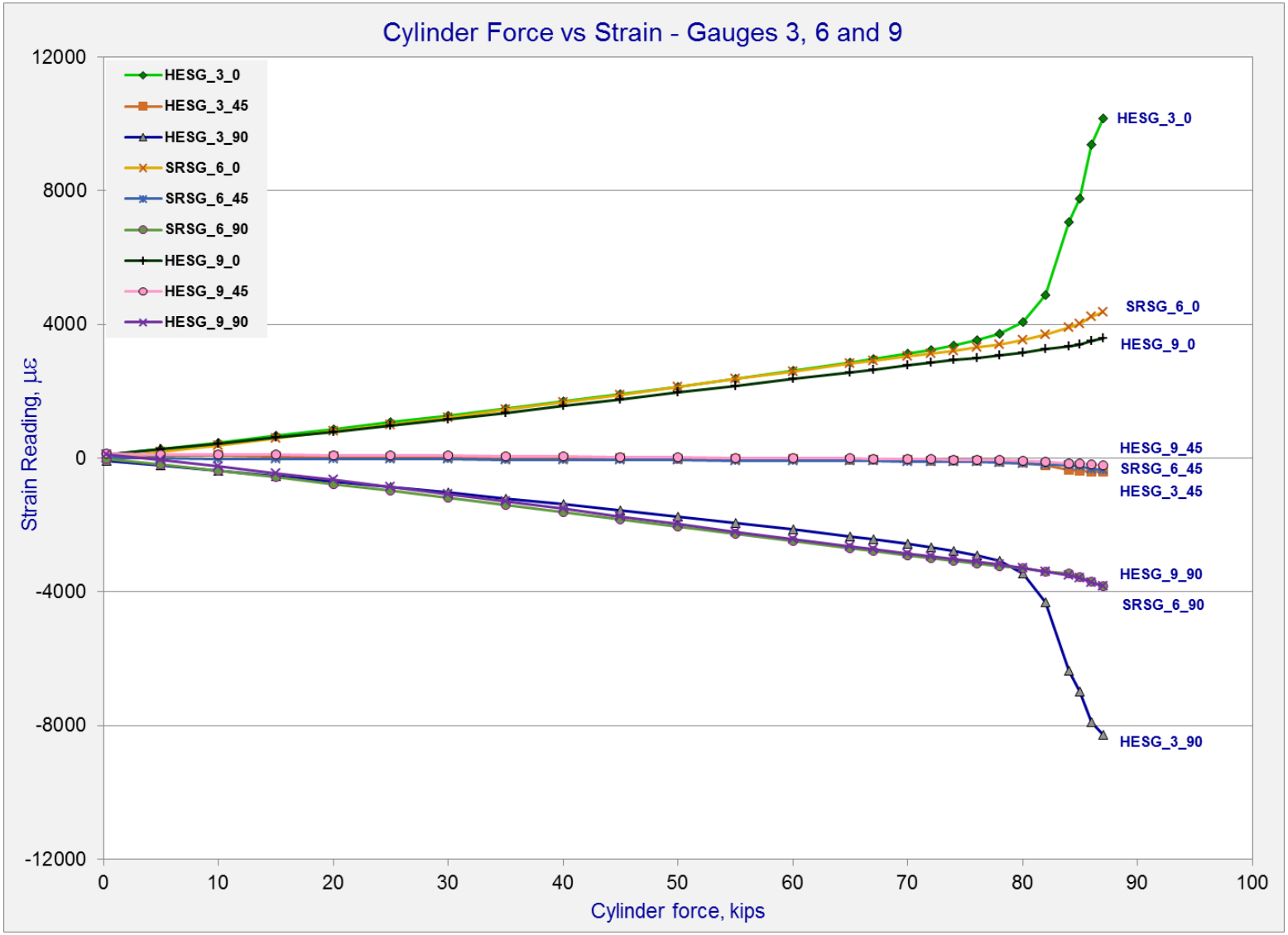

Figure B 7. Test Strains Plot for the Coupler Gauges 3, 6 and 9 – Coupler Failure Test – Specimen 1

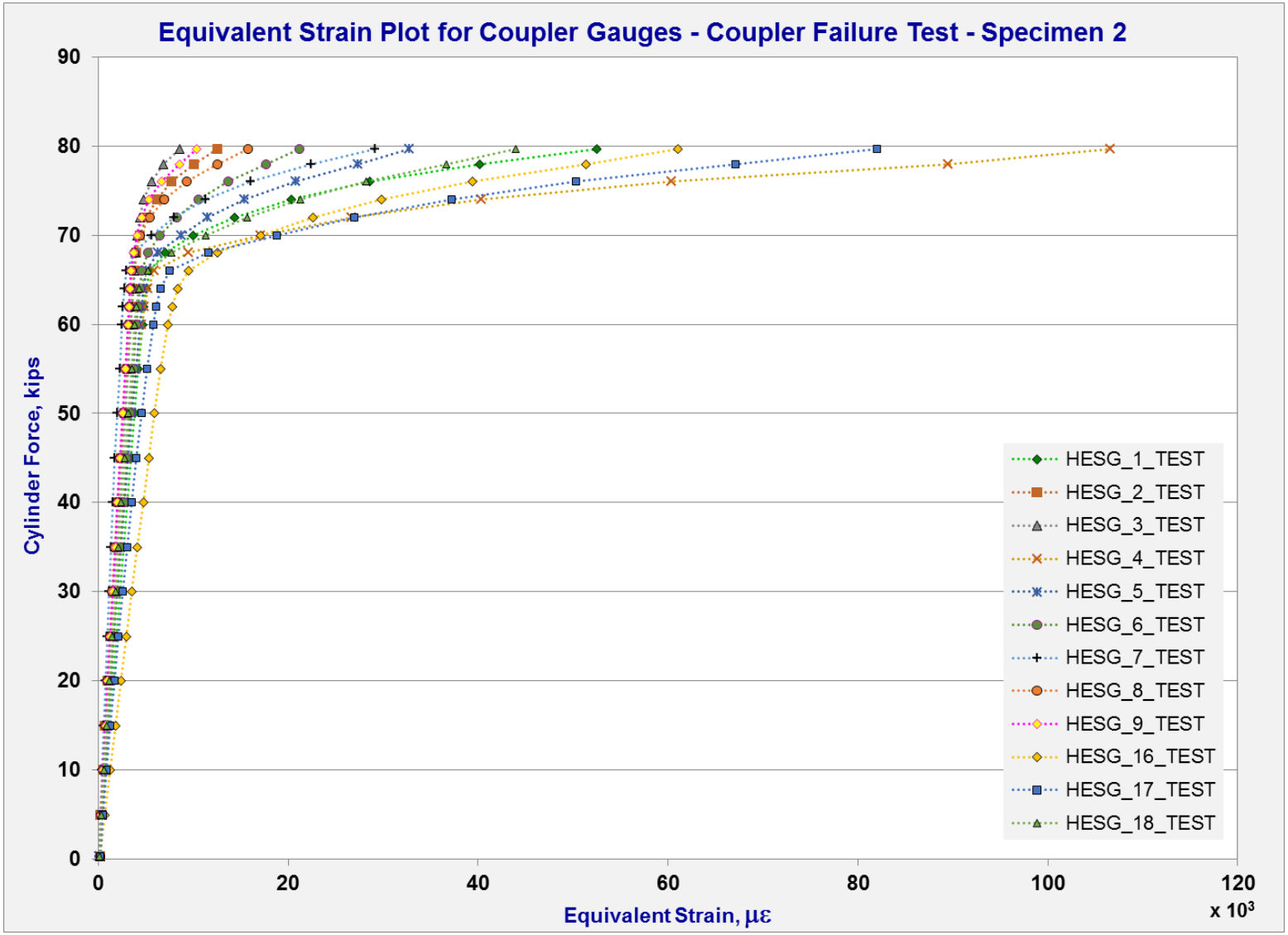

Figure B 8. Equivalent Strain Plot for the Coupler Gauges – Coupler Failure Test – Specimen 2

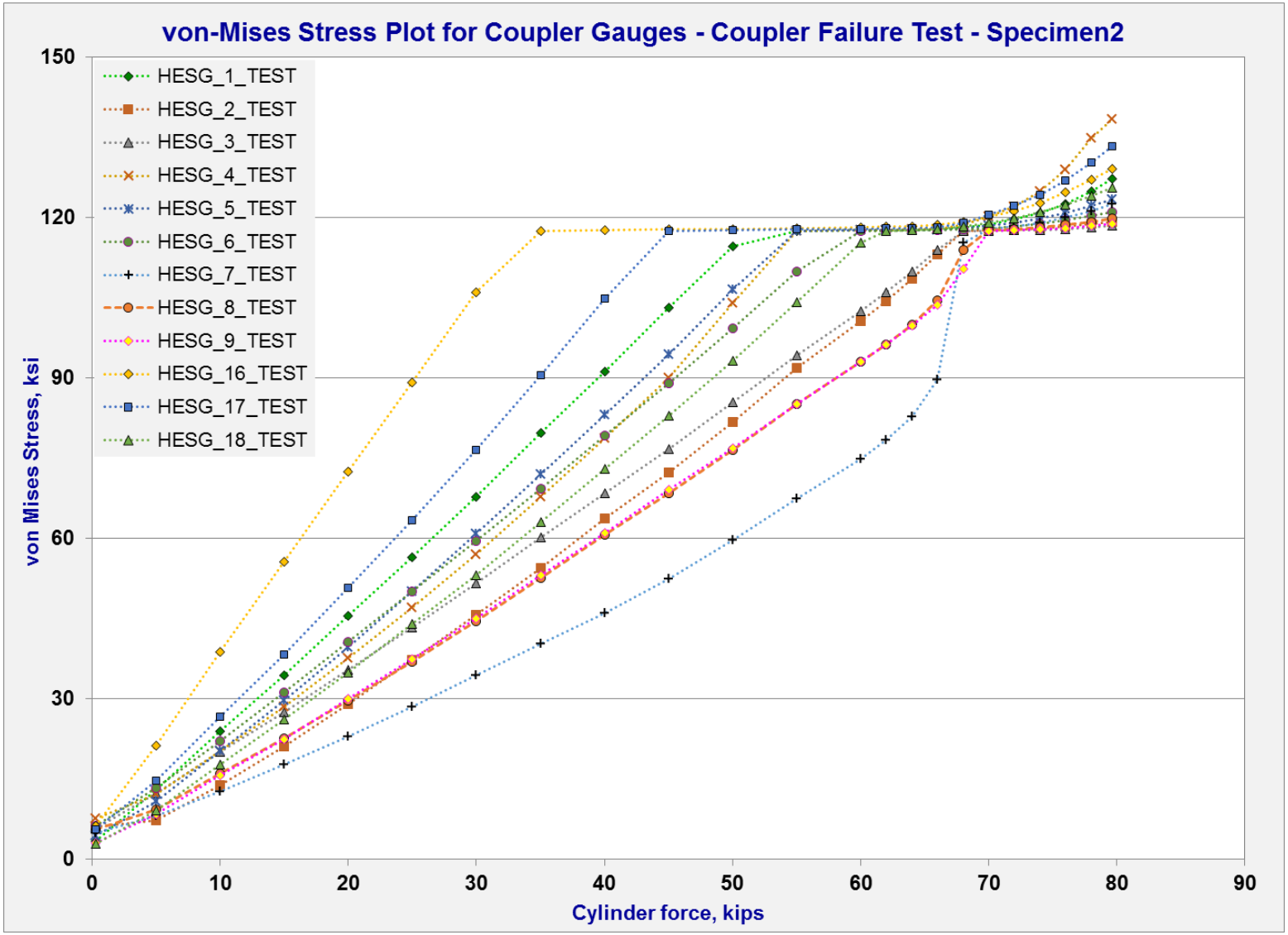

Figure B 9. Equivalent Stress Plot for the Coupler Gauges – Coupler Failure Test – Specimen 2

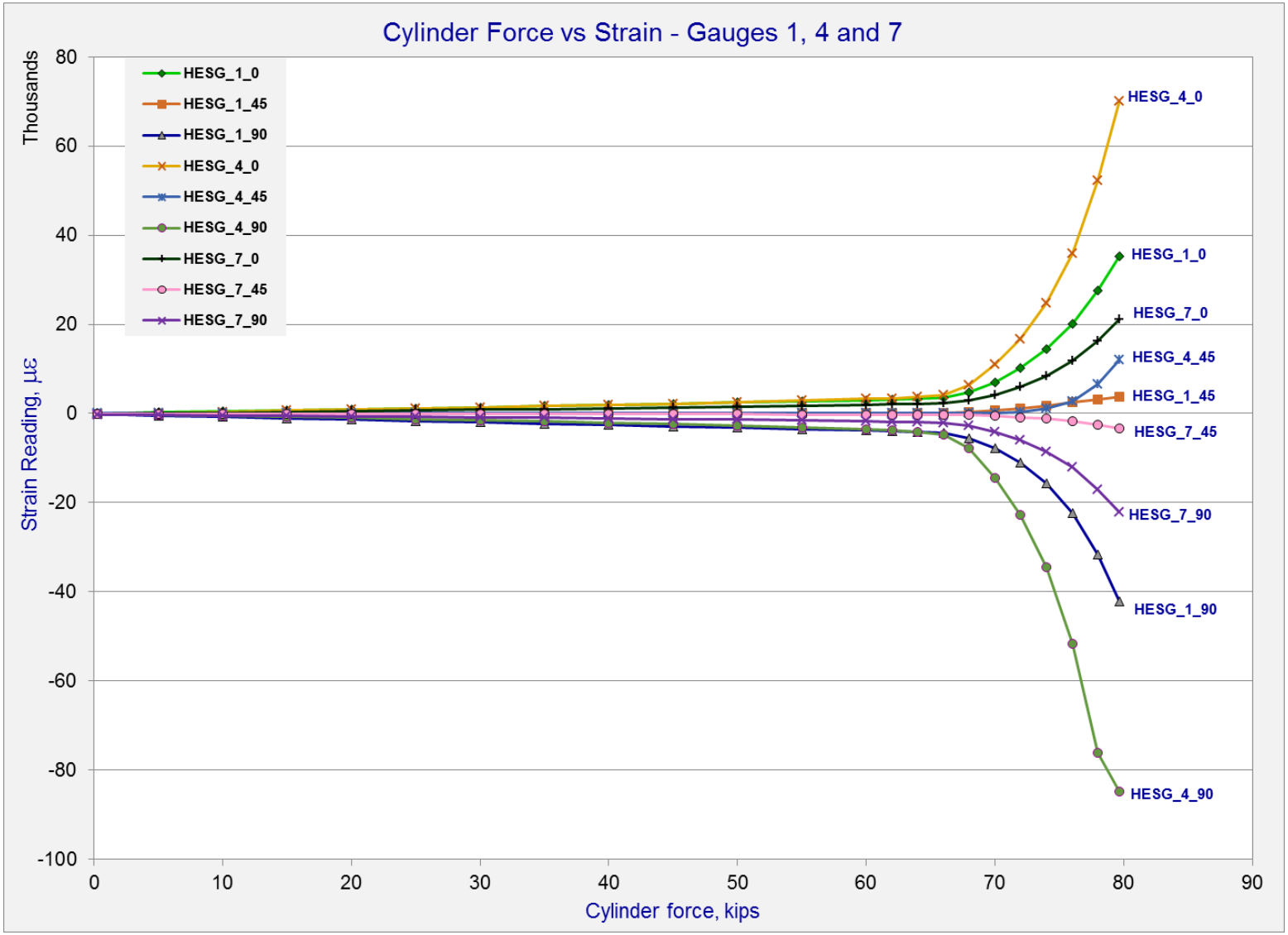

Figure B 10. Test Strains Plot for the Coupler Gauges 1, 4 and 7 – Coupler Failure Test – Specimen 2

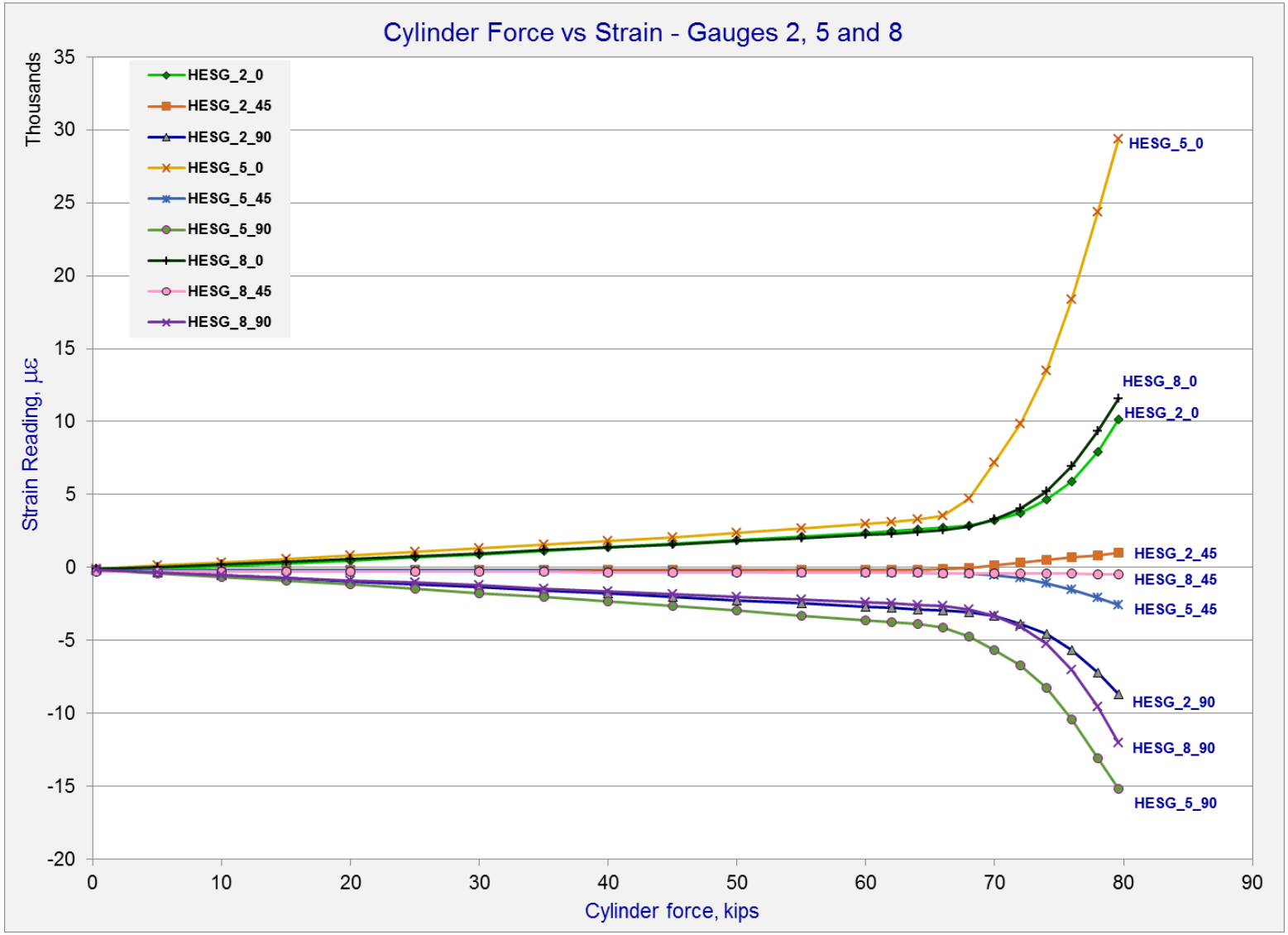

Figure B 11. Test Strains Plot for the Coupler Gauges 2, 5 and 8 – Coupler Failure Test – Specimen 2

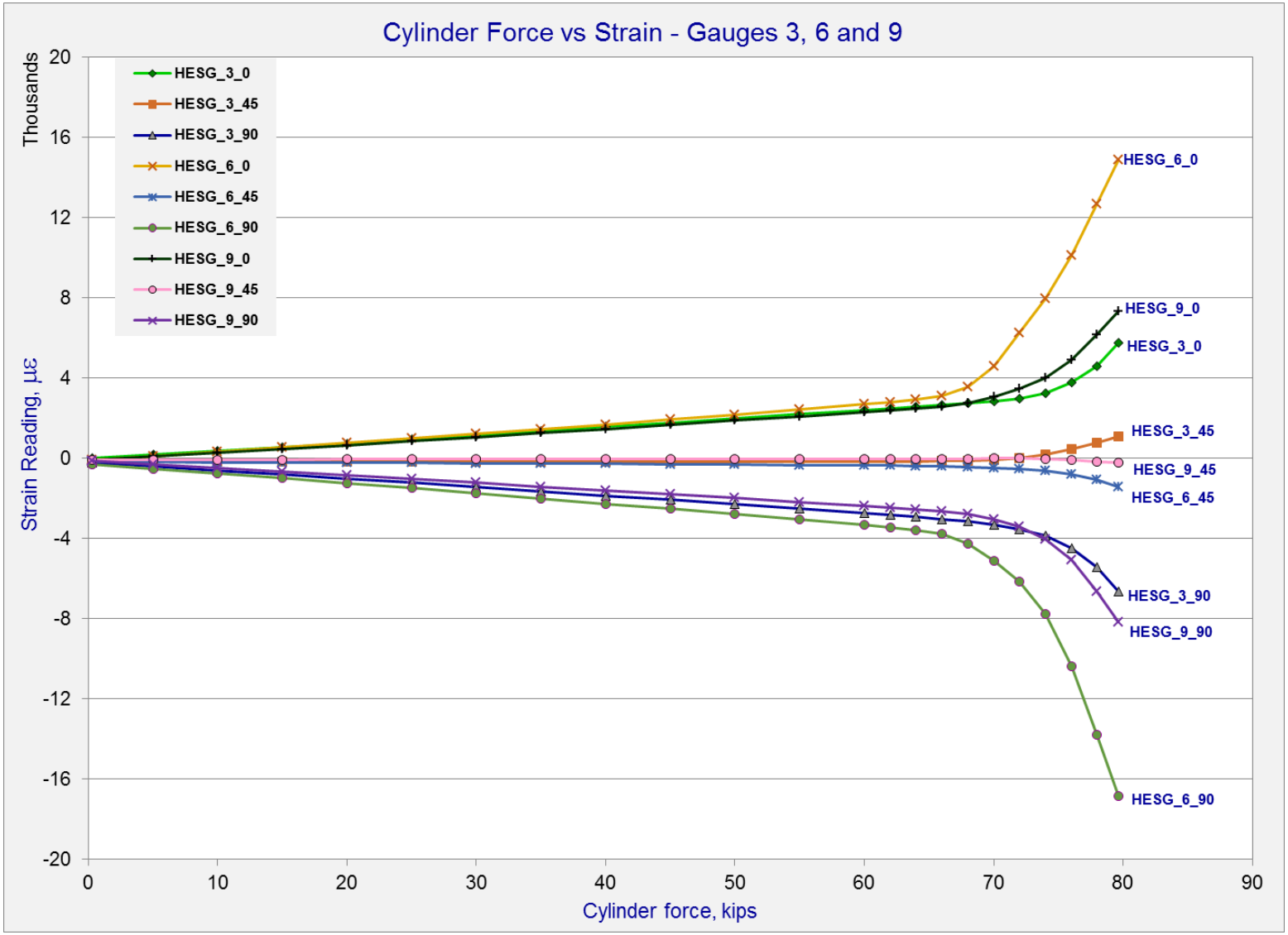

Figure B 12. Test Strains Plot for the Coupler Gauges 3, 6 and 9 – Coupler Failure Test – Specimen 2

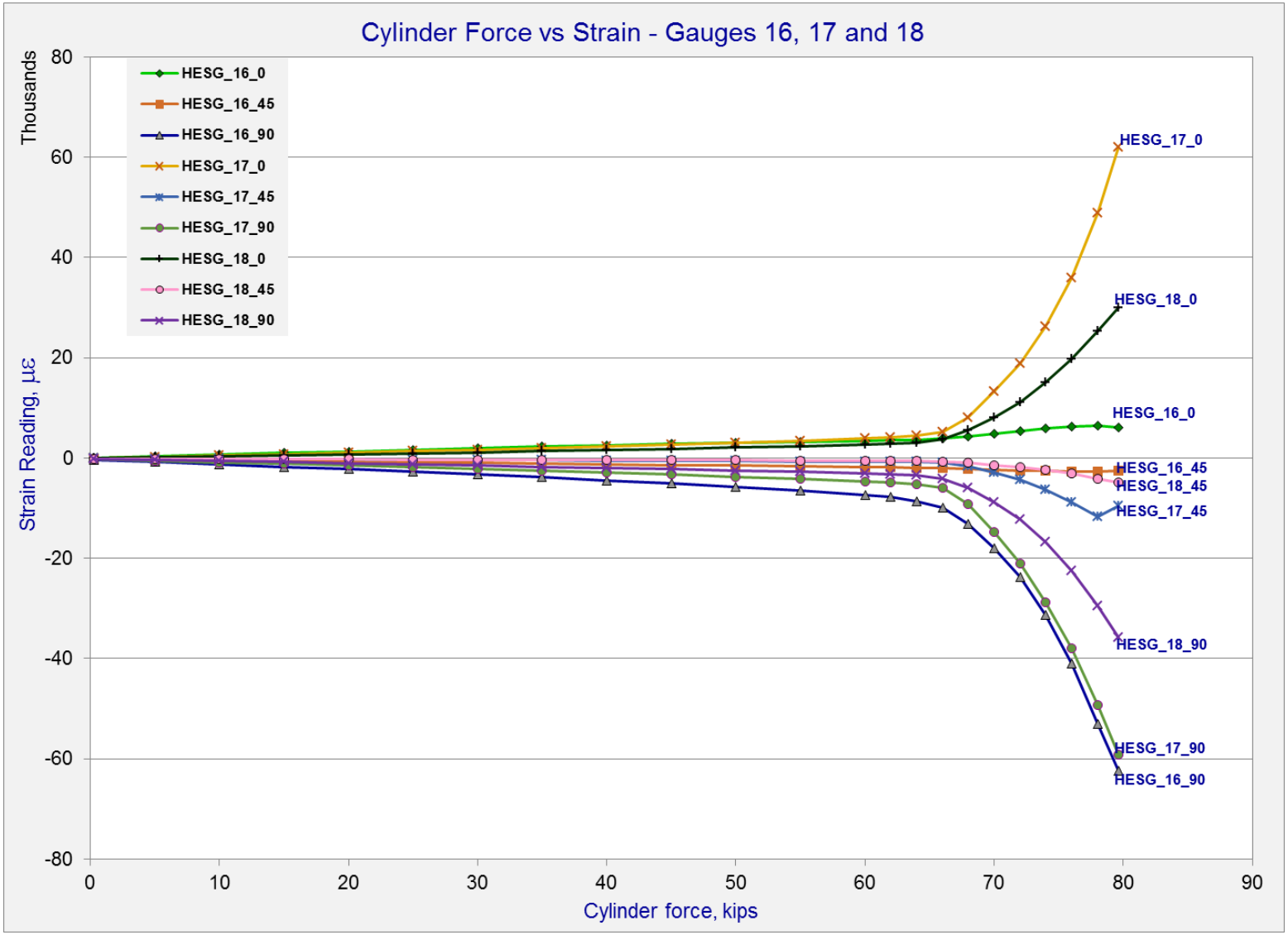

Figure B 13. Test Strains Plot for the Coupler Gauges 16, 17 and 18 – Coupler Failure Test – Specimen 2

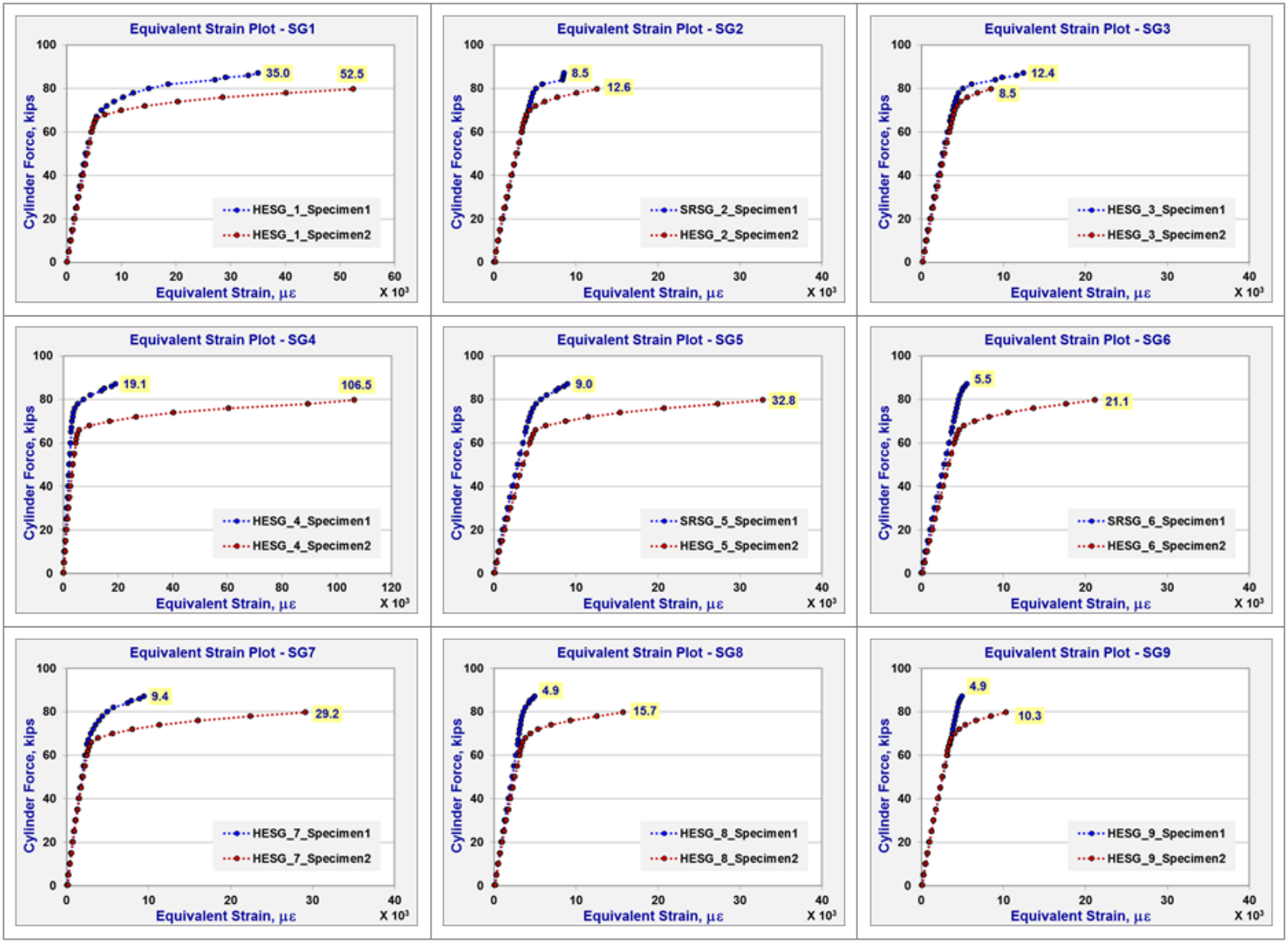

Figure B 14. Equivalent Strain Plots for the Coupler Gauges – Coupler Failure Test - Specimen1 and Specimen 2

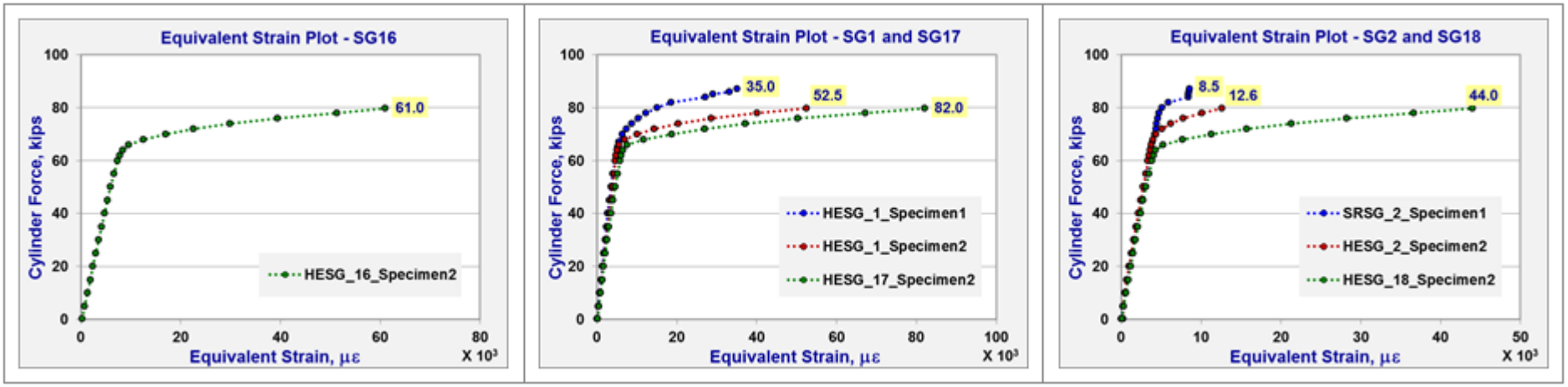

Figure B 15. Equivalent Strain Plots for the Coupler Gauges – Coupler Failure Test - Specimen1 and Specimen 2

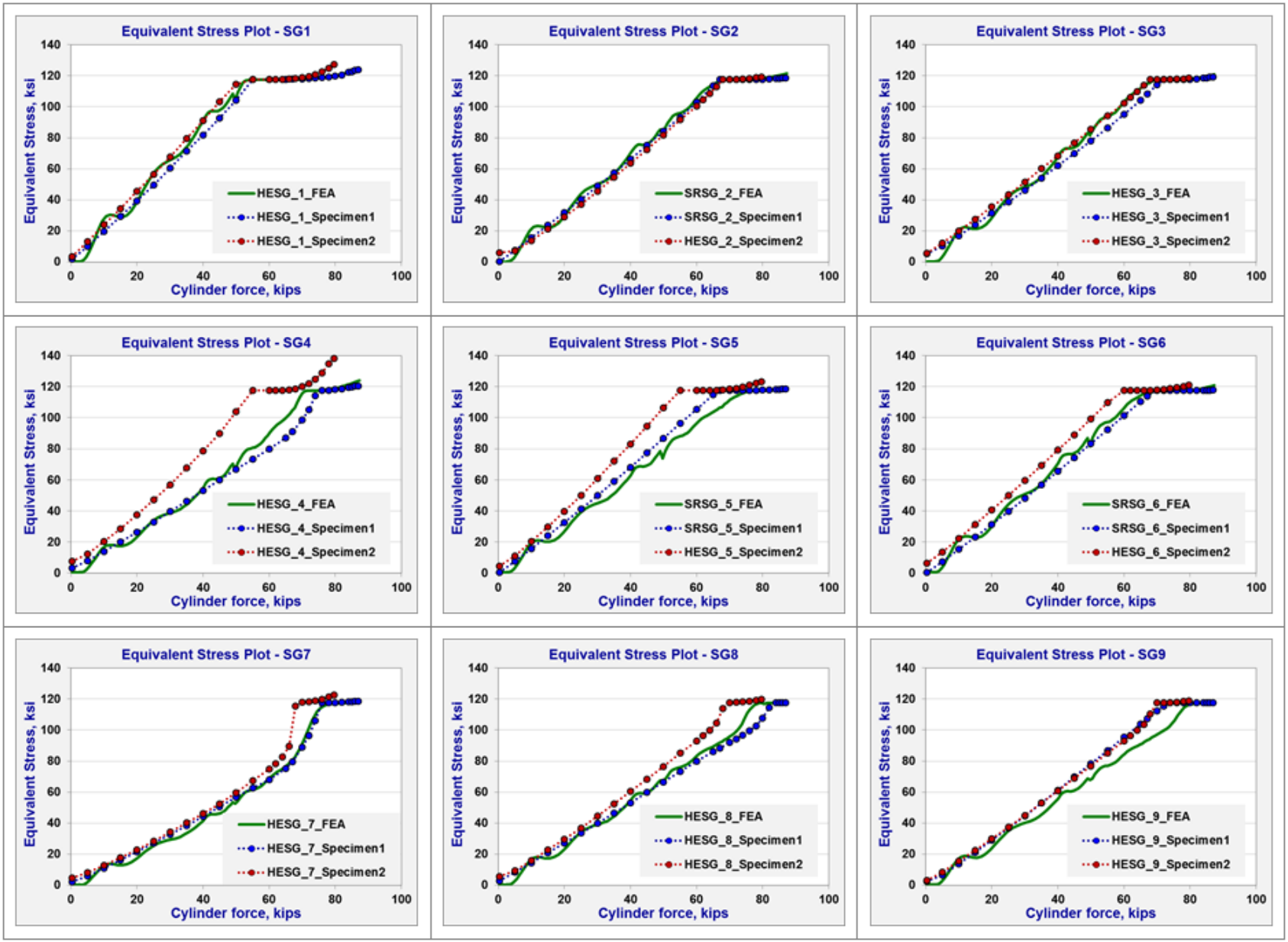

Figure B 16. Equivalent Stress Plots for the Coupler Gauges – Coupler Failure Test - Specimen1, Specimen 2, and FE simulation

Appendix C.
Classical Rollover Calculations

Treating carbody and trucks as a rigid body, and considering rolling of car about wheel

Determine if carbody will rollover based on torque applied to coupler shank.

$\circlearrowleft + \sum \downarrow Pt.a = 0$:

$$T - LW + 2LR = 0$$

$$R = LW - T/2L$$

If $R \leq 0$, then carbody will roll over

Given:
L = 30 in
W = 100,000 lbs
T = $3.556e^6$ in-lb

R = -9,267 lbs

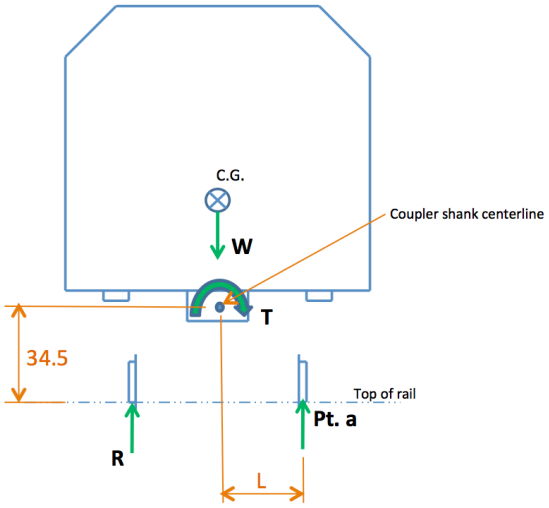

Considering rolling of carbody about side bearing

Assuming: No suspension compression

Determine if carbody will rollover based on torque applied to coupler shank

$\circlearrowleft + \sum \downarrow Pt.b = 0$:

$$SR_c - SW + T = 0$$

$$R_c = SW - T/S$$

IF $R_c \leq 0$, then carbody will roll over

Given:
S = 26 in
W = 100,000 lbs
T = $3.556e^6$ in-lb

R_c = -36,769 lbs

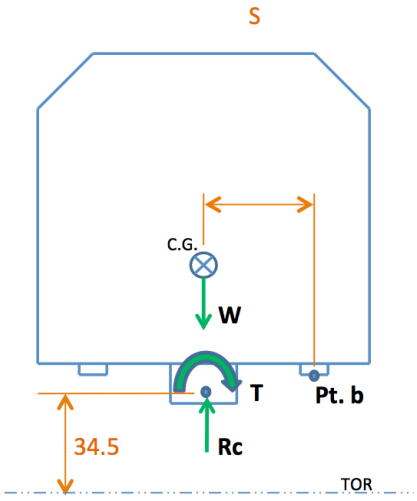

Abbreviations and Acronyms

ACRONYM	DEFINITION
AAR	Association of American Railroads
APTA	American Public Transportation Association
CAD	Computer Aided Design
CEM	Crash Energy Management
DOT	Department of Transportation
FE	Finite Element
FEA	Finite Element Analysis
FRA	Federal Railroad Administration
NTSB	National Transportation Safety Board
RAIRS	Railroad Accident and Incident Reporting System